SI MICROWIRE ARRAY PHOTOANODES FOR ARTIFICIAL PHOTOSYNTHETIC DEVICES

Thesis by
Elizabeth Santori

In Partial Fulfillment of the Requirements
for the Degree of
Doctor of Philosophy

CALIFORNIA INSTITUTE OF TECHNOLOGY
Pasadena, California
2013
(Defended October 2, 2012)

ACKNOWLEDGEMENTS

I have a great number of people to thank for their critical contributions to the work contained in this thesis, as well as for their support, which ultimately allowed me to finish this degree. First, I would like to thank my mentor, Nate Lewis. Nate, you gave me the reason to go to graduate school and to stay. Your passion for energy research and energy policy struck a chord with me, and made me remember why science was ever interesting to me in the first place: as a potential means to solve great societal problems. Your group was the perfect choice for me, and I thank you for giving me a chance. Besides the ability to epoxy small features with great precision, my experience in your group has really provided me with the tools to analyze situations and solve problems. I have always admired your ability to condense complicated problems into like 2 equations in 5 seconds, and will continually strive to match your speed, accuracy, and elegance in performing back-of-the-envelope calculations.

I would also like to thank my collaborator, Harry Atwater, for his support and enthusiasm. Harry, every time I would meet with you, you would really have great advice, or be thinking about something really interesting and share your ideas with me. Thank you for that. Your group is a joy to work with and to learn from, and I am glad that I had a second home there. Bruce Brunschwig must be acknowledged for his thoughtful advice, patience, and hilarity. Thank you, Bruce, for being the scientist that everyone wants to be, including myself. The additional members of my thesis committee—Theo Agapie and Mitchio Okumura—provided me with great feedback, and were very supportive of both my work at Caltech and my D.C. ambitions. Thank you all for taking the time to be mentors to me.

Several people directly contributed to the contents of this thesis. Nick Strandwitz closely collaborated with me on experiments on undoped Si microwires, and performed all of the device physics simulations contained herein. Thank you Nick for being the best scientific sounding board, and for increasing the depth of this project. Shane Ardo took up the torch of n-Si microwire arrays, completing many of the calibrations for n-Si

microwires, and demonstrated the successful performance of thermally oxidized n-Si microwires. Shane also graciously allowed me to include his work on n^+-i-Si microwire arrays with diffused radial junctions. Matt Bierman made this whole thesis possible by building a Si microwire CVD that actually produced…wires. He must also be acknowledged for his relentlessly upbeat attitude that buoyed my spirits and made me want to be a better person. Ron Grimm maintained and overhauled the Si CVD with me, supplied reagents for measurements in cobaltocene, helped me with photoconductivity measurements, and generally just made everything work better. Emily Warren was my 'go-to' wire guru, providing me with invaluable advice on wire processing and experiments. Emily also supplied me with p-Si microwires for some critical experiments and helped me with measurements using $MV^{2+/+}$.

I was fortunate enough to have the opportunity to pursue my interest in science policy during graduate school, as a Christine Mirzayan Science and Technology Policy Fellow at the National Academies. The program directors, Rebecca Burke and Anne-Marie Mazza, and my mentor, John Holmes, were absolutely wonderful and made the experience challenging and fulfilling. I cannot thank you enough for your complete dedication to the program. John, you kept me super busy and involved, and were the reason that I was able to learn so much in a short time. Thank you!

I would also like to acknowledge my undergraduate advisor Milan Mrksich, for taking a chance on me as an undergraduate and for encouraging me to get in the lab and figure things out for myself. Milan, your showmanship and powers of persuasion are something to aspire to, in addition to your scientific creativity. I hope one day to give a talk as well as you can.

My colleagues in both the Lewis and Atwater groups over these past five years have been my surrogate family. There was always a draw to come into Noyes, to talk, to share the latest disappointing or amazing results, or just go to the white board to hash things out. You made me work harder and helped me to understand things better. In particular, I would like to thank Leslie O'Leary and Emily Warren for being the best colleagues and friends. We really did have a unique experience. I'm glad I got to work so

closely with two amazing people, as we united together as the women of the Lewis Group. Jim Maiolo shared his electrochemistry skills with me and so generously mentored me in the very beginning. Kate Plass showed me the ropes as a young first year and was also a good friend. Whenever I think of kitties on a piece of glass over a flame, I think of you. Greg Kimball, thank you for being crazy and excited about everything all of the time—you really are an inspiration. Don Walker, you are hilarious and it was great to be able to work with you on the spectral response system. We ultimately got our way, and that feels good. Shannon Boettcher, your energy and determination pushed me to work faster and harder. To the first wave of postdocs, you made the Lewis Group a better place to do science and work. We were all a little trepidatious and territorial when you arrived, but you quickly made the group smarter, more positive, and a little more functional. Thank you and I do apologize for potentially glaring at you when you first arrived. Barbara Miralles and Elyse Garlock pretty much kept our group thriving and surviving, and made sure that I was successful in my time here. I cannot thank you both enough.

I would also like to collectively acknowledge all of my Atwater and wire friends—Brendan Kayes, Mike Filler, Josh Spurgeon, Mike Kelzenberg, Morgan Putnam, Dan Turner-Evans, Emily Warren, Mike Deseglie, Shannon Boettcher, Hal Emmer, Chris Chen, Emily Kosten, Nick Strandwitz, Emily Kosten, Anna Beck, Matt Shaner, and Heather Audesirk. I came to grad school wanting to work on a collaborative project, and after sitting in the dark alone for a year with some printers that I use to talk to, I finally got that chance. Thanks for letting me on the team. In particular, Mike K, thank you for your help in understanding the angle-resolved optical and photoelectrochemical measurements. I'm sorry for my relentless questions, and I'm glad that you always seemed to humor me. Josh, thank you for showing me how to grow wires in the very beginning. Dan, thank you for being ever so helpful and gracious all the time. You made the wire project an actual team project and fun as hell.

I would like to thank Zak Gates for both dragging me to meet with Nate during the visitation weekend and for setting the highest standards for what science should be; Rachel Klet and Matt Winston for always being there, even when I was being a total kvetch; and

the Okumura crew, for being chill, fun, and like in-laws that sometimes you like better than your own crazy family that you just need to get away from sometimes.

As Milan told me when I had decided on Caltech, his alma mater, 'Caltech is a monastery for science.' I shrugged off the comment, thinking I could handle at least five years of scientific solitude. I was naïve. I want to thank my family—David, Cathy, Matt, John, Christine, Rob, Rowan, Grandma, Aunt Cindy, Eric, and all the Santoris—for bearing with me during my monastic absence for five years. Your support, love, and understanding were critical to my success at Caltech, and I am looking forward to seeing more of you in the coming years.

And Dave, I wouldn't have made it through without you, literally. Would I have finished this Ph.D. if I hadn't met you? Uncertain. I am so glad that I had your unwavering support and your love through these five years. You pushed me to accomplish more, while simultaneously reassuring me that I was doing okay. I reverse-dedicate this thesis to you! Please don't read it, though.

Elizabeth Santori
September 18, 2012

ABSTRACT

To realize the large-scale deployment of solar power, new materials and strategies must be developed for the fabrication of economical and sustainable artificial photosynthetic devices. These systems have multiple constraints, which are typically met by employing expensive, multi-junction solar cells coupled to noble-metal catalysts. However, to supply and store power on a global, terawatt scale, these technologies must shift towards utilizing abundant elements and low-cost deposition techniques, while maintaining device efficiency. Driven by these challenges, this thesis presents achievements in Si microwire arrays to realize cost-competitive and sustainable artificial photosynthetic devices.

The device performance of Si microwire arrays, a thin-film photovoltaic technology, was investigated using photoelectrochemical methods. Both n-type and lightly doped Si microwire arrays demonstrated improved performance as photoanodes, and may be used in an artificial photosynthetic device to perform oxidative reactions. In addition, lightly doped Si microwire arrays operating under high-level injection conditions achieved performance comparable to that of optimally doped p-type Si microwire array photocathodes, with V_{oc} values exceeding 450 mV and carrier-collection efficiencies of ~ 0.85. A model of these devices operating under high-level injection conditions was developed, using finite-element device physics simulations. These simulations predicted that the carrier-collection efficiencies of the devices should deviate from unity, even for minority-carrier diffusion lengths greater than the radius. Such behavior was confirmed by experimental internal quantum yield measurements, reaffirming that these devices are limited by axial transport of carriers along the length of the wire. However, optimized arrays have the potential to generate voltages that exceed those generated by arrays operating under low-level injection conditions. Such studies offer increased understanding of the performance of structured, concentrator photovoltaics and considerations for structuring lightly doped materials on the nano- and microscale.

TABLE OF CONTENTS

LIST OF FIGURES

1. Artificial Photosynthetic Devices

2. Si Microwire Array Photoanodes

3. Si Microwire Arrays Operating under High-Level Injection Conditions

4. Optimization of the Photoanodic Performance of Undoped Si Microwires

5. Angle–Resolved Spectral Response of n^+-i-Si Microwire Arrays

Appendix: Non-aqueous Dimethylferrocene Electrochemical Measurements

LIST OF TABLES

Chapter 1

ARTIFICIAL PHOTOSYNTHETIC DEVICES

The inability to store electricity is one of the most significant barriers to achieving the large-scale penetration of electricity generation from renewable resources, such as solar and wind power.[1] Such renewable energy sources vary substantially over time, making their generation difficult to forecast and subsequently integrate into the electric grid.[2] In particular, solar photovoltaic plants can experience variation in output on the timescale of seconds to minutes, with variations in output of ± 50% in a 30–90 second time frame and ± 70% in a five to ten minute time frame under partly cloudy conditions.[3] Wind power generation, while relatively more stable than generation from photovoltaic plants, is more difficult to forecast. Moreover, onshore wind power can be inversely correlated with demand, attaining peak generation during hours of limited demand at night.[4] In contrast, conventional energy sources, such as coal and nuclear, provide constant, reliable base-load power for the entire electricity grid,[4] while power from natural gas-fired and hydroelectric plants can be dispatched at high ramp rates to meet demand on the short time scales required.

Electricity generation from renewable energy resources is both uncertain and variable, allowing for limited control to maintain stable and reliable grid operation at high penetration. From these characteristics, its average contribution to electricity generation in

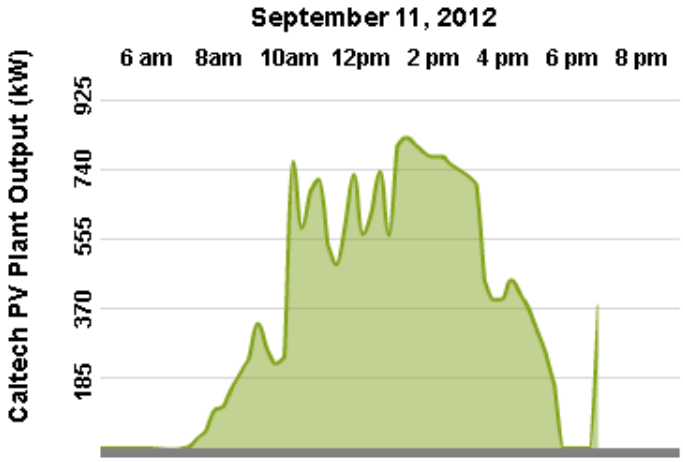

Figure 1.1. Power generation from Caltech's photovoltaic installations, on the day I wrote this introduction, September 11, 2012
Acquired from: *http://buildingdashboard.net/caltech/*

the U.S. will be approximately limited to 30%.[1, 5] To ultimately achieve large-scale penetration of renewable power in electricity generation, storage technologies are needed that are energy dense, cost-effective, and amenable to most locations. However, no current energy storage technology meets all of these three criteria.

Given these demands, directly collecting and storing solar energy in energy-dense chemical bonds, as nature accomplishes through photosynthesis, is a highly desirable approach.[6, 7] Photosynthetic organisms, however, are very inefficient at converting energy from photons into stored chemical energy, with a typical average yearly energy-conversion efficiency of $< 1\%$.[8] Given this low efficiency, plants compete for valuable and scarce resources, including arable land, fertilizer, and fresh water, making the large-scale storage of energy from sunlight through photosynthesis not currently viable.[9, 10] To improve upon this efficiency, inorganic solar cells, which typically achieve efficiencies of ~ 15–20%, and robust inorganic catalysts can be employed to create an artificial photosynthetic device, where solar energy can be directly converted to a chemical fuel (Figure 1.2). In its simplest

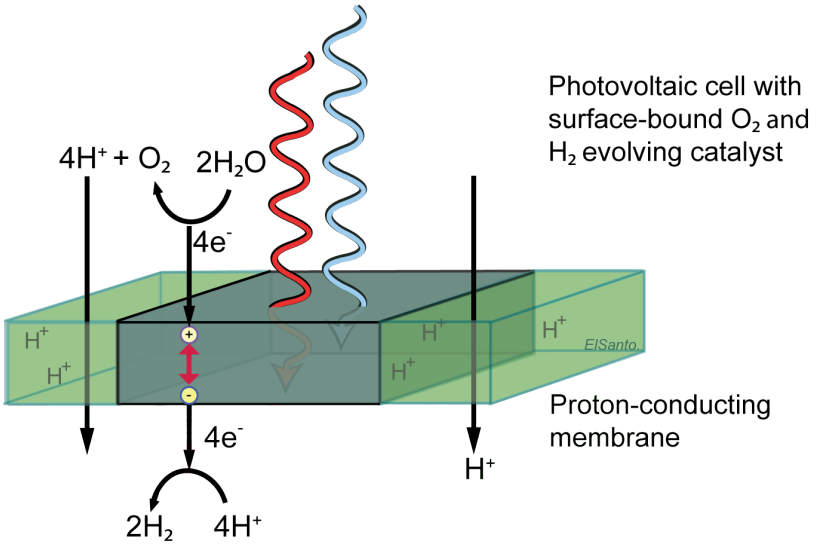

Figure 1.2. Schematic of a planar, artificial photosynthetic device. The device harnesses energy from the incident light to generate hydrogen fuel and oxygen. The photoexcited electrons and holes are separated, and are subsequently coupled with catalysts at the surface of the cell, generating H_2 and O_2 from H_2O.

design, the artificial photosynthetic device would reduce water (H_2O) to form hydrogen (H_2) fuel and oxygen (O_2), with sunlight providing the energy for the reaction, which under standard conditions is $\Delta G = 237.2$ kJ mol^{-1}, or $\Delta E° = 1.23$ V per electron transferred.

Wireless, artificial photosynthetic devices have gained solar to fuel efficiencies from over 2% to 18%, greatly improved over the energy-conversion efficiencies of photosynthetic organisms.[7, 11-15] However, these devices are fabricated with expensive, crystalline solar cells and/or noble-metal catalysts such as Pt and RuO_2, making these devices not viable for commercialization. To supply and store power on a global, terawatt scale, these technologies must shift towards utilizing abundant elements and low-cost deposition techniques, while maintaining device efficiency. Driven by these challenges, this thesis presents achievements in the fabrication and characterization of a structured semiconductor, Si microwires, to realize cost-competitive and sustainable artificial photosynthetic devices.

1.1 Structuring semiconductors for efficient artificial photosynthetic devices

The structuring of semiconductors on the nano- and microscale is a promising approach for the fabrication of scalable and efficient devices for the production of electricity and fuels from sunlight.[7, 16, 17] In contrast to a traditional geometry that is characterized by planar light absorbers and planar electrical junctions, wire-based architectures orthogonalize the directions of light absorption and carrier collection (Figure 1.3).[18] Such a structure provides both a long optical path length (α^{-1}) for efficient light absorption and a short distance for minority-carrier (L) collection, therefore allowing the incorporation of inexpensive, defective materials with short minority-carrier diffusion lengths into devices that can produce high energy-conversion efficiencies. For semiconductors with characteristically short diffusion lengths, including GaP, Fe_2O_3, and WO_3, improvements have been observed in the carrier-collection efficiency by structuring these semiconductors,[19-21] making this an important strategy for fabricating both an economical and efficient artificial photosynthetic device.

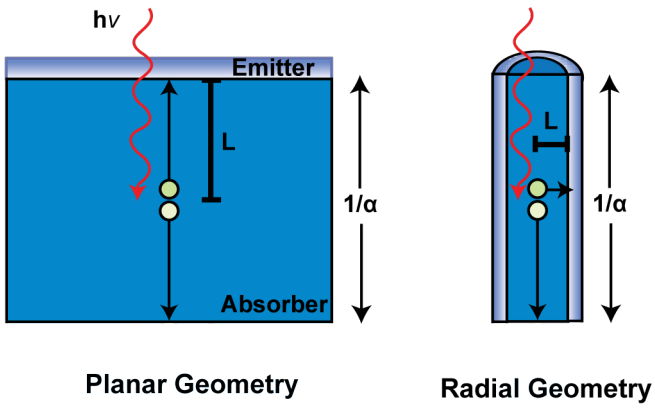

Figure 1.3. Schematic of a planar and a wire array solar cell. In a traditional planar device, the minority-carrier diffusion length *L* should comparable to the absorption length *1/α* for maximum efficiency. Using a radial geometry, the minority carrier is collected radially, while light can be absorbed along the length of the wire.

In addition to improving the carrier collection in low-quality, inexpensive semiconductor materials, structuring the semiconductor should allow for the use of lower loadings of the catalyst material or the use of an inexpensive catalyst that is less efficient. Currently, one of the main barriers to the efficient conversion of solar energy to hydrogen fuel is the significant energy loss associated with overcoming the kinetic barriers to performing the multi-step, multi-electron reactions for the generation of oxygen and hydrogen. The most efficient electrocatalysts are typically expensive, noble metals, such as RuO_2 and IrO_2, and Pt, for the oxygen and hydrogen evolution reaction, respectively. However, even the highest activity water oxidation catalyst RuO_2 requires an applied voltage in excess of the reversible potential for the reaction, or an overpotential, of $\eta \sim 400$ mV to achieve a current density J of ~ 1 A cm^{-2}, as a compact film with no geometric enhancement.[22] The catalyst's exchange current density J_o, or the forward reaction rate under dynamic equilibrium (i.e., at $\eta = 0.0$ V), is extremely low, on the order of $J_o \sim 1 \times 10^{-5}$ to 1×10^{-6} A cm^{-2}.[22] The best catalyst for the hydrogen evolution reaction, Pt metal, has been shown to require an η less than 100 mV to operate at a $J \sim 1$ A cm^{-2} in acidic conditions, with $J_o \sim 1 \times 10^{-2}$ to 1×10^{-3} A cm^{-2}.[23] Thus, to electrolyze water at current densities of 1 A cm^{-2}, an additional voltage of ~ 500 mV would be required, in addition to the thermodynamic requirement of 1.23 V per electron transferred. Even to operate at more reasonable current densities matched to the solar flux at ~ 10 mA cm^{-2}, an additional

potential exceeding 250 mV would be required.[24-26] The most active non-noble, earth-abundant metal catalysts have substantially lower activities, and, thus, high catalyst loadings are required to achieve substantial turnover frequencies.

However, by employing a structured semiconductor, the flux of photogenerated carriers to the surface, to perform the fuel–forming reactions, is distributed over a larger area. Thus, the electrocatalyst at the semiconductor surface will ultimately have to support a decreased carrier flux from this geometric enhancement, allowing for the use of catalysts with lower activity. By employing a structured semiconductor, earth-abundant catalysts with lower activities can achieve comparable performance, as has been previously demonstrated for a Ni-Mo alloy hydrogen evolution catalyst on Si microwires.[27]

Thus, structuring semiconductors allows for both the use of inexpensive semiconductors and catalysts in an artificial photosynthetic device. Such a device has been schematically depicted (Figure 1.4), with a dual–material system consisting of a separate

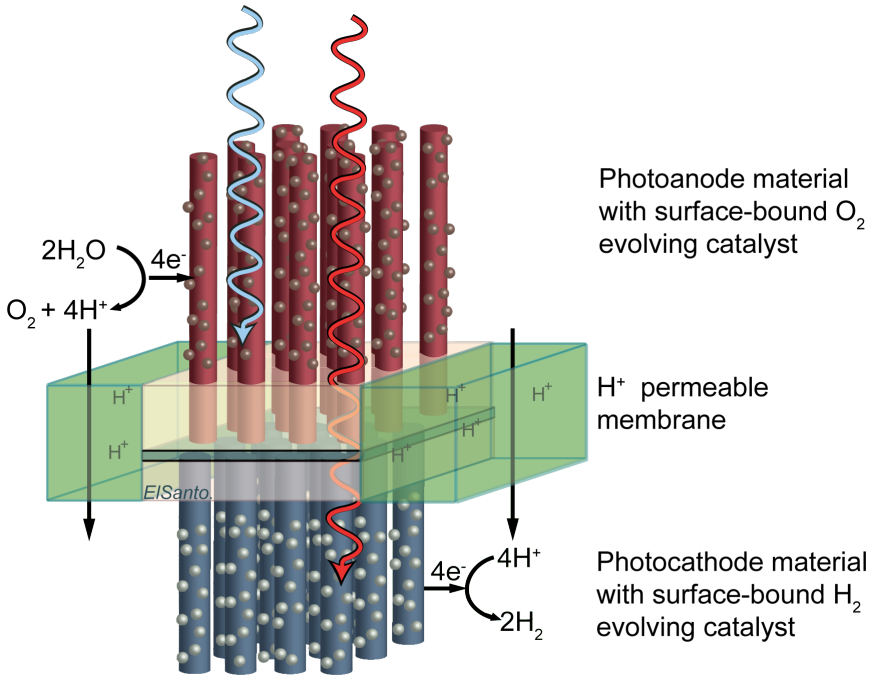

Figure 1.4. Schematic of a structured artificial photosynthetic device

photoanode and photocathode, to allow for the most efficient absorption of the solar spectrum and to generate the photovoltage required to split water; earth-abundant catalysts, such as those based on alloys of Ni, Co, and Mn; and an integrated proton or hydroxide conducting membrane, to manage the flux of these generated species while minimizing the *iR* drop in the device and simultaneously separating the generated O_2 and H_2 gases. Many variations on this basic device structure are possible, to optimize for light absorption and transport of reactants and products, in addition to allowing for the use of new materials systems.

1.2 Si microwires for scalable, efficient devices

1.2.1 Si microwire photocathodes

Recently, Si wire arrays grown by the vapor–liquid–solid (VLS) technique have emerged as a promising technology for the fabrication of efficient and potentially inexpensive artificial photosynthetic devices. Crystalline, planar Si decorated with Pt nanoparticles has been extensively studied as a photocathode material to reduce H_2O, demonstrating stable performance with photon to H_2 conversion efficiencies of ~ 6%.[28, 29] However, the growth of planar Si for efficient devices is both capital and energy intensive, requiring extremely pure Si and high temperatures for extended periods of time for the crystallization of Si, with large associated losses in material when forming the resulting wafers.[30] In contrast, the growth of Si wire arrays utilizes an atmospheric pressure, rapid chemical vapor deposition growth process; inexpensive Si precursors; and earth-abundant VLS catalysts. The resulting arrays of p-Si microwires have already demonstrated promising performance in regenerative[31, 32] and fuel–forming[33] photoelectrochemical cells, as well as in photovoltaic devices.[34, 35] In particular, arrays of radial junction n^+p-Si microwire photocathodes have demonstrated thermodynamically based photoelectrode energy-conversion efficiencies of > 5% for the production of H_2 from H_2O.[33]

1.2.2 Si microwire photoanodes

Even with the excellent demonstrated performance of n^+p-Si microwire photocathodes, an additional photovoltaic device or photoanode must be placed in series, to supply the additional voltage needed to split water at an appreciable current density. This photoanode must meet several criteria, including that this semiconductor must absorb in the visible spectrum, possess good material properties, and be stable under extremely oxidizing conditions. Currently, there is no ideal candidate for providing the other half of this structured artificial photosynthetic device; metal oxides typically possess wide-band gaps and poor mobilities, and smaller band gap materials, such as GaAs and Si, are unstable under anodic conditions and also unable to provide the additional voltage in excess of 1.0 V to split water. To begin fabricating wireless devices that utilize new structured materials, more thermodynamically and kinetically facile reactions than the splitting of water can be attempted, including HBr to H_2 and Br_2/Br_3^-, and HI to H_2 and I_2/I_3^-, which thermodynamically require $\Delta E°$ =1.05 V and $\Delta E°$ =0.536 per electron transferred, respectively.[36, 37] In these devices, Si microwires may be used as the photoanode (Figure 1.5), and both the operational challenges and fundamental properties of a dual-material,

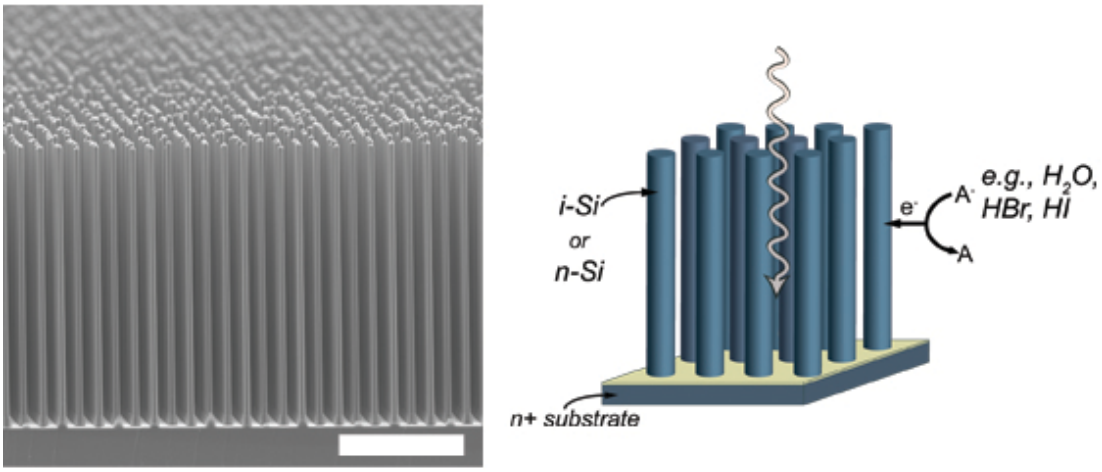

Figure 1.5. Scanning electron microscopy (SEM) image of undoped Si microwires, scale bar = 30 μm, with a schematic of the potential photoanodic, fuel-forming reactions that could be accomplished using undoped or n-Si microwire arrays

membrane-based, artificial photosynthetic device can begin to be explored.

Thus, this thesis presents achievements in improving the device performance of Si microwire arrays, which can be used as either a photoanode or photocathode in an artificial photosynthetic device. Arrays of n-Si microwires were fabricated and subsequently measured for their photoanodic performance using regenerative non-aqueous photoelectrochemistry, as presented in Chapter 2. The use of these non-aqueous redox systems allowed for a well–defined, conformal junction to the highly structured arrays. This electrochemical characterization obviates the need to fabricate a diffused metallurgical junction, and, thus, the material properties of the as-grown wires and incremental processing steps could be easily monitored.

Moreover, to potentially improve upon the device performance of Si microwire anodes and cathodes, undoped wires, as opposed to doped n-type or p-type microwires, can be utilized. As discussed in Chapter 3, lightly-doped microwires under the conditions of high-level injection have the potential to match or exceed the photovoltages produced by optimally doped Si microwires operating under low-level injection conditions. The device performance of the undoped Si microwire arrays was extensively probed using regenerative non-aqueous photoelectrochemistry, to gain understanding of the *J-E* performance, carrier-collection efficiency, and effect of processing on the behavior of these arrays. In addition, a device physics model of these devices operating under high-level injection conditions was developed, using finite-element device physics simulations. Such studies offer increased understanding of the performance of structured, concentrator photovoltaics and considerations for structuring lightly-doped materials on the nano- and microscale.

1.3 References

1. National Research Council, *Electricity from Renewable Resources: Status, Prospects, and Impediments*, The National Academies Press, Washington, D.C., 2010.
2. J. G. Kassakian and R. Schmalensee, co-chairs, *The Future of the Electric Grid: An Interdisciplinary MIT Study*, MIT Press, Cambridge, 2011.
3. North American Electric Reliability Corporation, *Accommodating High Levels of Variable Generation*, 2009, Available online at http://www.nerc.com/files/IVGTF_Report_041609.pdf, Accessed September 10, 2012.
4. MIT Energy Initiative Symposium, April 20, 2011, *Managing Large-scale Penetration of Intermittent Renewables*, Available online at http://web.mit.edu/mitei/research/energy-studies.html, Accessed March 17, 2012.
5. P. Denholm, in *Fundamentals of Materials for Energy and Environmental Sustainability*, eds. D. S. Ginley and D. Cahen, Cambridge University Press, New York, 2012.
6. N. S. Lewis and D. G. Nocera, *Proc. Natl. Acad. Sci. U.S.A.*, 2006, **103**, 15729-15735.
7. M. G. Walter, E. L. Warren, J. R. McKone, S. W. Boettcher, Q. X. Mi, E. A. Santori and N. S. Lewis, *Chem. Rev.*, 2010, **110**, 6446-6473.
8. JASON, *Engineering Microorganism for Energy Production*, JSR-05-300, 2006.
9. H. Michel, *Angew. Chem. Int. Ed.*, 2012, **51**, 2516-2518.
10. National Research Council, *Renewable Fuel Standard: Potential Economic and Environmental Effects of U.S. Biofuel Policy*, The National Academies Press, Washington, D.C., 2011.
11. S. Licht, B. Wang, S. Mukerji, T. Soga, M. Umeno and H. Tributsch, *J. Phys. Chem. B*, 2000, **104**, 8920-8924.
12. O. Khaselev, A. Bansal and J. A. Turner, *Int. J. Hydrogen Energy*, 2001, **26**, 127-132.

13. Y. Yamada, N. Matsuki, T. Ohmori, H. Mametsuka, M. Kondo, A. Matsuda and E. Suzuki, *Int. J. Hydrogen Energy*, 2003, **28**, 1167-1169.
14. S. Yamane, N. Kato, S. Kojima, A. Imanishi, S. Ogawa, N. Yoshida, S. Nonomura and Y. Nakato, *J. Phys. Chem. C*, 2009, **113**, 14575-14581.
15. S. Y. Reece, J. A. Hamel, K. Sung, T. D. Jarvi, A. J. Esswein, J. J. H. Pijpers and D. G. Nocera, *Science*, 2011, **334**, 645-648.
16. B. Tian, T. J. Kempa and C. M. Lieber, *Chem. Soc. Rev.*, 2009, **38**, 16-24.
17. A. I. Hochbaum and P. D. Yang, *Chem. Rev.*, 2010, **110**, 527-546.
18. B. M. Kayes, H. A. Atwater and N. S. Lewis, *J. Appl. Phys.*, 2005, **97**, 114302.
19. K. Hagedorn, S. Collins and S. Maldonado, *J. Electrochem. Soc.*, 2010, **157**, D588-D592.
20. K. Sivula, F. Le Formal and M. Grätzel, *ChemSusChem*, 2011, **4**, 432-449.
21. H. A. Atwater, J. M. Spurgeon and N. S. Lewis, *J. Phys. Chem. C*, 2008, **112**, 6186-6193.
22. S. Trasatti and G. Lodi, in *Electrodes of Conductive Metallic Oxides*, ed. S. Trasatti, Elsevier, Amsterdam, 1981, vol. B.
23. S. Trasatti, *J. Electroanal. Chem. Interfac.*, 1972, **39**, 163-184.
24. G. Lodi, E. Sivieri, A. Debattisti and S. Trasatti, *J. Appl. Electrochem.*, 1978, **8**, 135-143.
25. Y. Matsumoto and E. Sato, *Mater. Chem. Phys.*, 1986, **14**, 397-426.
26. J. O. Bockris, I. A. Ammar and A. K. M. S. Huq, *J. Phys. Chem.*, 1957, **61**, 879-886.
27. J. R. McKone, E. L. Warren, M. J. Bierman, S. W. Boettcher, B. S. Brunschwig, N. S. Lewis and H. B. Gray, *Energy Environ. Sci.*, 2011, **4**, 3573-3583.
28. R. N. Dominey, N. S. Lewis, J. A. Bruce, D. C. Bookbinder and M. S. Wrighton, *J. Am. Chem. Soc.*, 1982, **104**, 467-482.
29. Y. Nakato, H. Yano, S. Nishiura, T. Ueda and H. Tsubomura, *J. Electroanal. Chem.*, 1987, **228**, 97-108.
30. C. del Cañizo, G. del Coso and W. C. Sinke, *Prog. Photovolt: Res. Appl.*, 2009, **17**, 199-209.

31. S. W. Boettcher, J. M. Spurgeon, M. C. Putnam, E. L. Warren, D. B. Turner-Evans, M. D. Kelzenberg, J. R. Maiolo, H. A. Atwater and N. S. Lewis, *Science*, 2010, **327**, 185-187.

32. J. M. Spurgeon, S. W. Boettcher, M. D. Kelzenberg, B. S. Brunschwig, H. A. Atwater and N. S. Lewis, *Adv. Mater.*, 2010, **22**, 3277–3281.

33. S. W. Boettcher, E. L. Warren, M. C. Putnam, E. A. Santori, D. Turner-Evans, M. D. Kelzenberg, M. G. Walter, J. R. McKone, B. S. Brunschwig, H. A. Atwater and N. S. Lewis, *J. Am. Chem. Soc.*, 2011, **133**, 1216-1219.

34. C. E. Kendrick, H. P. Yoon, Y. A. Yuwen, G. D. Barber, H. T. Shen, T. E. Mallouk, E. C. Dickey, T. S. Mayer and J. M. Redwing, *Appl. Phys. Lett.*, 2010, **97**, 143108.

35. M. C. Putnam, S. W. Boettcher, M. D. Kelzenberg, D. B. Turner-Evans, J. M. Spurgeon, E. L. Warren, R. M. Briggs, N. S. Lewis and H. A. Atwater, *Energy Environ. Sci.*, 2010, **3**, 1037-1041.

36. M. Pourbaix, *Atlas of Electrochemical Equilibria in Aqueous Solutions*, Pergamon Press, New York, 1966.

37. A. J. Bard and L. R. Faulkner, *Electrochemical Methods: Fundamentals and Applications*, John Wiley & Sons, Hoboken, 2011.

C h a p t e r 2

SI MICROWIRE ARRAY PHOTOANODES

Components of this chapter were published in

E. A. Santori, J. R. Maiolo III, M. J. Bierman, N. C. Strandwitz, M. D. Kelzenberg, B. S. Brunschwig, H. A. Atwater, and N. S. Lewis, *Energy Environ. Sci.*, 2012, **5**, 6867-6871.

Summary

Arrays of n-Si microwires have to date exhibited low efficiencies when measured as photoanodes in contact with a 1-1'-dimethylferrocene ($Me_2Fc^{+/0}$)–CH_3OH solution. Using high-purity Au or Cu catalysts, arrays of crystalline Si microwires were grown by a vapor–liquid–solid process without dopants, which produced wires with electronically active dopant concentrations of 1 x 10^{13} cm^{-3}. When measured as photoanodes in contact with a $Me_2Fc^{+/0}$–CH_3OH solution, the lightly doped Si microwire arrays exhibited greatly increased fill factors and efficiencies as compared to n-Si microwires grown previously with a lower purity Au catalyst. In particular, the Cu–catalyzed Si microwire array photoanodes exhibited open-circuit voltages of ~ 0.44 V and an energy-conversion efficiency of 1.4% under simulated air mass 1.5 G illumination.

Arrays of n-Si microwires were also obtained using PH_3 as an in situ dopant source, allowing for the growth of microwires with electronically active dopant concentrations of 1 x 10^{15} – 1 x 10^{18} cm^{-3}. However, when measured contact with $Me_2Fc^{+/0}$–CH_3OH, the n-Si microwire arrays displayed poor fill factors and demonstrated little variation in photoresponse with changes in measured dopant density. Subsequent oxidation of the n-type microwire arrays improved their electrochemical performance, resulting in open-circuit voltages of exceeding 0.40 V and fill factors of ~ 0.5. Thus, both lightly doped Cu–catalyzed Si microwire array photoanodes and n-Si microwire arrays have demonstrated performance that is comparable to that of optimally doped p-type Si microwire array photocathodes in photoelectrochemical cells.

2.1 Introduction and motivation

Arrays of crystalline p-Si microwires grown by the vapor–liquid–solid (VLS) process have demonstrated promising performance in regenerative[1-3] and fuel–forming[4] photoelectrochemical cells, as well as in photovoltaic devices.[5, 6] For example, p-type Si microwire array photoelectrodes in contact with an aqueous methyl viologen ($MV^{2+/+}$) redox system have yielded open-circuit voltages (V_{oc}) approaching 0.45 V under 100 mW cm^{-2} of simulated air mass (AM) 1.5 G illumination, with near-unity internal quantum yields, demonstrating the efficient radial collection of carriers in the wire-array geometry. Arrays of radial junction n^+p-Si microwires have demonstrated thermodynamically based photoelectrode energy-conversion efficiencies of > 5% for the production of H_2 from H_2O. Analogous arrays in solid-state photovoltaic devices have achieved an efficiency of 7.8%, with V_{oc} values exceeding 0.5 V, under simulated AM 1.5 G illumination.

In contrast, initial experiments of n-Si microwire array photoanodes in contact with a 1-1'-dimethylferrocene ($Me_2Fc^{+/0}$)–CH_3OH solution under simulated AM 1.5 conditions only exhibited V_{oc} values of 0.39 V, in conjunction with low fill factors and low short-circuit photocurrent densities (J_{sc}), resulting in photoelectrode efficiencies, η, of ~ 0.1%.[7] Given that the $Me_2Fc^{+/0}$–CH_3OH electrolyte in contact with planar, crystalline n-Si photoanodes produces V_{oc} values that are only limited by bulk recombination/generation,[8] the comparatively low performance of n-Si microwire array photoanodes is presumably indicative of the inferior material quality of the n-Si microwires.

Two factors may have contributed to the poor electronic quality of the VLS–grown n-Si microwires: the purity of the catalyst used and the choice of metal catalyst. The n-Si microwire arrays were grown with a 99.999% (5N) Au VLS catalyst,[7, 9-11] as compared to the higher purity 99.9999% (6N) Cu catalyst that has been used to grow p-Si microwires.[1, 2, 4, 6, 12-14] Although the measured n-Si microwire array photoanodes possessed an electronically active dopant density, N_D, of 2.5×10^{16} cm^{-3}, four-point resistance measurements of several arrays of 5N Au–catalyzed microwires revealed that the wires had high variability in the observed N_D, with values ranging $1 \times 10^{14} - 1 \times 10^{20}$ cm^{-3}.[13] This doping cannot be attributed to the Au itself, which has been shown to actually

compensate n-type dopants in Si.[15] Uncontrolled impurities in the lower purity 5N catalyst may have resulted in the variable n-type doping of the as-grown Si microwires, and the cross-contamination of several metals that were formerly used in the reactor including Al, Mg, In, Zn, and 4N purity VLS catalysts could have also been the source of the unintentional doping. Additionally, the use of Au as the VLS catalyst, as opposed to Cu, may have limited the efficiency of the Si microwire arrays. Although both Au and Cu form mid-gap traps in Si, in planar Si solar cells Cu has a less detrimental effect than Au, with a minority-carrier lifetime degradation threshold concentration of 4 x 10^{17} cm^{-3} for Cu as compared to 3 x 10^{13} cm^{-3} for Au.[16, 17]

The focus of this work was to determine whether the low photoelectrode efficiencies observed for n-Si microwire arrays in contact with $Me_2Fc^{+/0}$–CH_3OH are an inherent, fundamental property of the system or whether improved performance could be obtained through control over the electronic properties of the bulk and surface properties of Si wire array photoelectrodes. We report herein the photoelectrochemical behavior of Si microwire arrays that have been fabricated using a 6N VLS catalyst, for both Au and Cu. Si microwire arrays were grown both with and without an in situ dopant source, to produce both relatively undoped Si wires, and intentionally doped n-Si wires. The device performance of the Si microwire arrays was subsequently probed using the $Me_2Fc^{+/0}$–CH_3OH junction. This system provides a conformal contact to the microwires, and obviates the need to fabricate a diffused metallurgical junction. Additionally, the Si/$Me_2Fc^{+/0}$–CH_3OH interface has been previously shown to have a low effective surface recombination velocity and to produce high V_{oc} values that are only limited by the bulk properties of the Si.[18] Thus, though these photoelectrochemical measurements, the highly structured Si microwire arrays can be easily contacted with a well–defined redox system, which should result in a photoresponse that is indicative of the material properties of the Si microwire arrays.

2.2 Growth and characterization of 6N Au–catalyzed Si microwire arrays

To produce the desired photoanodes, arrays of square–packed Si microwires were grown on a planar n^+-Si(111) substrate using the VLS process, without dopants, but with 6N Au as the growth catalyst. The resulting Si wires were oriented in the (111) direction, with diameters of 2.25–3.0 μm and heights of 65–75 μm, with an average areal packing fraction (η_f) of 11.0% (Figure 2.1 and Figure 2.2).

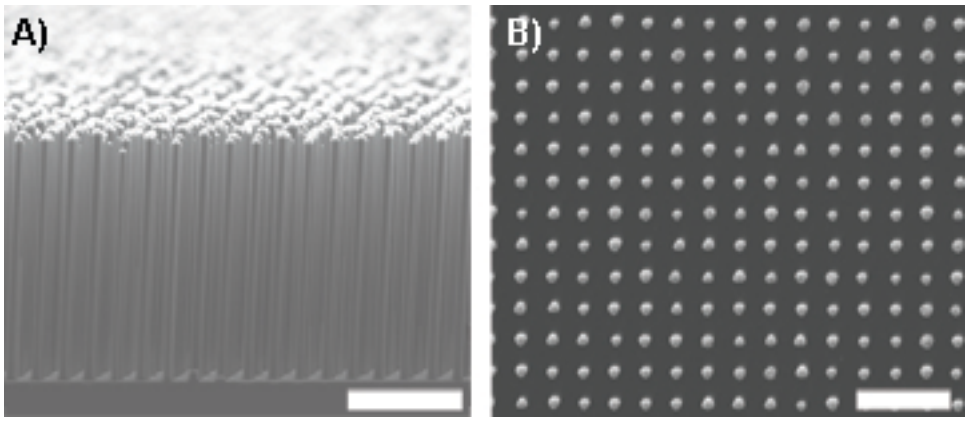

Figure 2.1. A) Side view SEM image of a cleaved array of Au–catalyzed Si microwires, scale bar = 30 μm. B) Top view of the same Si microwire array, scale bar = 20 μm

Four-point resistance and gate-dependent conductance measurements indicated that the undoped silicon microwires were nominally p-type, with consistent resistivities of ~ 1000 Ω-cm, corresponding to an acceptor concentration, N_a, of ~1 x 10^{13} cm^{-3} (Figure 2.3). Moreover, several different wire arrays were sampled to measure the variability in wire dopant density among growths, and, for each growth, at least ten wires were measured. The measured resistivities of wires from three different arrays were 1400 ± 900 Ω-cm, 800 ± 700 Ω-cm, and 600 ± 300 Ω-cm, demonstrating increased control of the impurity concentration in the Si microwires.

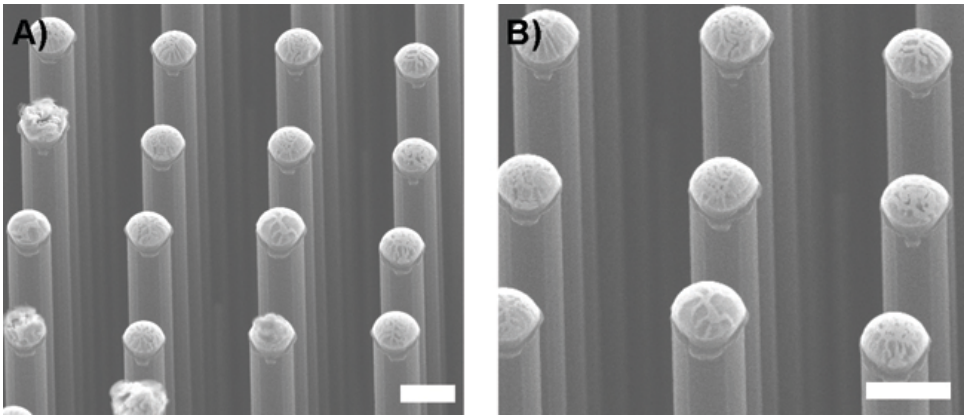

Figure 2.2. SEM images with an angled view of a Au–catalyzed Si microwire array prior to catalyst removal, scale bar = 3 μm. A) and B) are images of the same wire array, with increased magnification in B).

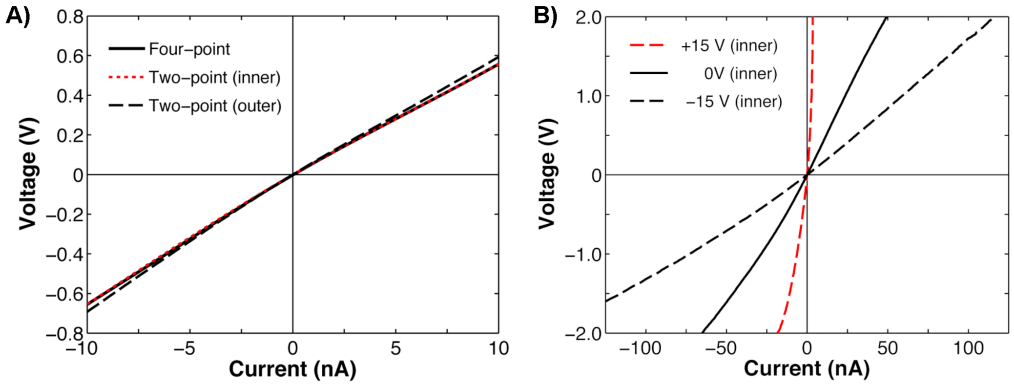

Figure 2.3. A) Two-point and four-point *I-V* characteristics of a representative undoped Au–catalyzed Si microwire. B) *I-V* behavior of a Au–catalyzed Si microwire, with varying back-gate bias, indicating p-type microwires

2.3 Photoanodic response of 6N Au–catalyzed Si microwire arrays

Current density vs. potential (*J-E*) measurements of Au–catalyzed Si microwire array photoanodes, and of control photoanodes in which the wires had been physically removed after growth on the n^+-Si substrate, were measured in contact with 200 mM Me_2Fc-0.4 mM Me_2FcBF_4 in CH_3OH under 100 mW cm^{-2} of simulated AM 1.5 G illumination (Figure 2.4). The simulated AM 1.5 G illumination was produced by a 150 W

Xe lamp, coupled to an AM 1.5 G filter (see Appendix A for experimental details). The Si wire array photoanodes exhibited V_{oc} = 334 ± 21 mV, J_{sc} = 10.0 ± 1.3 mA cm^{-2}, and fill factors, ff = 0.34 ± 0.05, with a photoelectrode energy-conversion efficiency η = 1.1 ± 0.3%. The n^{+}-Si(111) control substrates for which the wires had been physically removed after growth produced V_{oc} = 233 ± 38 mV, J_{sc} = 1.0 ± 0.2 mA cm^{-2}, and ff = 0.20 ± 0.04. The observed properties of the Si microwire array photoelectrodes can therefore predominately be attributed to the behavior of the VLS–grown crystalline Si wires in contact with the $Me_2Fc^{+/0}$–CH_3OH electrolyte.

In the previously published electrochemical experiments with 5N Au–catalyzed wire arrays, the control photoelectrodes consisted of the patterned, oxidized wafers, without deposited Au or subsequent wire growth. This control should result in an overestimation of the contributing photoresponse of the growth substrate, since the substrate will not have any lifetime degradation resulting from saturation with the VLS catalyst during the growth process. However, since the degenerate growth wafer is in direct contact with solution, which is not the case for Si microwire arrays with an existing oxide buffer, this control may actually overestimate the contribution of the growth

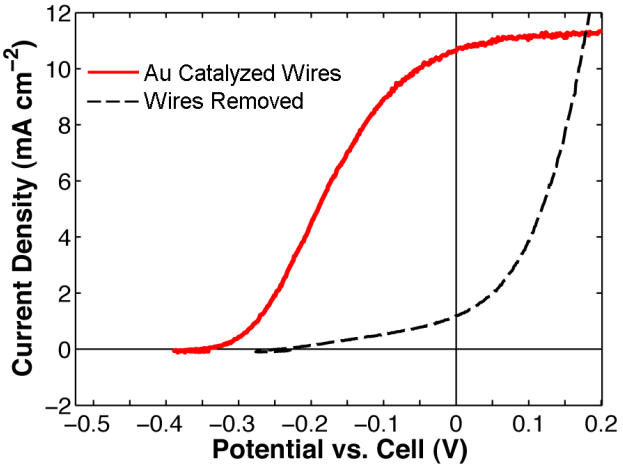

Figure 2.4. *J-E* data for Au–catalyzed Si microwire array photoelectrodes in contact with the $Me_2Fc^{+/0}$–CH_3OH redox system under 100 mW cm^{-2} of simulated AM 1.5 G illumination

substrate in the photoresponse of the Si microwire arrays. In contrast, mechanically removing the wires from the substrate allows for the measurement of the photoresponse of the exact, contributing substrate after the measurement of the wires for their photoelectrochemical behavior. By employing non-abrasive mechanical force to the array, the wires were removed at the base, potentially leaving some Si growth on the substrate within the patterned holes which does not then expose the degenerate Si of the growth substrate.

The behavior of the same Au–catalyzed Si microwire photoanodes was also measured in contact with a higher concentration of the oxidized form of the redox couple, 25 mM Me_2FcBF_4, to reduce the concentration overpotential losses at the photoelectrode. The photoelectrodes were illuminated using an 808 nm laser diode, such that the J_{sc} value matched the value of J_{sc} that was obtained at low Me_2Fc^+ concentrations under 100 mW cm^{-2} of simulated AM 1.5 G illumination. Figure 2.5 shows the performance of the arrays in the presence of either 0.4 or 25 mM Me_2FcBF_4, with the latter cell exhibiting a fill factor of $ff_{808} = 0.47 \pm 0.04$ and an efficiency $\eta_{808} = 2.7 \pm 0.7\%$. After correcting both the 0.4 and

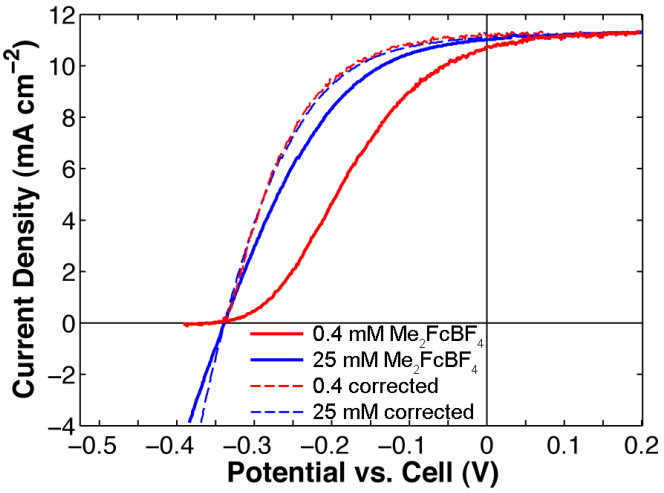

Figure 2.5. *J-E* data for Au–catalyzed Si microwire array photoelectrodes in contact with the $Me_2Fc^{+/0}$–CH_3OH redox system with varying amounts of Me_2FcBF_4, to demonstrate and correct for resistance losses in the cell. The *J-E* behavior was measured under both 100 mW cm^{-2} of simulated AM 1.5 G illumination and under 808 nm illumination, with 0.4 and 25 mM of Me_2FcBF_4, respectively.

25 mM Me_2FcBF_4 *J-E* data for concentration overpotential and uncompensated resistance losses, the corrected fill factor and photoelectrode efficiency values were $ff_{corr} = 0.57 \pm 0.05$ and $\eta_{corr} = 2.0 \pm 0.5\%$, respectively. The corrected *J-E* data are indicative of the inherent performance of the Si microwire arrays, without experimental artifacts arising from measurement in an unoptimized electrochemical cell configuration.

The photoelectrode efficiency of Si microwire arrays that were grown using the 6N–purity Au VLS catalyst represents a significant improvement relative to initial measurements of photoanodic performance of n-Si microwire arrays in contact with the $Me_2Fc^{+/0}$–CH_3OH system. However, the V_{oc} of the Si microwire arrays grown with Au was still substantially less than the V_{oc} values produced by either p-type or n^+p-Si microwire array photocathodes that were grown with Cu and tested in contact with the $MV^{2+/+}$(aq) redox system. For Si microwires grown with a Au VLS catalyst, bulk Au concentrations up to 1.7×10^{16} cm^{-3} have been previously measured, corresponding to the thermodynamic equilibrium concentration of Au in Si at the growth temperature.[11] The concentration of Au within the wires thus greatly exceeded the degradation threshold concentration of Au in planar Si solar cells, and could have contributed to the lower V_{oc} values that were measured for wires that were grown with a Au catalyst. Indeed, Si microwire arrays that were grown by a Au–catalyzed VLS process have previously shown V_{oc} values up to 500 mV in photovoltaic device structures, but only after repeated thermal oxidation and etching steps that should getter Au at the surfaces of the Si wires.[5] Given the low tolerance for Au in Si solar cells and the relative cost and scarcity of Au, Cu was subsequently used exclusively for the VLS growth of Si microwire arrays, and no attempts were made to getter the Au to improve an array's device performance.

2.4 Growth and characterization of 6N Cu–catalyzed Si microwire arrays

Thus, 6N Cu was subsequently used for VLS–catalyzed Si wire growth. Cu catalyzed, hexagonally–packed Si microwire arrays were fabricated on an n^+ substrate without dopants. The resulting wires were 2.0–2.5 μm in diameter and 70–80 μm in height, providing an average areal packing fraction (η_f) of 9.4% (Figure 2.6 and 2.7).

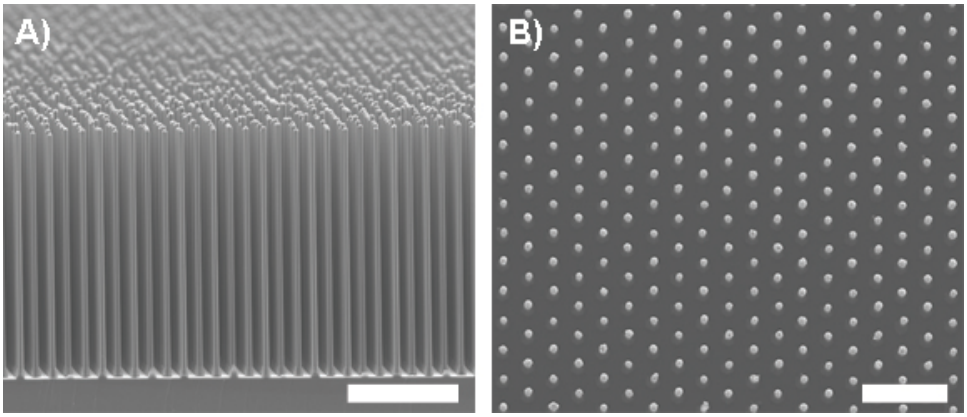

Figure 2.6. A) Side view SEM image of a cleaved array of Cu–catalyzed Si microwires, scale bar = 40 μm. B) Top view of a Si microwire hexagonal array, scale bar = 20 μm

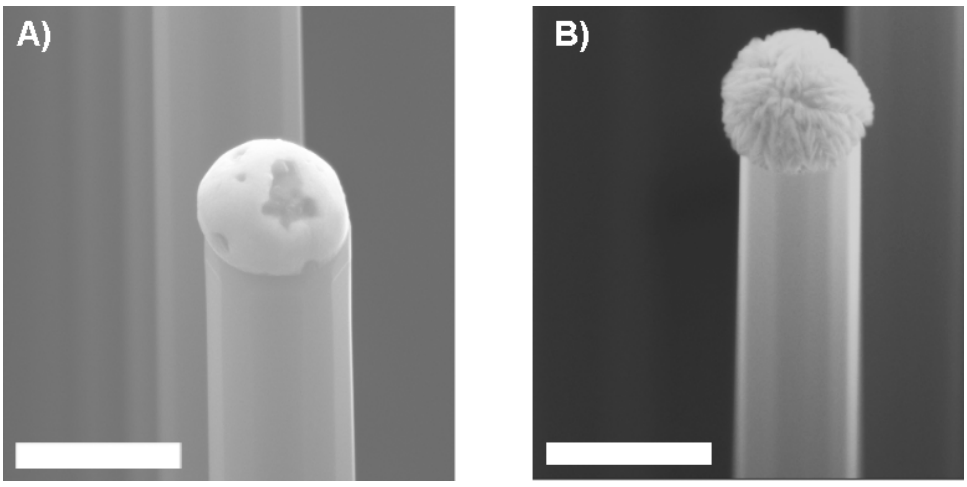

Figure 2.7. SEM images with an angled view of a Cu–catalyzed Si microwire array prior to catalyst removal for a A) quickly cooled array and B) a slowly cooled array. Scale bar = 2 μm.

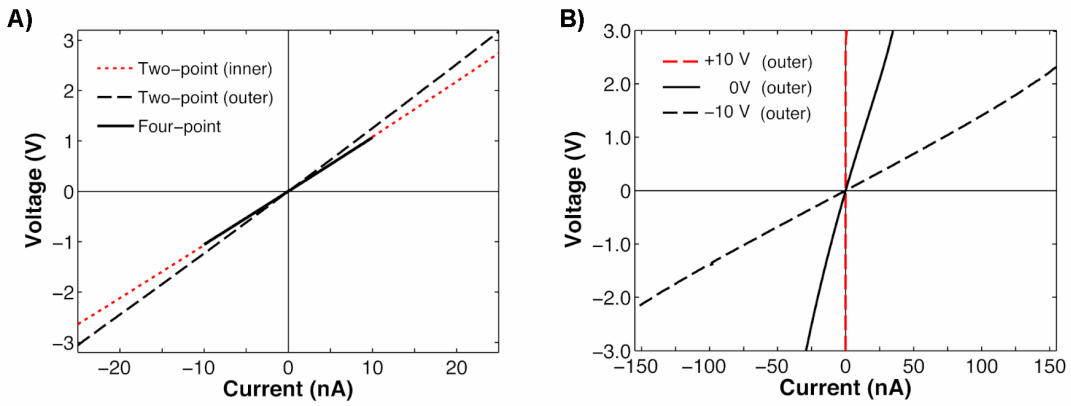

Figure 2.8. A) Two-point and four-point *I-V* characteristics of a representative undoped Cu–catalyzed Si microwire. B) *I-V* behavior of a Cu–catalyzed Si microwire, with varying back-gate bias, indicating p-type doping

Similar to the Au–catalyzed wires, the Cu–catalyzed wires were slightly p-type, with resistivities of ~ 1000 Ω-cm, as measured by four-point resistance measurements, corresponding to N_a of ~ 1 x 10^{13} cm^{-3} (Figure 2.8). To measure the variability in wire dopant density among growths, the resistivities of several different wire arrays from different growths were measured, and, for each growth, at least ten wires were measured. The measured resistivities of wires from three different arrays were 310 ± 70 Ω-cm, 1000 ± 600 Ω-cm, and 600 ± 400 Ω-cm. Even though these wire arrays were grown in a different, new reactor (Dorothy), the Cu–catalyzed wires possessed similar resistivities to the previous Au–catalyzed microwires. This consistency attests to the minimal contamination of the Watson reactor (Big Blue), after more vigorous procedures were implemented to separate evaporation boats, growth tubes, and growth boats for different metal catalysts, as well as no longer employing lower purity catalysts (3N, 4N, 5N) for VLS growth.

2.5 Photoanodic response of 6N Cu–catalyzed Si microwire arrays

J-E measurements of the Cu–catalyzed Si microwire arrays in contact with the $Me_2Fc^{+/0}$–CH_3OH electrolyte under 100 mW cm^{-2} of simulated AM 1.5 G illumination (Figure 2.9) showed V_{oc} = 437 ± 8 mV, J_{sc} = 7.9 ± 0.5 mA cm^{-2}, and *ff* = 0.40 ± 0.02, with a photoelectrode efficiency of η = 1.4 ± 0.1%. The Cu–catalyzed Si microwire array photoanodes measured herein exhibited a slightly smaller J_{sc} than the Au–catalyzed Si microwire array photoanodes, consistent with the Cu–catalyzed wire arrays possessing a smaller areal packing fraction than the Au–catalyzed wire arrays. The n^+-Si(111) control substrates with the wires physically removed produced V_{oc} = 262 ± 17 mV, J_{sc} = 1.3 ± 0.3 mA cm^{-2}, and *ff* = 0.21 ± 0.01, again demonstrating that the wafer substrate did not contribute substantially to the photoresponse of Si microwire photoelectrodes.

The same photoelectrodes were also measured under 100 mW cm^{-2} of ELH-type W halogen illumination. When illuminated with this different illumination source, which has a warmer spectrum than the AM 1.5 G spectrum, the photoelectrodes produced J_{sc} values that were ~ 10–15% higher than under AM 1.5 G illumination, with J_{sc} = 9.2 ± 1.0 mA cm^{-2} (Figure 2.10). This increase in current was consistent with previous measurements on n^+p-Si microwires, which showed a 15% increase in J_{sc} under ELH-type W illumination.[4]

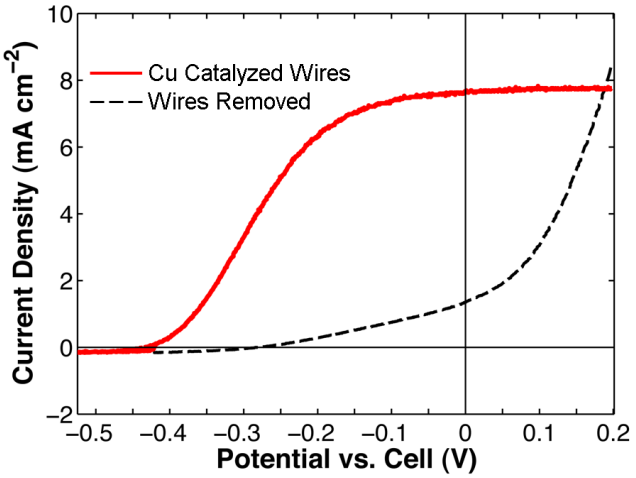

Figure 2.9. *J-E* data for Cu–catalyzed Si microwire array photoelectrodes in contact with the $Me_2Fc^{+/0}$–CH_3OH redox system under 100 mW cm^{-2} of simulated AM 1.5 G illumination

The difference between the photoresponse of the microwire arrays under these two illumination sources should vary strongly with angle, and the difference should diminish when the wires are measured at normal incidence, where the spectral response is more uniform across the visible spectrum.[19]

The Cu–catalyzed Si microwire array photoanodes measured under 808 nm illumination in contact with 25 mM Me_2FcBF_4, to reduce concentration overpotential losses, exhibited a fill factor of $ff_{808} = 0.60 \pm 0.02$ and an efficiency of $\eta_{808} = 3.4 \pm 0.2\%$ (Figure 2.11). After correcting for concentration overpotential and uncompensated resistance losses, the corrected fill factor and efficiency were $ff_{corr} = 0.61 \pm 0.04$ and $\eta_{corr} = 2.1 \pm 0.1\%$, respectively, for Si microwire photoanodes measured under AM 1.5 G

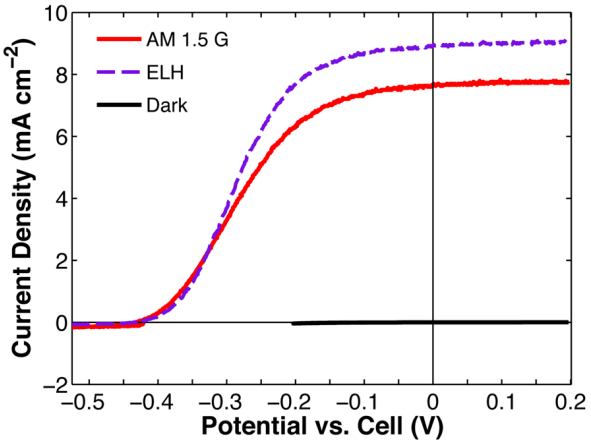

Figure 2.10. *J-E* data for the same Cu–catalyzed Si microwire array photoelectrode in contact with the $Me_2Fc^{+/0}$–CH_3OH redox system under 100 mW cm^{-2} of simulated AM 1.5 G illumination and under 100 mW cm^{-2} of ELH-type W halogen illumination

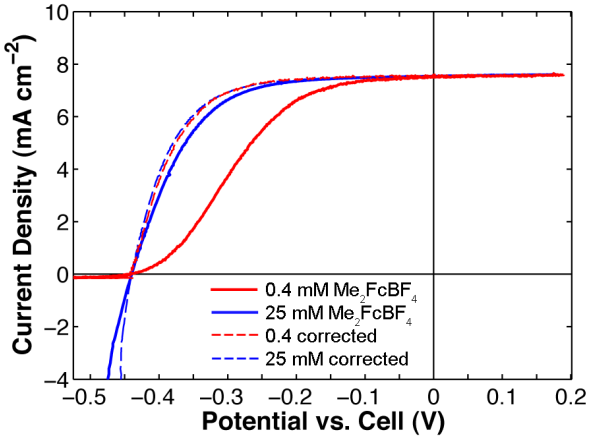

Figure 2.11. *J-E* data for Cu–catalyzed Si microwire array photoelectrodes with varying amounts of Me_2FcBF_4 in the cell, to demonstrate and correct for resistance losses in the cell. The *J-E* behavior was measured under both 100 mW cm^{-2} of simulated AM 1.5 G illumination and under 808 nm illumination, with 0.4 and 25 mM of Me_2FcBF_4, respectively.

illumination. Thus, the undoped Cu–catalyzed Si wire array photoanodes in contact with $Me_2Fc^{+/0}$–CH_3OH not only exhibited improved performance relative to the initial n-Si wire array measurements, but also yielded efficiencies that were very similar to those observed for optimally doped p-Si wire arrays photocathodes in contact with $MV^{2+/+}$(aq) (Table 2.1).[1, 2]

Table 2.1 Figures of merit of Si microwire array cells

	V_{oc} (mV)	J_{sc} (mA cm^{-2})	*ff*	Efficiency (%)
Au–Catalyzed (AM 1.5 G)	334 ± 21	10.0 ± 1.3	0.34 ± 0.05	1.1 ± 0.3
Au–Catalyzed (808 nm)	332 ± 18	10.2 ± 1.2	0.47 ± 0.04	2.7 ± 0.7
Corrected Au	334 ± 21	10.4 ± 1.4	0.57 ± 0.05	2.0 ± 0.5
Au Wires Removed	223 ± 38	1.0 ± 0.2	0.20 ± 0.04	0.04 ± 0.01
Cu–Catalyzed (AM 1.5 G)	437 ± 8	7.9 ± 0.6	0.40 ± 0.02	1.4 ± 0.1
Cu–Catalyzed (808 nm)	435 ± 10	7.8 ± 0.4	0.60 ± 0.02	3.4 ± 0.2
Corrected Cu	437 ± 8	8.0 ± 0.7	0.61 ± 0.04	2.1 ± 0.1
Wires Removed	274 ± 1	1.4 ± 0.1	0.22 ± 0.002	0.08 ± 0.006
Previous Result, 5N Au [7]	389 ± 18	1.43 ± 0.14	0.16 ± 0.02	0.09 ± 0.01
p-Si Microwires / $MV^{2+/+}$ (808 nm) [1]	410 ± 40	7.7 ± 0.9	0.50 ± 0.10	2.6 ± 0.4

2.6 Growth and characterization of n-Si microwire arrays using in situ PH_3

With enhanced control over the material properties of undoped wires grown with a high-purity Cu catalyst, intentionally doped n-Si microwires were subsequently fabricated using a 6N Cu growth catalyst and PH_3 introduced in situ during the VLS growth. A PH_3 source (100 ppm in H_2, Matteson) was added to the Dorothy reactor, with the capability to flow in two different regimes using two mass flow controllers (MFC) with maximum flow rates of 2 and 20 sccm. Initial calibration of the PH_3 flow rate using the 20 sccm MFC showed that electronically active doping concentrations N_D of 1 x 10^{15} – 1 x 10^{18} cm^{-3} could be attained using this MFC (Figure 2.12). Using a flow rate of 1 sccm, microwires with an N_D of ~ 5 x 10^{17} cm^{-3} were produced, which should be a near optimal carrier concentration for the Si microwires. Given that the accuracy of the MFCs

are ±1% or ±0.2 sccm for a 20 sccm MFC, a second MFC with a flow rate of 2 sccm was added to the reactor, to increase control over the possible doping levels below an N_D of 1 x 10^{17} cm^{-3}. Using this MFC, carrier concentrations of 1 x 10^{16} cm^{-3} could be attained, opening up the possibility of conducting experiments on the dependence of the *J-E* behavior, particularly variation of the photoelectrodes' V_{oc} values, on the N_D of the microwire arrays.

Within the calibration of the PH_3 dopant source, it should be noted that the effective carrier concentration measured at a flow rate of 0 sccm varied from ~ 5 x 10^{14} – 1 x 10^{15} cm^{-3}. These values were significantly higher than the N_a values typically measured for undoped Si microwires as grown in both Dorothy and Big Blue. For resistivity measurements conducted using the 20 sccm MFC, the growths at 0 sccm produced lower fidelity arrays than would typically be measured for both resistivity and *J-E* measurements, and these arrays may have possessed markedly different electronic properties from high-fidelity arrays. In addition, the number of the growth run for each array was not closely tracked and may be significant, with variable contamination arising from the quartz tube or the reactor itself.

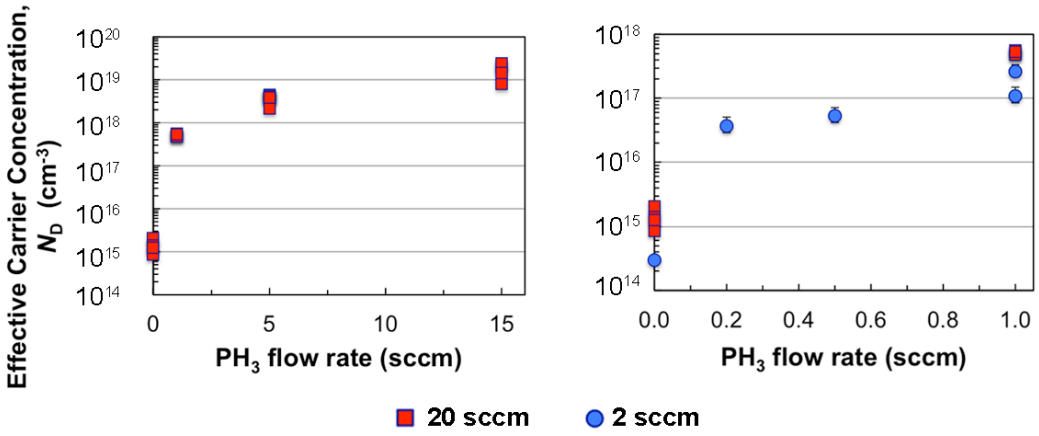

Figure 2.12. Calibration of the resulting effective carrier concentration of Si microwires with the flow rate of the PH_3 dopant source, using a 20 sccm mass flow controller (red squares) and with a 2 sccm mass flow controller (blue dots). *Calibration of PH_3 by Shane Ardo and Elizabeth Santori.*

2.7 *J-E* response of n-Si microwire arrays

Initial measurements of the photoresponse of the PH_3 doped Si microwire arrays were made on arrays grown with a PH_3 flow rate of 1 sccm. From single-wire measurements, the microwires from these electrodes possessed an N_D of ~ 5.0 x 10^{17} cm^{-3}, a near optimal carrier concentration for the base material (Figure 2.13B). When measured in contact with the $Me_2Fc^{+/0}$–CH_3OH redox system, the n-Si microwire array photoelectrodes produced V_{oc} = 487 ± 12 mV, J_{sc} = 13.2 ± 1.2 mA cm^{-2}, and *ff* = 0.16 ± 0.01 under 100 mW cm^{-2} of simulated 1 Sun's (ELH-type) illumination (Figure 2.13A). The photoelectrodes exhibited *J-E* behavior consistent with the expected behavior of a degenerate semiconductor, with low *ff* values, large V_{oc} values, and large dark current in reverse bias.

Thus, to further investigate the relationship between the measured effective carrier concentration in the wires and their *J-E* performance, and to potentially optimize the performance of the n-Si microwire arrays, wire arrays were subsequently grown at several PH_3 flow rates, ranging from 0.10–0.40 sccm. The *J-E* behavior of representative n-Si photoelectrodes in contact with $Me_2Fc^{+/0}$–CH_3OH is shown in Figure 2.14. The electrodes' photoresponse, particularly their *ff*, varied little with the PH_3 flow rate used during growth,

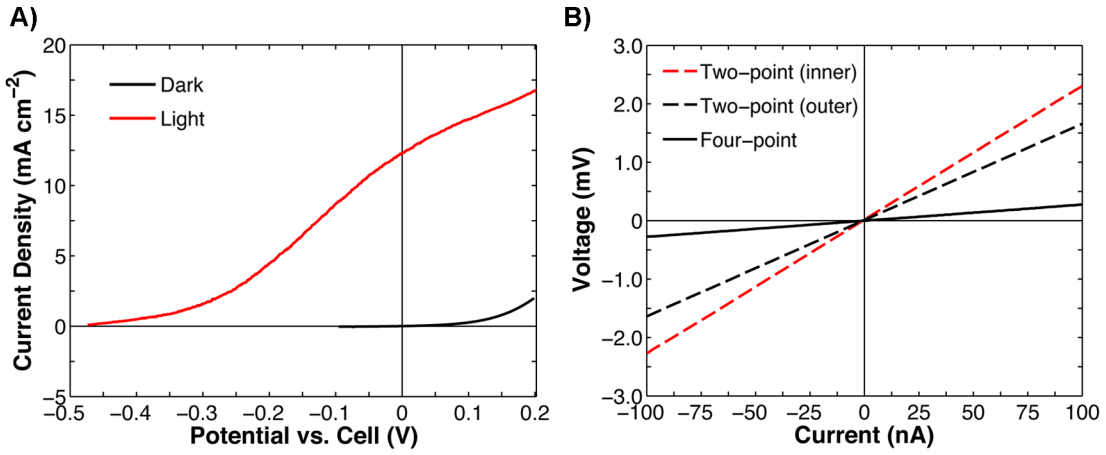

Figure 2.13. A) Representative *J-E* performance of n-Si photoelectrodes in contact with $Me_2Fc^{+/0}$–CH_3OH under 1 Sun's ELH-type illumination. B) Corresponding *I-V* characteristics of wires from the array grown at a 1 sccm PH_3 flow rate, with wires possessing a N_D of ~ 5.0 x 10^{17} cm^{-3}

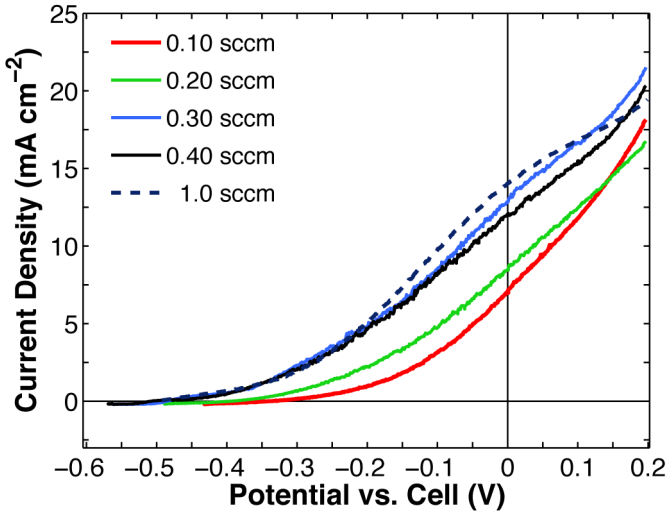

Figure 2.14. *J-E* behavior of electrodes of n-Si microwire arrays, grown with varying flow rates of PH_3, measured in contact with $Me_2Fc^{+/0}$–CH_3OH under 1 Sun's ELH-type illumination

with *ff* ~ 0.16 ± 0.02 across all electrodes measured. The V_{oc} of the photoelectrodes increased with increasing N_D, with V_{oc} values increasing from 330 mV to 470 mV, with corresponding N_D of ~ 1 x 10^{15} (0.1 sccm PH_3) to 5 x 10^{15} cm^{-3} (0.4 sccm PH_3), respectively. Chemical etching of the arrays with KOH(aq) to remove the near-surface region of the wires (~ 50 nm radially) generally increased the measured V_{oc}, but did not result in an improvement of the *ff* of the photoelectrodes. The degenerate behavior of the n-Si microwire arrays, regardless of measured N_D, suggested that an inhomogeneous doping profile existed in the wires, either radially or axially, with P-enriched surfaces potentially located along the length or at the base of the wire.

To investigate the radial doping profile of the microwires, the resistivity of microwires from a single array was repeatedly measured as a function of KOH chemical etching (experiment conducted by Shane Ardo). Preliminary measurements showed that the resistivity would increase with increased chemical etching with KOH, indicating non-uniform radial doping and higher P concentrations at the surface. Further work is

ongoing to determine the radial doping profile, as well as the doping profile along the length of the wire.

2.8 *J-E* response of thermally oxidized n-Si microwire arrays

To improve upon the device performance of the n-Si microwire arrays, thermal oxide 'boots' were fabricated, as demonstrated previously.[4, 6, 14] Following a standard catalyst removal procedure and subsequent KOH etch, arrays of n-Si microwires were thermally oxidized at 1100ºC for ~ 100 min, to produce a thermal oxide with a thickness of ~ 120 nm. To expose the majority of the Si wire, a polymer mask was employed, using polydimethylsiloxane (PDMS) infilled into the array to a height of ~ 10 μm from the base of the wires. The exposed thermal oxide was etched using BHF, and the PDMS was subsequently removed, resulting in wire arrays with selective oxide passivation at the bottom of the wire.

Figure 2.15 shows the *J-E* response of a representative n-Si electrode grown under 0.2 sccm PH_3, with a thermal oxide boot, measured in contact with the $Me_2Fc^{+/0}$–

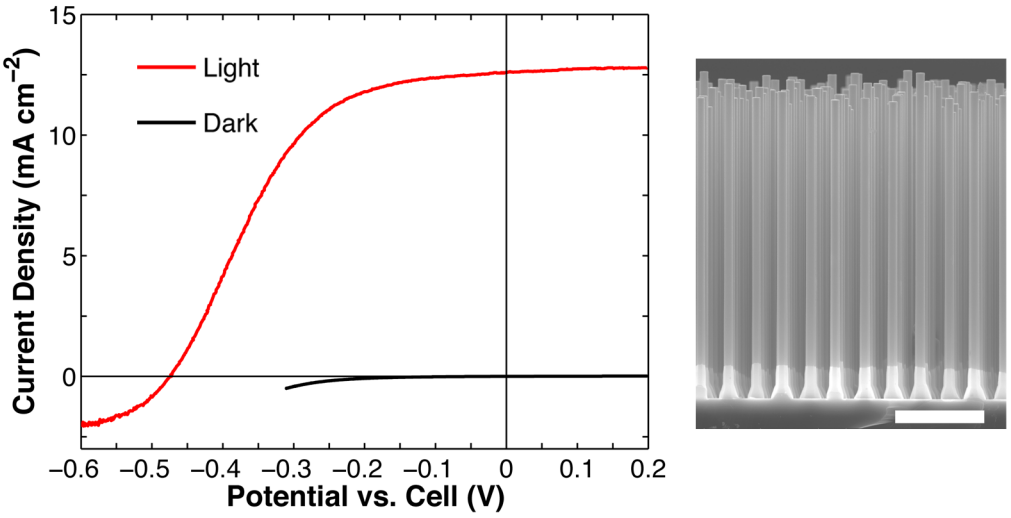

Figure 2.15. *J-E* performance of a n-Si microwire photoelectrode with a thermal oxide 'boot' in contact with $Me_2Fc^{+/0}$–CH_3OH under ELH illumination and in the dark. *Experiment conducted by Shane Ardo.* Included is a representative SEM image of a Si microwire array with a thermal oxide boot, scale bar = 20 μm.

CH_3OH redox system under ELH-type W halogen illumination. The photoresponse of the n-Si electrodes drastically improved with the subsequent processing, with the representative electrode producing a J_{sc} = 12.6 mA cm^{-2}, V_{oc} = 475 mV, and a *ff* = 0.49. Due to the small electrode area of ~ .007 cm^{-2} and thus lower operating currents, the fill factors were slightly improved relative to the undoped Si microwire arrays, which had larger electrode areas of ~ 0.025 cm^{-2}. The n-Si microwire/$Me_2Fc^{+/0}$ contact was more rectifying in dark, as compared to the contact with as-grown n-Si microwire arrays, consistent with the improved response of these electrodes.

From this experimental result, it is unclear whether the improvement in the device properties of the n-Si microwire arrays was the result of gettering of P at the surface of the wires from the growth of a thermal oxide, or from eliminating direct contact of a highly doped base region of the wire from solution. To distinguish between these two possibilities, an insulating, Si nitride (*a*-SiN_x:H) boot could be fabricated, which proceeds through a plasma-enhanced chemical vapor deposition at relatively low substrate temperatures for short times (~ 350ºC, 25 min deposition). In addition, the *a*-SiN_x:H should produce a surface with a lower surface recombination velocity than the dry thermal oxide, and could thus improve the performance of this device.

2.9 Conclusions

For both undoped and n-Si microwire arrays photoanodes, improvements have been made in their photoelectrochemical performance by gaining control over the material properties of the microwires, in particular by employing higher purity VLS catalysts. The n-Si microwires, although demonstrating poor photoresponse as grown, showed greatly improved *J-E* response when subject to subsequent thermal oxidation to form an insulating oxide at the bottom of the array.

For the undoped microwire arrays, due to their very low dopant concentration, the Si wires are expected to be operating under high-level injection conditions, in which the concentration of photogenerated carriers exceeds the equilibrium concentration of majority carriers in the wire.[20] The initial device physics model only encompassed wires under

low-level injection that were not fully depleted, making the model potentially not applicable to undoped microwires operating under field-free conditions. Modeling of radial junction nanowire devices under high-level injection conditions predicts that these devices should have poor carrier-collection efficiencies, due to the full depletion within the nanowire resulting in large majority-carrier recombination losses.[13, 21] Work is currently underway to understand in more detail the properties of both nano- and microscale radial geometry devices with low dopant densities that are operating under high-level injection conditions, as presented in subsequent chapters of this thesis.

2.10 Experimental methods

2.10.1 Synthesis of 5N Au–catalyzed Si microwire arrays

Si microwire arrays were grown using the vapor–liquid–solid (VLS) growth method, using thermally evaporated Au (ESPI, 99.999%) as the VLS growth catalyst. Degenerately doped (111)–oriented n-Si wafers with a resistivity of $\rho \sim 0.004$ Ω-cm were thermally oxidized to produce an oxide film with a thickness of 285 nm. A positive photoresist (Microchem S1813) was used to pattern the wafers with 3 μm diameter circular holes, with a 7 μm center-to-center spacing, in a square array. The exposed thermal oxide was etched in buffered HF(aq) (BHF, Transene Inc.) for 4 min. Immediately following the HF etch, 500 nm of Au was thermally evaporated onto the patterned growth substrate and lift-off was performed in acetone. To perform VLS growth, the samples were introduced to the CVD reactor (Watson, 'Big Blue') at 1050º C under N_2 flow, and subsequently annealed in H_2 for 20 min at a flow rate of 1000 sccm at atmospheric pressure. Wire growth was induced by introduction of a mixture of 20 sccm of $SiCl_4$ (6N, Strem) and 1000 sccm of H_2 (Research grade, Matheson) into the reactor for 20 min.

After VLS growth, the Au VLS catalyst was subsequently removed by a 10 s 10% HF etch followed by etching in a Au etchant solution (gold etch TFA, Transene Inc.) for 10 min. The wire array samples were subsequently dipped in 1 M HCl(aq) and rinsed with H_2O. The samples were then etched for 10 s in 10% HF(aq) to remove the native oxide,

rinsed with H_2O, and dried under a stream of N_2.

2.10.2 Synthesis of 6N Au–catalyzed Si microwire arrays

Arrays of Si microwires were grown using thermally evaporated Au (ESPI, 99.9999%) as the VLS growth catalyst, and degenerately doped (111)–oriented n-Si wafers with a resistivity of $\rho < 0.007$ Ω-cm and with 300 nm of thermal oxide (Addison Engineering, Inc.) were used as the growth substrates. A positive photoresist (Microchem S1813) was used to pattern the wafers with 3 μm diameter circular holes, with a 7 μm center-to-center spacing, in a square array. The exposed thermal oxide was etched in buffered HF(aq) (BHF, Transene Inc.) for 4 min. Immediately following the HF etch, 400 nm of Au was thermally evaporated onto the patterned growth substrate. Lift-off was performed in acetone, and the patterned wafers were then cleaved into 1.3 x 1.5 cm pieces. To perform VLS growth, the samples were introduced to the CVD reactor (Watson, 'Big Blue') at 1000º C under N_2 flow, and subsequently annealed in H_2 (Research Grade, Matheson) for 20 min at a flow rate of 1000 sccm at atmospheric pressure. Wire growth was induced by introduction of a mixture of 5 sccm of $SiCl_4$ (6N, Strem) and 1000 sccm of H_2 into the reactor for 45 min. Following growth, the tube was purged with N_2 at 200 sccm and was allowed cool to ~ 650 °C over the course of ~ 20 min. The wires were subsequently quickly cooled to RT for 5 min and removed from the reactor. After VLS growth, the Au VLS catalyst was removed by a 10 s BHF etch followed by etching in a Au etchant solution (gold etch TFA, Transene Inc.) for 45 min. Following a 5s BHF etch to remove the native oxide on the microwires, the arrays were etched in 30% KOH(aq) at room temperature (~20ºC) for 2 min. Given a corresponding Si etch rate of ~ 1.5–2.1 μm hr^{-1},[22, 23] approximately 60 nm of Si was removed radially from the wires.

2.10.3 Synthesis of 6N Cu–catalyzed Si microwire arrays

Si microwire arrays were grown using the vapor–liquid–solid (VLS) growth method, using thermally evaporated Cu (ESPI, 99.9999%) as the VLS growth catalyst.

Degenerately doped (111)–oriented n-Si wafers with a resistivity of $\rho < 0.007$ Ω-cm and with 300 nm of thermal oxide (Addison Engineering, Inc.) were used as the growth substrates. The wafers were patterned as described previously, with 3 μm x 7 μm hexagonal array of 400 nm of evaporated Cu catalyst. To perform VLS growth, the samples were annealed in a tube furnace ('Dorothy') at 1000º C for 20 min with 500 sccm of H_2 (Research grade 'AlphaGaz 2,' Air Liquide) at atmospheric pressure. Wire growth was induced by the introduction of $SiCl_4$ (6N, Strem) in 50 sccm of He (Research grade, Air Liquide) into the reactor for 20 min. The wires were subsequently cooled to 750ºC under H_2 for 15 min, then cooled to RT under He for 20 min and subsequently removed from the reactor. After VLS growth, the Cu growth catalyst was removed by a 10 s BHF etch, immediately followed by an etch in 6:1:1 (by volume) of H_2O:HCl:H_2O_2 at 70º C (RCA 2) for 15 min. A KOH etch was not employed on the Cu–catalyzed wires, as the *J-E* performance of the microwires was not shown to improve with subsequent etching. In fact, increasing the total time of HF etching generally decreased the observed V_{oc}, from increased etching of the Si oxide buffer layer.

2.10.4 Synthesis of n-Si microwire arrays with in situ PH_3

Si microwire arrays were grown using the vapor–liquid–solid (VLS) growth method, using thermally evaporated Cu (ESPI, 99.9999%) as the VLS growth catalyst. Degenerately doped (111)–oriented n-Si wafers with a resistivity of $\rho < 0.001$–0.003 Ω-cm and with 450 nm of thermal oxide (University Wafer) were used as the growth substrates. These wafers were subsequently patterned with a 3 x 7 μm hexagonal array of the Cu metal catalyst, with a thickness of 450 nm. To perform VLS growth, the samples were annealed in a tube furnace ('Dorothy') at 1000º C for 20 min with 500 sccm of H_2 (Research grade, Air Liquide) at atmospheric pressure. Wire growth was induced by introduction of $SiCl_4$ (6N, Strem) in 50 sccm of He (Research grade, Air Liquide) into the reactor for 20 min, in conjunction with 0.1–15.0 sccm of PH_3 (100 ppm in H_2, Matheson). The wires were subsequently cooled to 750ºC under H_2 for 15 min, then cooled to RT under He for 20 min and subsequently removed from the reactor. After VLS growth, the Cu growth

catalyst was removed by a 5 s BHF etch, immediately followed by an etch in 6:1:1 (by volume) of H_2O:HCl:H_2O_2 at 70º C (RCA 2) for 15 min ('BHF/RCA2 cleaning procedure'). This BHF/RCA2 step was repeated once more, to ensure that all the catalyst had been removed. No KOH etch steps were performed prior to electrochemical measurement.

2.10.5 Four-point resistance and gate-dependent measurements

Four-point resistance measurements were performed as described previously.[9] After removal of the VLS catalyst, a thin surface region of the Si microwires arrays of ~ 60 nm in thickness was chemically removed using a 30% KOH etch at RT (~ 20ºC) for 2 min. The wire arrays were thoroughly rinsed in H_2O to terminate the chemical etch, and dried under N_2. Various regions of the Si microwire arrays were mechanically removed from the growth substrate with a razor blade and were suspended in isopropanol. Care was taken not to remove wires from the edge of the array, where the wires were generally non-uniform and highly tapered. The wires were then spin-coated onto a silicon wafer that had been coated with 300 nm of Si_3N_4 (University Wafer). Contacts were patterned on individual wires using a lift-off resist (LOR10A, Microchem) and a positive photoresist (S1813, Microchem). Immediately following a 5 s BHF etch, 800 nm of Al (5N, Kurt J. Lesker) and 200 nm of Ag (4N, Kurt J. Lesker) were deposited by electron-beam evaporation onto the patterned wafer, to form ohmic contacts to the wires. The conductivity of the wires was measured with varying back-gate bias potentials, between -15 V and +15 V, to determine the carrier type in the wires.

2.10.6 Photoelectrochemical measurements

Please refer to Appendix A for the standard configuration of the $Me_2Fc^{+/0}$–CH_3OH electrochemical cell, under AM 1.5 G, ELH-type W halogen, and 808 nm illumination. For results given in 2.3 and 2.5, data were collected and averaged for six wire array samples, for both Au– and Cu–catalyzed Si microwire arrays. For the 200 mM Me_2Fc/25

mM Me_2FcBF_4 cell, ~ 60 mW cm^{-2} of 808 nm illumination was required to match each electrode's J_{sc} as measured under 100 mW cm^{-2} simulated 1 Sun's illumination. For correction of the Au– and Cu–catalyzed *J-E* data, the limiting anodic current density was 80 mA cm^{-2} and the limiting cathodic current densities were 0.15 and 9.8 mA cm^{-2}, for 0.4 mM and 25 mM Me_2FcBF_4, respectively. The measured values of the uncompensated series resistance of the cell, R_s ranged from 50–150 Ω. A value of R_s = 50 Ω was used in the correction of the *J-E* data, to avoid overcorrecting any individual photoelectrode's response. For *J-E* measurements of n-Si microwire arrays in 2.7, the electrochemical cell was operated under standard conditions (see Appendix A), with 200 mM Me_2Fc/0.4 mM Me_2FcBF_4 under 100 mW cm^{-2} of ELH-type W halogen illumination. Data was collected for n-Si grown for PH_3 flow rates of 0.10, 0.20, 0.25, 0.30, 0.40, and 1.00 sccm, with three electrodes measured at each PH_3 flow rate.

2.10.7 Oxidation and formation of a thermal oxide 'boot' on n-Si microwire arrays

A Cu–catalyzed, n-Si microwire array was grown with 0.2 sccm PH_3 and the resulting wires were 60 μm in height. The Cu catalyst was subsequently removed by the BHF/RCA2 cleaning procedure, followed by etching in 30 % wt. KOH(aq) for 90 s. The wire arrays were then subjected to the BHF/RCA2 cleaning procedure again, to fully remove the Cu catalyst and also any resulting metal contamination from the KOH etching step. The array was then oxidized at 1100ºC for 100 min under a pure O_2 ambient (2 lpm flow rate), producing a conformal, dry SiO_2 layer with a thickness of ~ 120 nm. To produce the polymer mask, the array was then coated with a solution that contained 1 g polydimethylsiloxane PDMS and 0.10 g of PDMS curing agent (Sylgard 184, Dow Corning) in 4.35 g (5 mL) of toluene. These samples were then spun at 30 s at 150 RPM, 30 s at 750 RPM, and 60 s at 1500 RPM. The array was then placed in a vacuum oven at 40–60ºC overnight, and was then fully cured at 150 °C for 30 min, producing a 10 μm thick PDMS layer at the base of the wire array. Residual PDMS was removed from the tops of the wires by first wetting the array with *N*-Methyl-2-pyrrolidone (NMP), and then subsequently employing a ~ 5 s etch in a 1:3 mixture of 75 wt. % tetrabutylammonium

fluoride in water (Sigma-Aldrich): NMP ('PDMS' etch), followed by a H_2O rinse. The arrays were then etched for 5 min in BHF to remove the exposed thermal oxide. The PDMS was completely removed by etching for 0.5–2 hr in the PDMS etch, followed by a H_2O rinse. To remove residual organics on the array, a piranha etch (3:1 aq. conc. H_2SO_4:H_2O_2) was used, for at least 10 min.

2.11 References

1. S. W. Boettcher, J. M. Spurgeon, M. C. Putnam, E. L. Warren, D. B. Turner-Evans, M. D. Kelzenberg, J. R. Maiolo, H. A. Atwater and N. S. Lewis, *Science*, 2010, **327**, 185-187.
2. E. L. Warren, S. W. Boettcher, M. G. Walter, H. A. Atwater and N. S. Lewis, *J. Phys. Chem. C*, 2011, **115**, 594-598.
3. J. M. Spurgeon, S. W. Boettcher, M. D. Kelzenberg, B. S. Brunschwig, H. A. Atwater and N. S. Lewis, *Adv. Mater.*, 2010, **22**, 3277–3281.
4. S. W. Boettcher, E. L. Warren, M. C. Putnam, E. A. Santori, D. Turner-Evans, M. D. Kelzenberg, M. G. Walter, J. R. McKone, B. S. Brunschwig, H. A. Atwater and N. S. Lewis, *J. Am. Chem. Soc.*, 2011, **133**, 1216-1219.
5. C. E. Kendrick, H. P. Yoon, Y. A. Yuwen, G. D. Barber, H. T. Shen, T. E. Mallouk, E. C. Dickey, T. S. Mayer and J. M. Redwing, *Appl. Phys. Lett.*, 2010, **97**, 143108.
6. M. C. Putnam, S. W. Boettcher, M. D. Kelzenberg, D. B. Turner-Evans, J. M. Spurgeon, E. L. Warren, R. M. Briggs, N. S. Lewis and H. A. Atwater, *Energy Environ. Sci.*, 2010, **3**, 1037-1041.
7. J. R. Maiolo, B. M. Kayes, M. A. Filler, M. C. Putnam, M. D. Kelzenberg, H. A. Atwater and N. S. Lewis, *J. Am. Chem. Soc.*, 2007, **129**, 12346-12347.
8. M. L. Rosenbluth and N. S. Lewis, *J. Am. Chem. Soc.*, 1986, **108**, 4689-4695.
9. M. D. Kelzenberg, D. B. Turner-Evans, B. M. Kayes, M. A. Filler, M. C. Putnam, N. S. Lewis and H. A. Atwater, *Nano Lett.*, 2008, **8**, 710-714.
10. B. M. Kayes, M. A. Filler, M. C. Putnam, M. D. Kelzenberg, N. S. Lewis and H. A. Atwater, *Appl. Phys. Lett.*, 2007, **91**, 103110.

11. M. C. Putnam, M. A. Filler, B. M. Kayes, M. D. Kelzenberg, Y. B. Guan, N. S. Lewis, J. M. Eiler and H. A. Atwater, *Nano Lett.*, 2008, **8**, 3109-3113.
12. M. C. Putnam, D. B. Turner-Evans, M. D. Kelzenberg, S. W. Boettcher, N. S. Lewis and H. A. Atwater, *Appl. Phys. Lett.*, 2009, **95**, 163116.
13. M. D. Kelzenberg Ph.D., *Silicon Microwire Photovoltaics*, California Institute of Technology, Pasadena, 2010.
14. M. D. Kelzenberg, D. B. Turner-Evans, M. C. Putnam, S. W. Boettcher, R. M. Briggs, J. Y. Baek, N. S. Lewis and H. A. Atwater, *Energy Environ. Sci.*, 2011, **4**, 866-871.
15. W. M. Bullis, *Solid State Electron.*, 1966, **9**, 143-168.
16. J. R. Davis, A. Rohatgi, R. H. Hopkins, P. D. Blais, P. Raichoudhury, J. R. Mccormick and H. C. Mollenkopf, *IEEE Trans. Electron. Dev.*, 1980, **27**, 677-687.
17. R. H. Hopkins and A. Rohatgi, *J. Cryst. Growth*, 1986, **75**, 67-79.
18. F. Gstrein, D. J. Michalak, W. J. Royea and N. S. Lewis, *J. Phys. Chem. B*, 2002, **106**, 2950-2961.
19. M. D. Kelzenberg, S. W. Boettcher, J. A. Petykiewicz, D. B. Turner-Evans, M. C. Putnam, E. L. Warren, J. M. Spurgeon, R. M. Briggs, N. S. Lewis and H. A. Atwater, *Nat. Mater.*, 2010, **9**, 239-244.
20. A. Luque and S. Hegedus, eds., *Handbook of Photovoltaic Science and Engineering*, Wiley, Chichester, England ; Hoboken, NJ 2003.
21. J. M. Foley, M. J. Price, J. I. Feldblyum and S. Maldonado, *Energy Environ. Sci.*, 2012, **5**, 5203-5220.
22. H. Seidel, L. Csepregi, A. Heuberger and H. Baumgartel, *J. Electrochem. Soc.*, 1990, **137**, 3626-3632.
23. H. Seidel, L. Csepregi, A. Heuberger and H. Baumgartel, *J. Electrochem. Soc.*, 1990, **137**, 3612-3626.

Chapter 3

SI MICROWIRE ARRAYS OPERATING UNDER HIGH-LEVEL INJECTION CONDITIONS

Summary

The device properties of undoped Si microwire arrays were further investigated, using single-wire and photoelectrochemical measurements. Wires grown with a Cu VLS catalyst on both n^+ and p^+ degenerate, planar substrates were slightly p-type, displaying resistivities of ~ 100–1000 Ω-cm corresponding to electronically active dopant concentrations of 1 x 10^{13} –1 x 10^{14} cm^{-3}. Photoconductivity measurements of single wires showed a decrease in resistance of the wires under illumination, consistent with an increase in carrier concentration under illumination for lightly doped Si.

Arrays of such wires were characterized electrochemically, using non-aqueous 1,1'-dimethylferrocene $(Me_2Fe)^{+/0}$ and cobaltocene $(CoCp)^{+/0}$ redox couples, which produce conformal, radial, high barrier-height contacts to n-Si and p-Si, respectively. In particular, arrays with a n^+ back contact measured in radial contact with $Me_2Fe^{+/0}$ exhibited photovoltages of 0.45 V and an energy-conversion efficiency of 2.3% under simulated 1 Sun's illumination, with diode quality factors of 1.90 ± 0.06. Similar behavior was observed for an identical array with a p^+ back contact in radial contact with $CoCp^{+/0}$, demonstrating that the arrays were operating under high-level injection conditions, in which kinetic asymmetries at the back contact determined the charge separation in the device.

3.1 Introduction and motivation

Si wire arrays grown by the vapor–liquid–solid (VLS) process have emerged as a promising technology for the fabrication of efficient, scalable photovoltaics and artificial photosynthetic devices. However, to ultimately achieve efficiencies comparable to wafer-based solar cells, higher open-circuit voltages must be obtained. One potential strategy to improve the attainable photovoltage of Si microwire arrays is to operate under the condition of high-level injection using lightly doped Si, where the change in the concentration of photogenerated electrons and holes (Δn and Δp, respectively) greatly exceeds their equilibrium concentration in the dark (n_0 and p_0). Under these conditions, the Shockley–Read–Hall recombination rate (eq. 3.1) for a single, mid-gap trap reduces to eq 3.2,

$$R_{SLT} = \frac{pn - n_i^2}{\tau_{SLT,n}\left(p + n_i e^{\frac{E_i - E_T}{kT}}\right) + \tau_{SLT,p}\left(n + n_i e^{\frac{E_T - E_i}{kT}}\right)} \tag{3.1}$$

$$R_{SLT} \approx \frac{n}{\tau_{SLT,n} + \tau_{SLT,p}} \approx \frac{p}{\tau_{SLT,n} + \tau_{SLT,p}} \qquad \text{when } p \approx n \gg n_0, p_0 \tag{3.2}$$

where n and p are the concentrations of electrons and holes under illumination, respectively; and $\tau_{SLT,\,n}$ and $\tau_{SLT,\,p}$ are the carrier lifetimes of electrons and holes, respectively.[1, 2] Under high-level injection conditions, the recombination lifetime is proportional to the sum of both the carrier lifetimes, and is thus longer than the lifetime under low-level injection conditions for a doped semiconductor, where the lifetime is proportional to the minority-carrier lifetime.

Planar devices operating under these conditions, such as Si point-contact solar cells (Figure 3.1), have achieved the highest efficiencies for a single-junction Si photovoltaic, with cell efficiencies of exceeding 27% under concentrated illumination.[3-5] These devices utilize lightly doped, float-zone Si, and are fabricated with small interdigitated n^+ and p^+ back point-contacts for the selective collection of electrons and holes, respectively, and low saturation currents. Photogenerated carriers are driven by diffusion, not drift, within the device, which does not possess an electric field in the bulk of the semiconductor. Thus, to

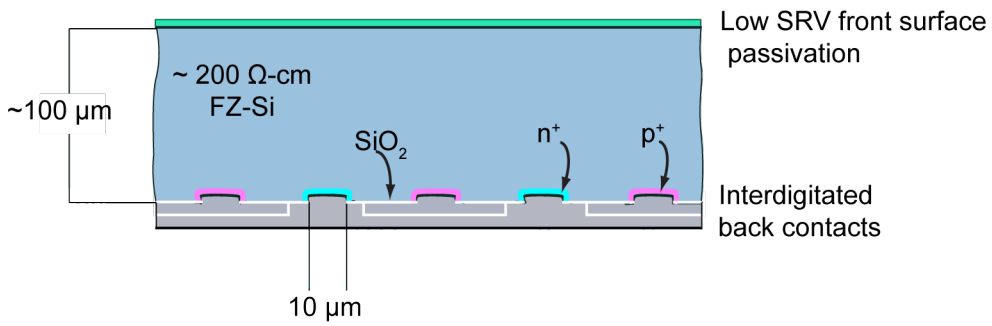

Figure 3.1. Schematic of a Si point-contact cell

elicit an efficient device, the Si must possess an extremely long lifetime exceeding 1 ms, and high-quality surface passivation on both the front and back of the cell are necessary to minimize recombination. This highly optimized device also benefits from having a highly reflective back surface, an antireflection coating on the front surface, and no shadowing from a top contact to achieve high efficiencies.

To translate the operational principles of planar devices operating under high-level injection conditions to a structured device, lightly doped, selectively contacted Si wire arrays were fabricated, by growing Cu–catalyzed Si microwires without dopants, on a n^+ or p^+-Si(111) substrate (Figure 3.2). Using non-aqueous redox couples with varying electrochemical potentials, including the $Me_2Fc^{+/0}$–CH_3OH and $CoCp_2^{+/0}$–CH_3CN redox systems, the *J-E* behavior of the wire arrays was systematically probed, following previous experiments using planar, modified point-contact solar cells.[6, 7] Both the $Me_2Fc^{+/0}$–CH_3OH and $CoCp_2^{+/0}$–CH_3CN systems have been shown to generate an inversion layer in contact with Si, resulting in semiconductor/liquid interfaces with high selectivity for holes and electrons, respectively, and low effective surface recombination velocities, *S*.[8]

However, unlike these planar devices, the lightly doped Si microwires are expected to be fully depleted in contact with the stated redox couples, for $N_A \sim 1 \times 10^{-13}$ –1×10^{-14} cm^{-3} and wire diameters of ~ 2.5–3.0 μm. For doped wires, device physics simulations predict that depleted wires should have extremely low carrier-collection efficiencies, due to the absence of an electric field within the wire and the lack of majority carriers to facilitate axial carrier transport.[9, 10] For undoped Si microwires in contact with $Me_2Fc^{+/0}$–

CH_3OH, in contrast, the surface of the wire is also expected to be strongly inverted, as previously demonstrated for the n-Si/$Me_2Fc^{+/0}$–CH_3OH junction.[8, 11, 12] Thus, undoped microwires may possess an electric field, with a large concentration of holes at the surface, to enable efficient carrier collection. Moreover, prior device physics models have examined fully depleted materials with relatively short lifetimes, with effective diffusion lengths on the order of, or smaller than, the length of the wire. Given the longer anticipated lifetime of the lightly doped Si microwires operating under high-level injection conditions as compared to doped Si microwires, which have demonstrated effective diffusion lengths >> 30 μm,[13] further modeling of structured materials with lifetimes exceeding 1 μs are needed to fully understand the device properties of these systems.

It is clear from preliminary experiments of undoped Si microwires in contact with $Me_2Fc^{+/0}$–CH_3OH that these arrays have high carrier-collection efficiencies, producing *J-E* performance similar to optimally doped wire arrays. Chapters 3–5 within this thesis will provide a thorough investigation of the device properties of these microwire arrays, through electrochemical experiments in contact with varying electrochemical systems; modification of the as-grown wires with thermal processing, surface passivation for the formation of axial devices, and the formation of diffused emitters; spectral response measurements; and device physics modeling of the undoped wires in contact with $Me_2Fc^{+/0}$–CH_3OH. These experiments will provide fundamental insight into the performance lightly doped,

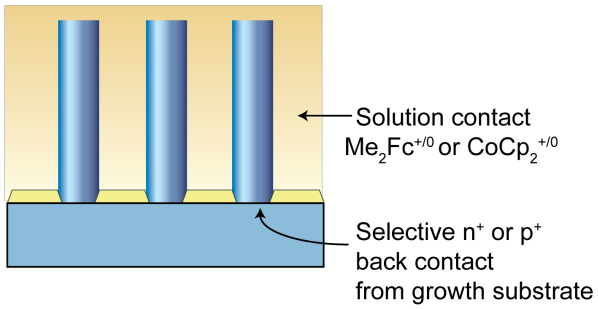

Figure 3.2. Schematic of a selectively contacted, undoped Si microwire array, in contact with redox couples with very positive ($Me_2Fc^{+/0}$) and negative ($CoCp_2^{+/0}$) electrochemical potentials. With the ability to vary both the solution contact and the back contact, several combinations of devices are possible to fully investigate the behavior of undoped microwires operating under high-level injection conditions.

structured semiconductor electrodes that are operated under high-level injection conditions.

3.2 VLS–catalyzed Si microwire growth and characterization

Arrays of lightly doped Si microwires were grown on a planar n^+-Si(111) substrate using the VLS process, without dopants, but with 6N Cu as the growth catalyst. The resulting Si wires were oriented in the (111) direction, with diameters of 2.7–2.9 μm and heights of 67–80 μm, with an average areal packing fraction (η_f) of 12.5% (Figure 3.3 and Figure 3.4). To potentially improve upon their performance, wires with larger diameters of ~ 3 μm were intentionally fabricated, by increasing the amount of deposited Cu metal catalyst from the typical thickness of 450 nm to 750 nm. An interfacial region between the faceted Si microwire and the metallic Cu catalyst existed at the top of the wires, with a minimum thickness of ~ 100 nm. This region was visually characterized by its scalloped appearance, in contrast to the highly faceted faces of the Si microwire. The interfacial region appeared in all wires grown in the Dorothy reactor, regardless of cooling conditions, and could not be removed with repeated HF/RCA2 chemical etching.

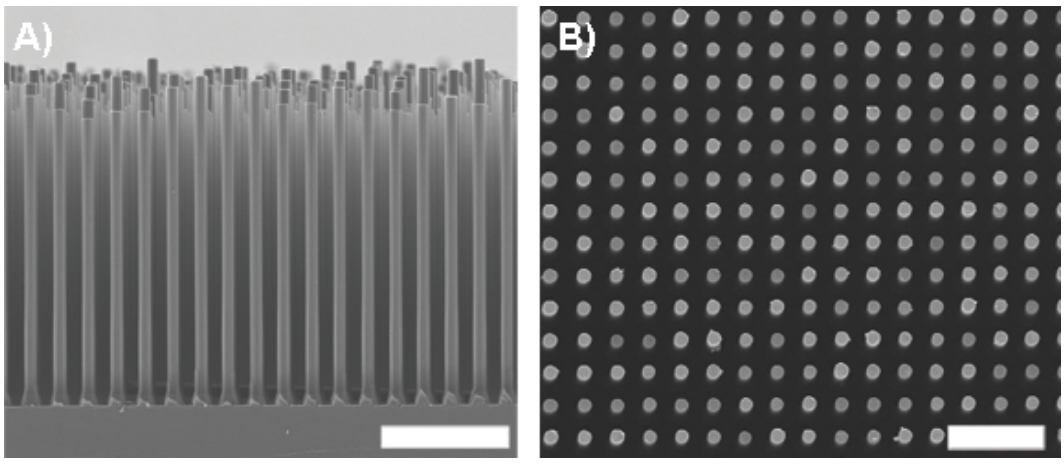

Figure 3.3. A) Side view SEM image of a cleaved array of square–packed Si microwires, scale bar = 30 μm. B) Top view of the same Si microwire array, scale bar = 20 μm.

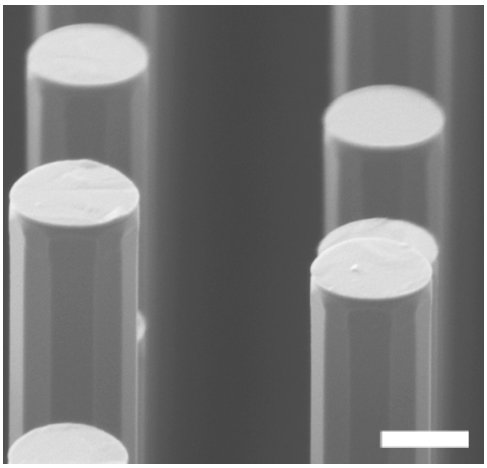

Figure 3.4. SEM image with an angled view of the Si microwire array after catalyst removal, scale bar = 2 μm.

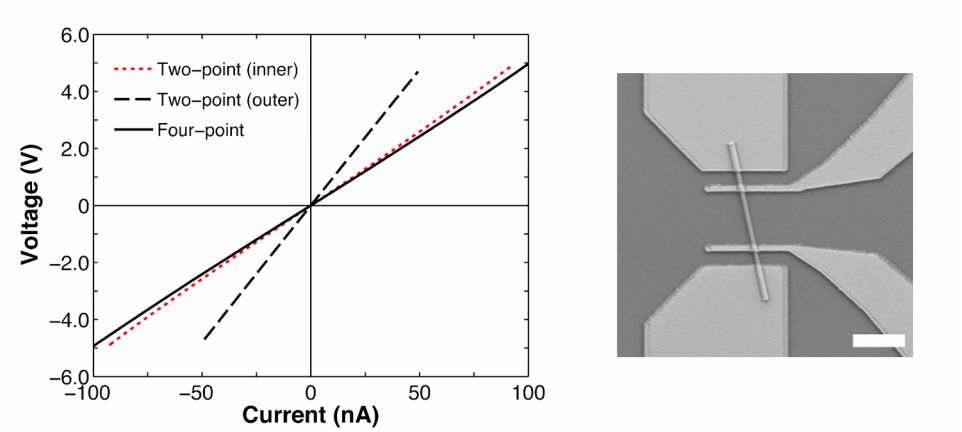

Figure 3.5. Representative two-point and four-point *I-V* behavior of an undoped Si microwire grown on an n^+ substrate, with a SEM image of the single-wire contact, scale bar = 30 μm.

Four-point resistance measurements indicated that the Si microwires grown without in situ dopants had resistivities of ~ 800 ± 500 Ω-cm, and gate-dependent conductance measurements demonstrated that the microwires were slightly p-type, with the wires showing an increase in conductivity with a negative applied gate-bias. Thus, the as-grown microwires possessed an electronically active acceptor concentration, N_a, of ~ 1 x 10^{13} cm^{-3} (Figure 3.5). These measurements were in good agreement with previous measurements on undoped Si microwires grown on degenerate n^+ substrates, as discussed in Chapter 2.4.

In addition, under illumination, the single-wire devices with native oxide passivation showed a decrease in resistance relative to their resistance in the dark (Figure 3.6), with a factor of 1.5 decrease of resistance under several Suns of ELH-type W halogen illumination. The small change in conductance of the microwires, even under several Suns of illumination, could be attributed to the low absorption of light by a single microwire. The ELH-type W halogen spectrum contains very little short wavelength radiation, with a maximum irradiance at $\lambda_{max} \sim 660$ nm. The spectrum's lack of short wavelength radiation, in conjunction with the thin (~ 3 μm) optical path length of a single wire, limited the absorption within the wire and, thus, its overall change in conductivity. Also, the native oxide surface of the microwire was expected to have a high surface recombination velocity. With this dominant recombination mechanism, the concentration of photogenerated carriers should decrease due to an overall increased recombination rate, resulting in a small change in conductance under illumination. The surface recombination velocity, *S,* of microwires with various surface passivations have been extrapolated from measurements of the effective diffusion length L_{eff} of single-wire Si p-n junctions.[13] In particular, a very high $S \geq 4 \times 10^5$ cm s^{-1} was calculated for the native oxide surface, from a measured $L_{eff} \leq 0.5\ \mu m$. A very low $S < 10$ cm s^{-1} was similarly computed for silicon nitride (a-SiN_x:H) surface passivation of the device from a measured $L_{eff} >> 30\ \mu m$, with all carriers being collected

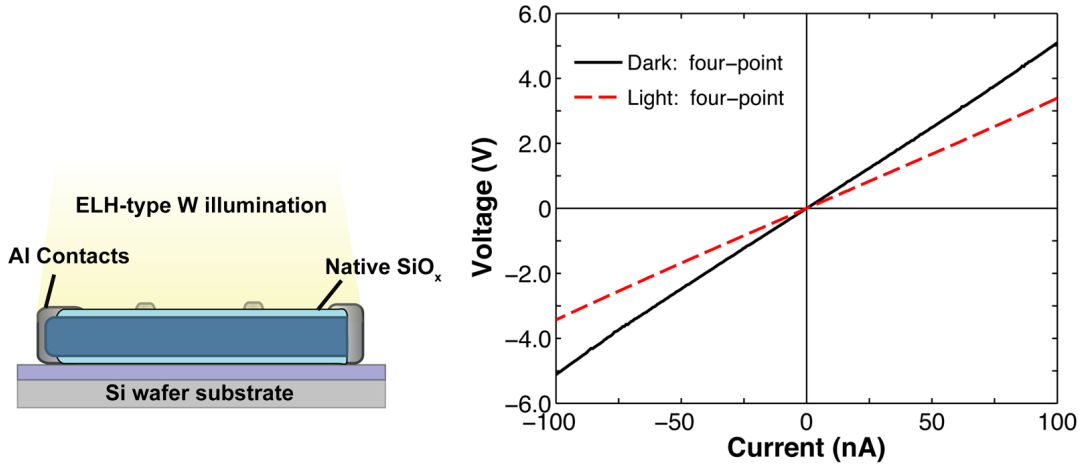

Figure 3.6. *I-V* behavior of a four-point contacted single-wire device with native oxide passivation, in the dark and under several Suns of ELH-type illumination, with a corresponding schematic of the device

from axial region of the device.

Given the known, high-quality passivation of the Si microwires by *a*-SiN_x:H, single-wire devices with low-stress, plasma-enhanced chemical vapor deposition (PECVD) *a*-SiN_x:H passivation were fabricated (Figure 3.7). After standard catalyst removal and subsequent cleaning of the Si microwire arrays by an RCA1/RCA2 procedure, PECVD *a*-SiN_x:H was deposited on the arrays. The *a*-SiN_x:H film was grown using SiH_4 (5% in N_2) and NH_3 precursors, with the substrate held at 350ºC. For a typical 25 min deposition, the thickness of the deposited a-SiN_x:H film on the Si microwires ranged from ~ 120 nm at the wire tips to ~ 60 nm at the wire bases, as measured previously.[13] The PECVD film was also deposited on planar, high-resistivity, double side polished, float-zone n-Si(111) with a lifetime > 2 ms. A *S* of ~ 25 cm s^{-1} was measured using microwave-frequency photoconductivity decay measurements, indicating the high quality of the deposited film.[8, 11]

To obtain single wires with both ohmic terminal contacts and *a* -SiN_x:H passivation over the entirety of the non-contacted area, a polymer mask was employed to allow for the selective removal of the Si nitride from the wire tips. At the base of the Si wire, contact could be made to the center of the wire once removed from the substrate in the fabrication of the single-wire device. Figure 3.7 shows the schematic for an *a*-SiN_x:H

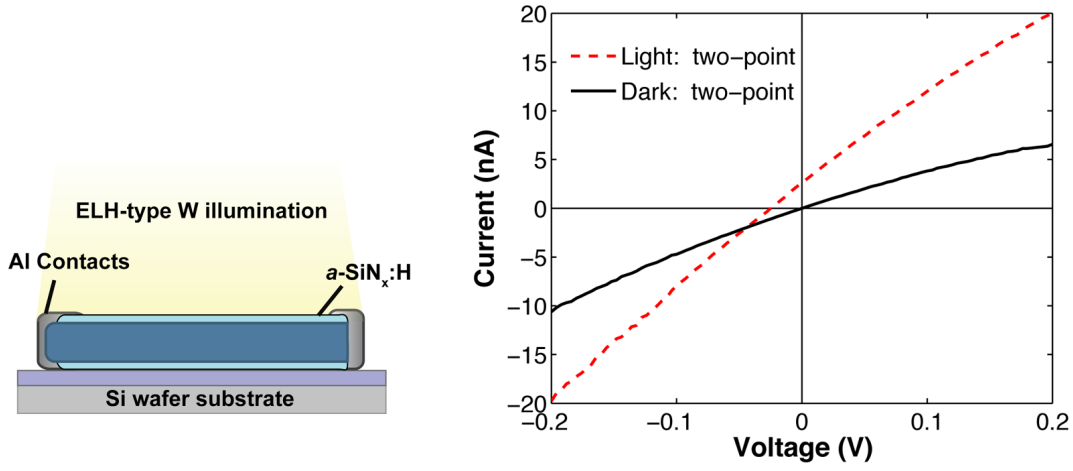

Figure 3.7. *I-V* behavior of a Si nitride coated microwire in the dark and under illumination, with a corresponding schematic of the single-wire device

passivated single-wire device with two-point contacts, as well as the *I-V* response of the *a*-SiN_x:H coated wire in the dark and under several Suns of ELH-type W halogen illumination. The *a*-SiN_x:H coated wire under illumination decreased in resistance by a factor of ~ 2.5; however, the real decrease in resistance cannot be properly calculated, given the presence of a rectifying contact in the device. To really measure the change in conductivity under illumination, a four-point contacted wire should be fabricated, to both maximize the change in resistance by eliminating contact resistance and to produce a linear response in the device. However, the change in conductivity for a single-wire device would not be representative of the actual change in conductivity of a wire in contact with $Me_2Fc^{+/0}$–CH_3OH, since this junction should create an accumulation layer at the surface of the lightly doped p-type microwires.

3.3 *J-E* response of lightly doped Si microwire arrays: n^+-i-Si/$Me_2Fc^{+/0}$–CH_3OH

Current density vs. potential (*J-E*) measurements of the undoped Si microwire arrays grown on a n^+ substrate (n^+-i-Si**)** were measured in contact with 200 mM Me_2Fc-0.4 mM Me_2FcBF_4 in CH_3OH under 100 mW cm^{-2} of simulated 1 Sun illumination, using an ELH-type W halogen illumination source (Figure 3.8). The lightly doped Si wire array electrodes exhibited V_{oc} = 445 ± 13 mV, J_{sc} = 12.8 ± 2.1 mA cm^{-2}, and fill factors, *ff* = 0.41 ± 0.03, with a photoelectrode energy-conversion efficiency η = 2.3 ± 0.3%. The arrays demonstrated photoanodic behavior even though the wires were slightly p-type, indicating that the *J-E* behavior of the arrays was not dominated by their doping but by the formation of ohmic-selective contacts at the back of the wire through the n^+ substrate and through the conformal, high barrier-height contact to $Me_2Fc^{+/0}$.

From the *J-E* performance of this particular array of larger diameter wires, overall trends in the device performance of Si microwires can be observed. The larger diameter wires with D ~ 2.7–2.9 μm produced more photocurrent than wires previously measured, with D ~ 2.0–2.5 μm and a resulting J_{sc} = 7.9 ± 0.5 mA cm^{-2} under AM 1.5 G illumination and a J_{sc} = 9.2 ± 1.0 mA cm^{-2} under 100 mW cm^{-2} ELH-type W illumination (Chapter 2.4).

However, these larger diameter wires were particularly sensitive to repeated HF etching, with an observed decrease in V_{oc} of ~ 10 mV for each 5 s 5% HF etching step. The increased quantity of deposited Cu metal (750 nm versus the typical 450 nm) may have increased the concentration of metal inclusions or Cu silicides formed in the planar substrate or around the base of the wire, which could provide a direct shunt between the degenerate growth substrate and the redox solution when exposed. This effect should be most pronounced when measuring these arrays in an electrochemical configuration, which provides a conformal contact to the whole array, and may not ultimately diminish the observed V_{oc} in a solid-state device.

To estimate the contribution of the degenerate n^+-Si(111) growth substrate to the photoresponse of the wire array photoelectrodes, the wires were subsequently removed from the electrode through non-abrasive mechanical force, and the same electrodes were measured for their photoresponse. These n^+-Si(111) control substrates produced V_{oc} = 7.5 ± 0.7 mV, J_{sc} = 0.86 ± 0.01 mA cm^{-2}, and ff = 0.34 ± 0.07. With the demonstrated small photoresponse of the crystalline growth substrate, the observed photoresponse of the Si microwire array electrodes can be primarily attributed to the wires and not to the underlying growth substrate. For this particular experiment, the photoresponse of the n^+-Si

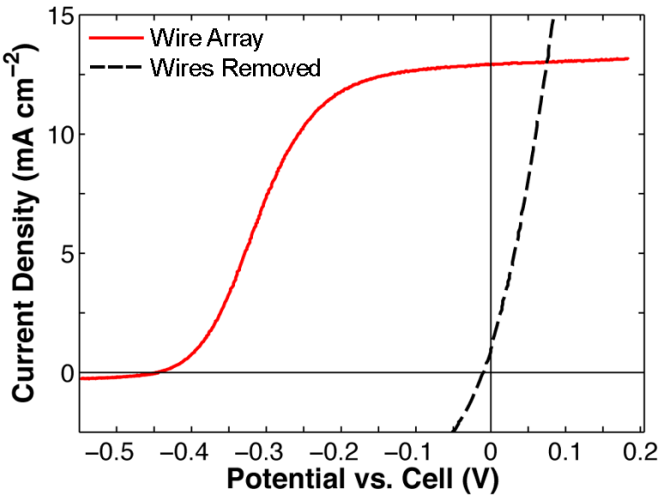

Figure 3.8. *J-E* behavior of lightly doped Si microwire arrays grown on a n^+-Si substrate, in contact with the $Me_2Fc^{+/0}$-CH_3OH redox system under 100 mW cm^{-2} simulated 1 Sun's illumination

growth substrate was greatly diminished, potentially due to the increased quantity of Cu metal that was deposited to achieve larger diameter wires.

After measuring the photoresponse of the Si microwire electrodes under 1 Sun's illumination, the concentration of the oxidized form of the redox couple, Me_2FcBF_4, was increased in the cell, to decrease the effect of concentration overpotential losses within the cell. The photoelectrodes were illuminated using an 808 nm laser diode, such that the J_{sc} value matched the value of J_{sc} that was obtained at low Me_2Fc^+ concentrations under 100 mW cm^{-2} of simulated 1 Sun illumination. Approximately 55 mW cm^{-2} of 808 nm illumination, as measured by a calibrated diode in the cell, was required to current match the photoelectrodes. Figure 3.9 shows the performance of the arrays in the presence of either 0.4 or 40 mM Me_2FcBF_4, with the latter cell exhibiting a fill factor of $ff_{808} = 0.58 \pm 0.02$ and an efficiency $\eta_{808nm} = 5.9 \pm 1.0\%$ under 55 mW cm^{-2} of 808 nm illumination. After correcting both the 0.4 Me_2FcBF_4 *J-E* data for concentration overpotential and uncompensated resistance losses, the corrected fill factor and photoelectrode efficiency values were $ff_{corr} = 0.62 \pm 0.04$ and $\eta_{corr} = 3.5 \pm 0.6\%$, respectively.

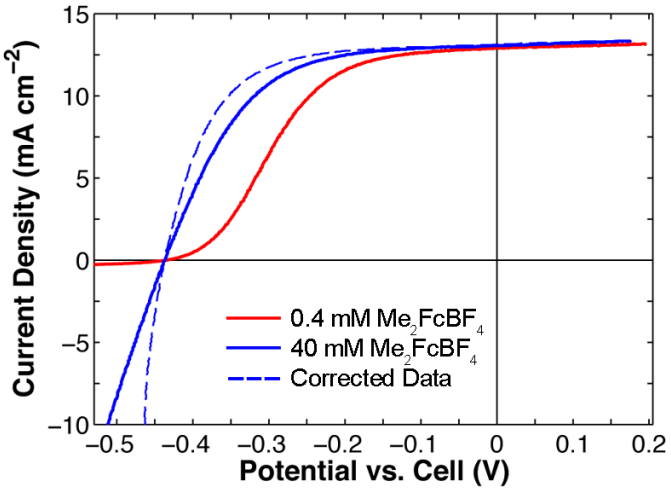

Figure 3.9. *J-E* behavior of lightly doped Si microwire arrays grown on a n^+-Si substrate, in contact with the $Me_2Fc^{+/0}$–CH_3OH redox system, with an increased concentration of Me_2FcBF_4 and the corrected *J-E* response

3.4 Diode quality factor measurement

To determine the diode quality factor of the undoped Si microwire photoelectrodes in contact with $Me_2Fc^{+/0}$–CH_3OH, the electrodes were measured at a series of light intensities under 808 nm illumination. At each light intensity, a photoelectrode's V_{oc} was initially measured using a Keithley 4-digit voltmeter, and the J_{sc} was measured from the *J-E* behavior of the electrode. The V_{oc} is expected to the have the general form:

$$V_{oc} = \frac{nkT}{q} \ln\left(\frac{J_{ph}}{J_0}\right) \tag{3.1}$$

where n is the diode quality factor, k is Boltzmann's constant, T is the temperature, q is the charge on an electron, J_{ph} is the photocurrent density, and J_0 is the dark saturation current density.[14] Therefore, a plot of V_{oc} versus J_{ph} should be linear with a slope of nkT/q, and the value of n can be readily determined. The Si microwire array photoelectrodes were measured under light intensities ranging from ~13 mW cm^{-2} to 165 mW cm^{-2} of 808 nm illumination, corresponding to ~ 0.24–3.0 Suns of illumination (Figure 3.10). Diode quality factors of n = 1.90 ± 0.06 were subsequently calculated from the variation of V_{oc} with J_{sc} (Figure 3.11).

These particular photoelectrodes showed typically lower *ff* values than previously measured, due to small variations in the Luggin capillary in the cell, and due to the electrodes' slightly larger active areas, > 0.033 cm^{-2} versus 0.024 cm^{-2} for electrodes previously measured. Higher concentration of Me_2FcBF_4 present in the cell (40 mM versus 25 mM) made aligning the electrodes relative to the Luggin capillary difficult, and most likely was the cause of the increase in the apparent resistance of the *J-E* behavior. As a comparison, the n^+-i-Si photoelectrodes described in Chapter 2.4 were also measured for their *J-E* behavior at various light intensities, from ~ 17–255 mW cm^{-2} of 808 nm illumination, from ~ .0.28–4.3 Suns (Figure 3.12). Diode quality factors of n =1.78 ± 0.01 were extrapolated from the electrodes' photoresponse (Figure 3.13).

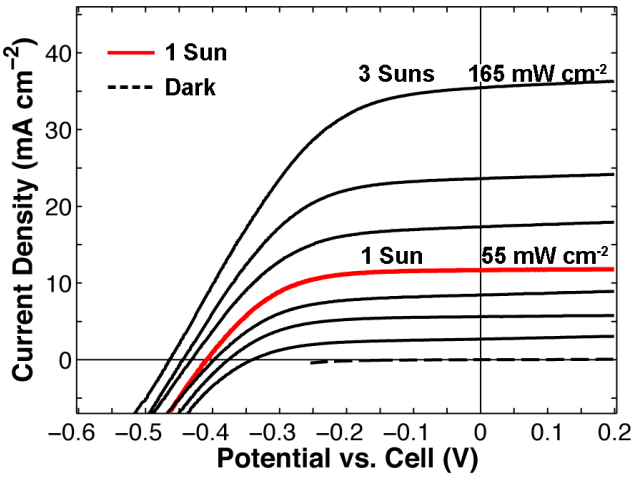

Figure 3.10. *J-E* data as a function of 808 nm illumination intensity for a representative n^+-i-Si microwire array photoelectrode measured in contact with 200 mM Me_2Fc/40 mM Me_2FcBF_4 in methanol

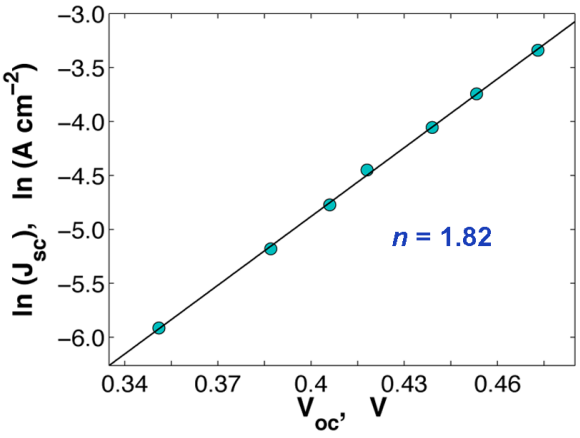

Figure 3.11. The corresponding natural logarithm of the short-circuit photocurrent density vs. the open-circuit photovoltage for the n^+-i-Si microwire array photoelectrode, yielding a diode quality factor of A = 1.82

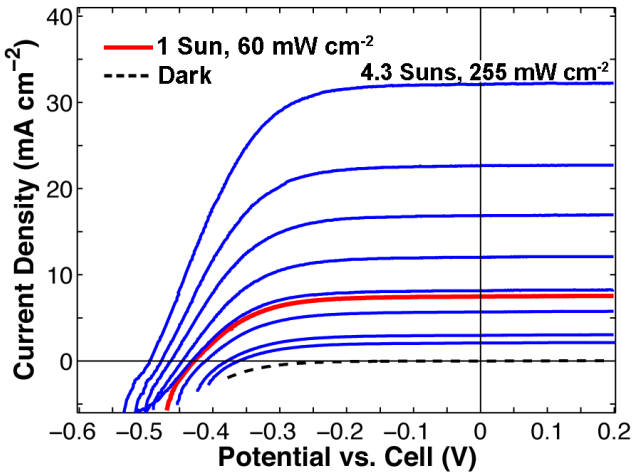

Figure 3.12. *J-E* data as a function of 808 nm illumination intensity for n^+-i-Si microwire array photoelectrodes (Chapter 2.4) measured in contact with 200 mM Me_2Fc/25 mM Me_2FcBF_4 in methanol

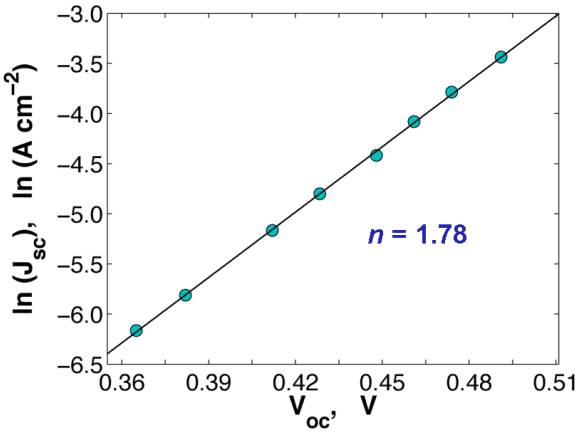

Figure 3.13. The corresponding natural logarithm of the short-circuit photocurrent density vs. the open-circuit photovoltage for the n^+-i-Si microwire array photoelectrode, yielding a diode quality factor of A = 1.78

Photoelectrodes of n^+-i-Si microwires in contact with $Me_2Fc^{+/0}$–CH_3OH consistently demonstrated measured diode quality factors of n ~ 1.8–2.0, which is characteristic of devices operating under the conditions of high-level injection. Diode quality factors of ~ 2.0, ranging from n = 1.6–1.8 have been measured previously for planar *p-i-n* concentrator devices in contact with the $Me_2Fc^{+/0}$–CH_3OH system.[6, 7] In contrast, previous measurements of p-type Si microwire arrays and diffused radial junction n^+p-Si microwire arrays measured in photoelectrochemical cells have produced diode quality factors closer to 1.0. Arrays of p-Si microwires in contact with $MV^{2+/+}$ have displayed n = 1.5–1.6 and Pt/n^+p-Si wire arrays in contact with aq. 0.5 M H_2SO_4 produced n = 1.10 ± 0.04.[15, 16] In addition, single-wire radial p-n junction wires have demonstrated n values between 1.0–1.2, indicating high-quality, low-recombination p–n junctions operating under low-level injection conditions.[13]

3.5 Variation of *ff* with light intensity

The change in the *ff* values of each electrode was calculated as a function of light intensity from the electrode's *J-E* behavior under 808 nm illumination. For these measurements, high concentrations of both the reduced and oxidized species were present in the cell, to reduce the total R_s of the cell. Under light intensities ranging from ~ 13 mW cm^{-2} to 165 mW cm^{-2}, the n^+-i-Si microwire photoelectrodes showed a maximum *ff* under approximately 1 Sun's illumination, with lower *ff* observed at low and high light intensities. The decreased *ff* at higher light intensities can be attributed to the dominance of uncompensated series resistance and concentration overpotential losses within the cell at higher operating currents. These particular n^+-i-Si electrodes possessed lower *ff* than were typically measured, due to the increased shunting from the degenerate substrate with increased HF etching. The decrease in *ff* at low light intensities was consistent with what is predicted by the diode equation. Thus, any decrease in the resistance of the wires would be convoluted with the diode behavior of the device, and the change in resistance cannot be calculated from this experiment.

3.6 Growth and characterization of Si microwires on p^+ substrates

To further investigate the effect of changing the back contact on the photoresponse of the undoped Si microwires, the microwires were grown without dopants on a p^+ substrate. The Si microwire arrays were grown with a similar procedure to that described in 3.2, using the Cu–catalyzed VLS process without dopants, but employing a degenerate p^+ substrate for the microwire growth. The resulting Si wires had diameters of 1.65–1.75 μm and heights of 90–97 μm (Figure 3.14). Four-point resistance and gate-dependent conductivity measurements demonstrated that the wires were nominally p-type, with resistivities of 200 ± 100 Ω-cm, corresponding to a N_a of ~ 5 x 10^{13} cm^{-3} (Figure 3.15). Thus, wires grown on degenerate p^+ substrates possessed similar electronic properties to those grown under the same conditions, on a n^+ substrate. Dopant atoms from the substrate were not expected to migrate a substantial distance into the wires, given that the wires were only held at high temperatures during their actual growth, for ~ 20 min.

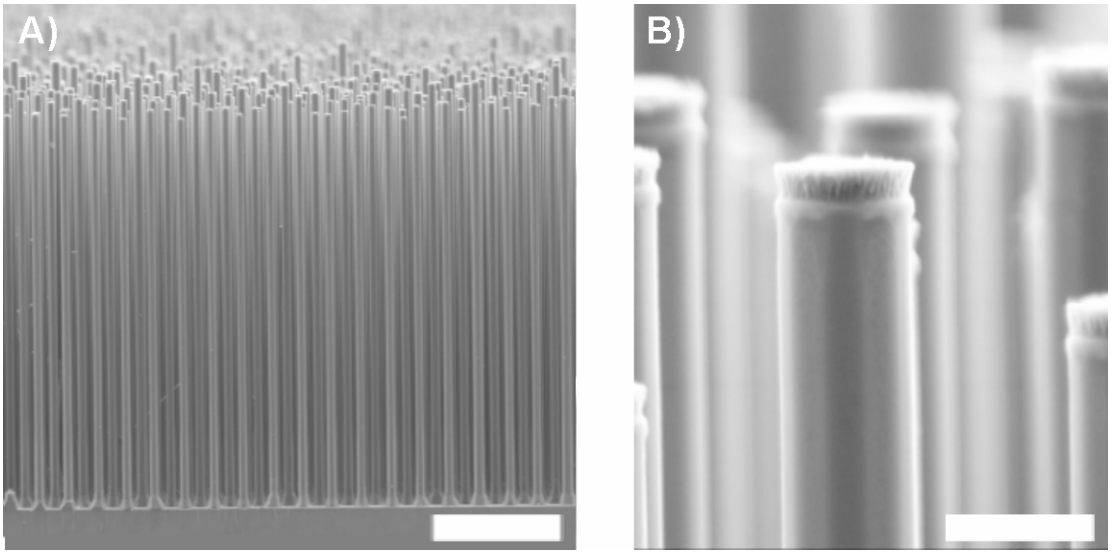

Figure 3.14. SEM images of undoped Si microwires grown on a p^+ substrate, with A) a side view of the microwire array, scale bar = 30 μm, and B) a magnified view of the top of an individual wire, scale bar = 2 μm.

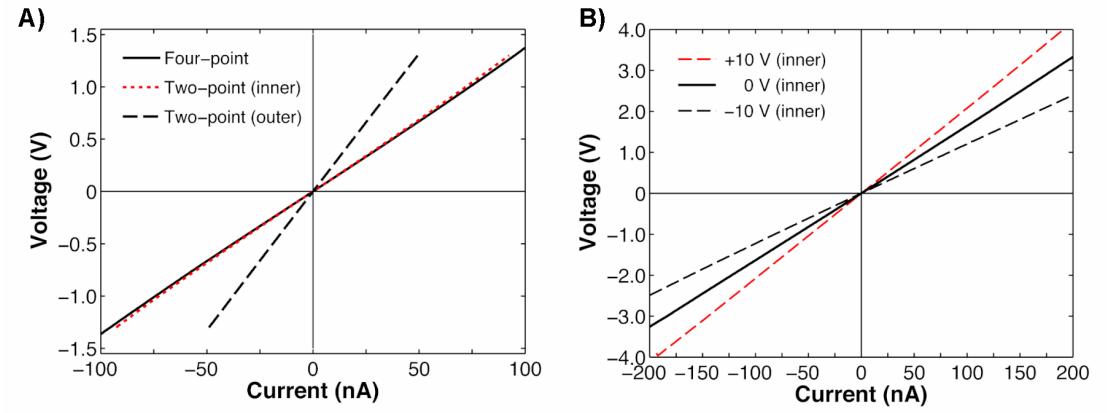

Figure 3.15. A) Two-point and four-point *I-V* behavior of an undoped Si microwire grown on an p^+ substrate and B) *I-V* behavior of the same Si microwire, with varying back-gate bias, indicating p-type doping

3.7 *J-E* response of undoped Si microwire arrays on a p^+ substrate: p^+-i-Si/$CoCp_2^{+/0}$–CH_3CN

Undoped Si microwires grown on planar p^+ substrates, with similar electronic properties to those grown on planar n^+ substrates, were subsequently measured for their photoelectrochemical performance. The wires arrays were initially measured in contact with the $CoCp_2^{+/0}$–CH_3CN redox system, which forms a high barrier-height contact to p-Si. The *J-E* performance of the p^+-i-Si microwire array electrodes in contact with 50 mM of $CoCp_2PF_6$/5.0 mM of $CoCp_2$ in acetonitrile under 100 mW cm^{-2} of ELH-type W halogen illumination is shown in Figure 3.16. The electrodes behaved as photocathodes in contact with the $CoCp_2^{+/0}$ redox couple, demonstrating V_{oc} = 421 ± 14 mV, J_{sc} = -10.9 ± 0.3 mA cm^{-2}, and fill factors, ff = 0.32 ± 0.02, with a photoelectrode energy-conversion efficiency η = 1.5 ± 0.1%. The planar p^+ substrates with the wires mechanically removed produced V_{oc} = 253 ± 1 mV, J_{sc} = -1.75 ± 0.11 mA cm^{-2}, and fill factors, ff = 0.27 ± 0.05.

The p^+-i-Si microwires in contact with $CoCp_2^{+/0}$–CH_3CN typically produced lower V_{oc} values than their n^+-i-Si/$Me_2Fc^{+/0}$ counterparts. This slight difference in the photoresponse could be attributed to slight differences in the effective surface

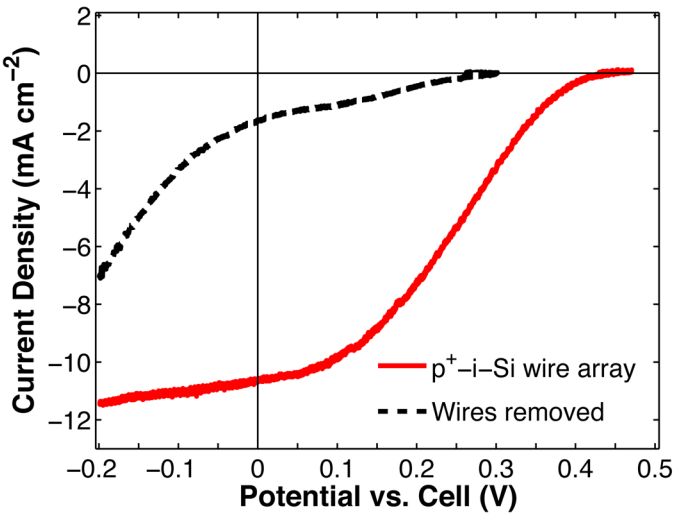

Figure 3.16. *J-E* performance of p^+-i-Si microwire arrays with and without the wires removed, in contact with the $CoCp_2^{+/0}$–CH_3CN redox system under 100 mW cm^{-2} of ELH-type W halogen illumination

recombination velocities for Si in contact with these redox couples, with previously measured $S \sim 20$ cm s^{-1} and $S \sim 55$ cm s^{-1} for Si in contact with the $Me_2Fc^{+/0}$–CH_3OH and $CoCp_2^{+/0}$–CH_3CN redox systems, respectively.[8] Even for planar n-type and p-type Si, the performance of the n-Si/$Me_2Fc^{+/0}$–CH_3OH electrochemical junction has typically produced higher V_{oc} values than the p-Si/$CoCp_2^{+/0}$–CH_3CN junction.[17-19] Recently, p-Si with a resistivity of ~ 0.24 Ω-cm in contact with $CoCp_2^{+/0}$–CH_3CN produced V_{oc} values of ~ 540 mV, while n-Si with the same resistivity measured in contact with $Me_2Fc^{+/0}$–CH_3OH has produced V_{oc} values of ~ 635 mV. In addition, redox couples with more negative electrochemical potentials, such as dimethylcobaltocene$^{+/0}$ in acetonitrile, have elicited higher V_{oc} values from p-Si, demonstrating that the cobaltocene redox system is not completely optimized to produce the maximum photoresponse in Si.

3.8 *J-E* response of lightly doped Si microwire arrays: n^+-i-Si/$CoCp_2^{+/0}$–MeCN and p^+-i-Si/$Me_2Fc^{+/0}$–CH_3OH

To further investigate the effect of altering both the contacting junction and the back contact, n^+-i-Si and p^+-i-Si microwire arrays were measured in contact with the $CoCp_2^{+/0}$–MeCN and $Me_2Fc^{+/0}$–CH_3OH redox systems, respectively. Figures 3.17 shows the response of these same electrodes under 100 mW^{-2} of ELH-type W halogen illumination and in the dark. These electrodes demonstrate no apparent photoresponse in contact with their respective redox systems, when the contacting junction and the back contact of the growth substrate were selective for the same carrier.

These combinations of electrochemical experiments and variation of the growth substrate demonstrated that the back contact of the array, in addition the electrochemical junction, ultimately determined the photoresponse of the wires. Kinetic asymmetries introduced into the device by the junction and the back contact were critical to achieve a photoresponse in the microwires, similar to previous observations with *p-i-n* type cells in contact with non-aqueous redox systems.

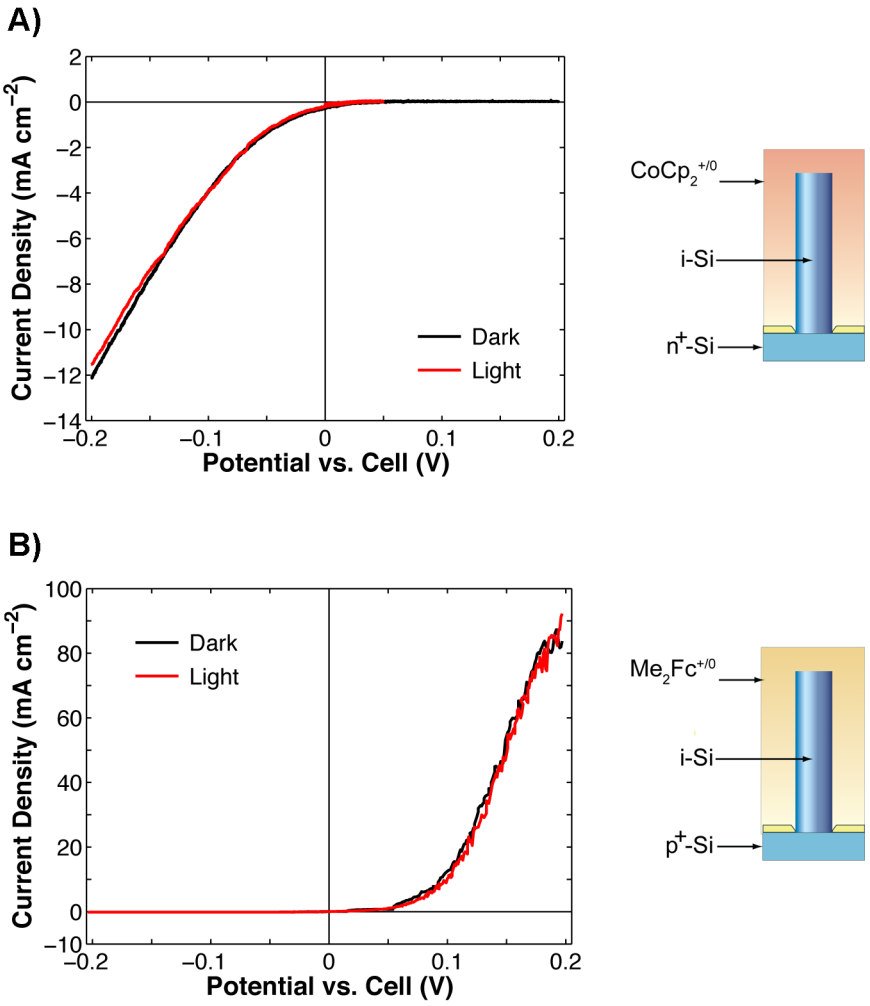

Figure 3.17. *J-E* performance of A) n^+-i-Si microwire arrays in contact with the $CoCp_2^{+/0}$–CH_3CN and B) p^+-i-Si microwire arrays in contact with the $CoCp_2^{+/0}$–CH_3CN under 100 mW cm^{-2} of ELH-type W halogen illumination and in the dark

Table 3.1. Figures of Merit of Undoped Si Microwire Array Cells				
	V_{oc} (mV)	J_{sc} (mA cm^{-2})	*ff*	Efficiency (%)
n^+-i-Si/ $Me_2Fc^{+/0}$–CH_3OH				
i-Si on n^+ substrate (ELH)	445 ± 13	12.8 ± 2.1	0.41 ± 0.03	2.3 ± 0.3
i-Si on n^+ substrate (808 nm)	436 ± 14	12.8 ± 2.1	0.58 ± 0.02	5.9 ± 1.0
Corrected i-Si on n^+ substrate	445 ± 13	12.9 ± 2.1	0.62 ± 0.04	3.5 ± 0.6
Wires Removed, n^+ substrate	7.5 ± 0.7	0.9 ± 0.01	0.34 ± 0.07	0.002 ± 0.003
p^+-i-Si/ $CoCp_2^{+/0}$–MeCN				
i-Si on p^+ substrate (ELH)	421 ± 14	-10.9 ± 0.3	0.32 ± 0.02	1.5 ± 0.1
Wires Removed, p^+ substrate	253 ± 1	-1.75 ± 0.11	0.27 ± 0.05	0.11 ± 0.01
p^+-i-Si/ $Me_2Fc^{+/0}$–CH_3OH				
i-Si on p^+ substrate (ELH)	-0.14 ± .07	-0.10 ± 0.03		
i-Si on p^+ substrate (dark)	-0.42 ± .09	-0.17 ± 0.04		
n^+-i-Si/ $CoCp_2^{+/0}$–MeCN				
i-Si on n^+ substrate (ELH)	0	0.02 ± 0.01		
i-Si on n^+ substrate (dark)	0	0.04 ± 0.02		

3.9 Experimental methods

3.9.1 Reagents

For the cobaltocene electrochemical cell, acetonitrile (99.8% anhydrous, Sigma-Aldrich) was purified first by sparging with nitrogen for 15 minutes, and then by passing the solvent under nitrogen pressure through a column of activated A2 alumina (Zapp's). Bis(cyclopentadienyl)cobalt(II) ($CoCp_2$, 98%, Strem) was purified by vacuum sublimation at 65 °C. Cobaltocenium hexafluorophosphate (Cp_2CoPF_6, 98%, Sigma-Aldrich) was recrystallized from an ethanol/acetonitrile mixture (ACS grade, EMD) and dried under vacuum. Water was obtained from a Barnstead Nanopure system and had a resistivity of 18.3 MΩ-cm. VLS–catalyzed Si microwire arrays were grown on both n^+- and p^+-Si (111)-oriented substrates, employing degenerately doped n^+-Si substrates with ρ ~ 0.001–0.004 Ω-cm and 450 nm of thermal oxide (University Wafer) and p^+-Si substrates with ρ ~ 0.001–0.005 Ω-cm and 500 nm of thermal oxide (International Wafer Service). Reagents for the 1,1′-dimethylferrocene (Me_2Fc)–MeOH cell were prepared and used as described in

Appendix A.

3.9.2 VLS–catalyzed Si microwire growth

Arrays of square– or hexagonally–packed Si microwires were grown on planar n^+- and p^+-Si(111) substrates using the vapor–liquid–solid (VLS) growth method with a Cu catalyst (6N, EPSI) and without dopants. A positive photoresist (Microchem S1813) was used to pattern the degenerately doped growth wafers with 3 μm diameter circular holes, with a 7 μm center–to–center spacing, in a square or hexagonal array. The exposed thermal oxide was etched in buffered HF(aq) (BHF, Transene Inc.) for 5 min. Immediately following the HF etch, 450–750 nm of Cu was thermally evaporated onto the patterned growth substrate. Lift-off proceeded in acetone, and the patterned wafers were then cleaved into 1.3 x 2.0 cm pieces. To perform VLS growth, the samples were annealed in a tube furnace at 1000º C for 20 min with 500 sccm of H_2 (Research grade, 'Alpha Gaz 2', Air Liquide) at atmospheric pressure. Wire growth was induced by introduction of $SiCl_4$ (6N, Strem) in 50 sccm of H_2 (Research grade, 'Alpha Gaz 2', Air Liquide) into the reactor for 20–45 min. After VLS growth, the Cu growth catalyst was removed by a 5 s BHF etch, immediately followed by an etch in 6:1:1 (by volume) of H_2O:HCl:H_2O_2 at 70º C (RCA 2) for 15 min. This BHF/RCA2 procedure was repeated an additional time, to ensure that all of the metal catalyst had been removed ('BHF/RCA2 x 2'). The removal of the metal catalyst was subsequently confirmed by SEM. Prior to photoelectrochemical measurements, the Si wire arrays were etched for 5 s in 5% HF(aq), rinsed with > 18 MΩ-cm resistivity H_2O, and dried thoroughly under a stream of N_2(g).

3.9.3 Four-point resistance and gate-dependent measurements

Four-point resistance measurements were performed as described previously.[20] After removal of the VLS catalyst, an area of 3 x 3 mm of Si microwires was mechanically removed from the growth substrate with a razor blade, and the microwires were suspended in isopropanol. The wires were then spin-coated onto a silicon wafer that had been coated with 300 nm of Si_3N_4 (University Wafer). Four-point contacts with an 30 μm and 60 μm inner and outer spacing, respectively, were patterned on individual wires using a lift-off

resist (LOR10A, Microchem) and a positive photoresist (S1813, Microchem). Immediately following a 5 s BHF etch, 800 nm of Al (5N, Kurt J. Lesker) and 200 nm of Ag (4N, Kurt J. Lesker) were deposited by electron-beam evaporation onto the patterned wafer, to form ohmic contacts to the wires. The conductivity of the wires was measured with varying gate bias potentials, typically between -10 V and +10 V, to determine the carrier type in the wires. For each wire growth, at least ten wires were measured. The resistivities of wires from the arrays measured for their *J-E* performance are provided in the main article.

3.9.4 Single-wire conductivity measurements under illumination

PECVD *a*-SiN_x:H deposition. The Cu VLS growth catalyst was initially removed through the standard BHF/RCA2 x 2 cleaning procedure and KOH etch. The Si microwire arrays were further cleaned for 15 min in 6:1:1 by volume H_2O:H_2O_2 (30 % in H_2O):conc. aq. NH_3OH at 70 °C (RCA 1), followed by a 5 s BHF etch, and then by 15 min etch in RCA 2. The arrays were then etched for 5 s in BHF, rinsed in H_2O, and dried before immediately placing under vacuum in the PECVD chamber. To ensure uniform deposition over the array, the Si microwire array chip was surrounded on each side by planar Si chips in the deposition chamber. The low-stress PECVD *a*-SiN_x:H was grown from SiH_4 (5% in N_2) and NH_3 at 350ºC, with a deposition time of ~ 25 min.

Mounting wax infill. The wire array sample was initially mounted on a glass slide using a small amount of mounting wax (Quickstick 135, South Bay Technology) at ~ 150ºC on a hot plate, to provide a stable handle for the array during processing. The sample remained at 150°C on the hot plate, and small chips of mounting wax (Quickstick 135, South Bay Technology) were melted into the array. Excess wax was placed in the array, to ensure that the wires were completely infilled with the polymer, and the sample was allowed to rest on the hot plate for at least 10 min, to allow air to escape from the array. The excess wax was removed from the array by gently applying lens paper to the array (Thorlabs), and placing a glass slide (1” x 3”) evenly on top of the array. This process was repeated multiple times, until a newly applied piece of lens paper did not absorb any wax. The sample was then placed on a clean glass slide, without any additional mounting wax.

Due to local variations in the heights of wires by ± 2.5 μm, the lowest wires were completely covered in wax, while the tallest wires in close proximity were fully exposed. To remove residual mounting wax from the surface of the wires, the sample on the glass slide was subsequently etched in an O_2 plasma (400 W, 300 mTorr) for ~ 5 min. The array was subsequently removed from the glass slide (should not be attached), and etched in BHF for ~ 5 min, to remove the exposed *a*-SiN_x:H. The mounting wax was then removed in acetone, and residual organics were removed by a 20 min piranha etch (3:1 aq. conc. H_2SO_4:H_2O_2).

The wires were subsequently removed from the growth substrate and single-wire measurements were made as described previously in 3.9.3., but using a different lithographic mask to define two-point contacts. The illumination was provided by a ELH-type W halogen lamp without a diffuser, but was uncalibrated, with the lamp's output ~ 5 inches from the device.

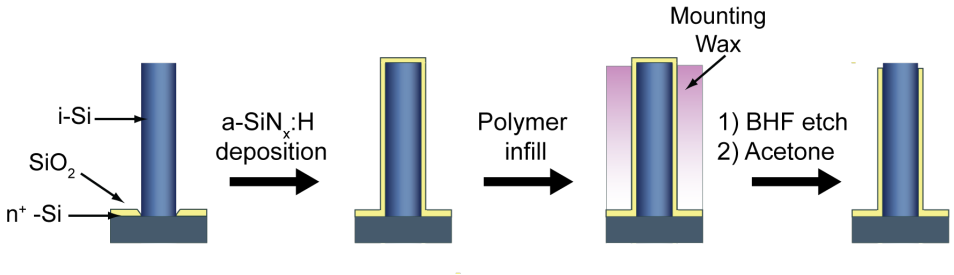

Figure 3.18. Schematic of the fabrication of *a*-SiN_x:H coated Si microwire arrays

3.9.5 Electrode fabrication

Arrays of Si microwires were cleaved into ~ 4 x 4 mm samples, to fabricate multiple electrodes for photoelectrochemical measurements. The electrodes were made as described in Appendix A, for both electrodes measured in the $CoCp_2^{+/0}$–CH_3CN and $Me_2Fc^{+/0}$–CH_3OH electrochemical cells. Prior to electrochemical measurements, the electrodes were placed for 4 h in an oven heated to 70º C, to further cure the epoxy to obtain enhanced chemical stability in both the CH_3OH and CH_3CN solutions. Electrode

areas were ~ 0.03 cm^2, as measured using a high-resolution scanner and Adobe Photoshop software.

3.9.6 Photoelectrochemical measurements

All non-aqueous photoelectrochemical *J-E* measurements were performed with bottom illumination in air-tight, flat-bottomed glass cells. The $Me_2Fc^{+/0}$–CH_3OH electrolyte solution consisted of 200 mM of Me_2Fc, 0.4 mM of Me_2FcBF_4, and 1.0 M $LiClO_4$ in 30 mL of methanol. The cell was assembled and sealed under an inert atmosphere (< 10 ppm O_2) before being placed under positive Ar pressure outside of the N_2 box. A methanol bubbler was used to prevent evaporation of the solution during an Ar purge. The three-electrode cell consisted of a high-area Pt mesh as the counter electrode, a Pt wire in a Luggin capillary filled with the cell's solution as the reference electrode, and a Si working electrode. The solution potential versus the reference was continuously monitored using a 4-digit voltmeter (Keithley), and deviated from the reference by < 10 mV. *J-E* measurements were obtained at a scan rate of 5 mV s^{-1}.

The $CoCp_2^{+/0}$–CH_3CN electrolyte solution consisted of 50 mM of $CoCp_2PF_6$, 5.0 mM of $CoCp_2$, and 1.0 M $LiClO_4$ in 20 mL of acetonitrile. The cell was assembled and utilized under an inert, dry atmosphere (< 0.50 ppm O_2; 0.5 ppm H_2O). The three-electrode cell consisted of a high-area Pt mesh as the counter electrode, a Si working electrode, and a Pt wire in the bulk of the solution as the reference electrode. A Luggin capillary was not used for as reference, due to the instability and relatively low concentrations of $CoCp_2$ present in the cell. The *J-E* measurements were obtained at a scan rate of 30 mV s^{-1}, to limit the solution absorption from the generated $CoCp_2$ species at the working electrode.

Both the $Me_2Fc^{+/0}$–CH_3OH and $CoCp_2^{+/0}$–CH_3CN cells were illuminated using ELH-type W halogen solar simulation. The incident light intensity was calibrated using a Si photodiode that was placed in the solution at the position of the working electrode. The light intensity was adjusted until the short-circuit photocurrent density on the Si diode was the same as the value produced by 100 mW cm^{-2} of AM 1.5G illumination.

To reduce concentration overpotential losses within the $Me_2Fc^{+/0}$–CH_3OH cell and demonstrate the validity of corrections for these losses, 40 mM Me_2FcBF_4 was added to the cell. A 1 W 808 nm diode laser (Thorlabs) was used as the illumination source, and *J-E* data were collected by matching the J_{sc} value to the value of J_{sc} that was obtained under simulated 1 Sun's illumination. This process required ~ 55 mW cm^{-2} of 808 nm illumination, as measured by a calibrated photodiode placed in the working electrode's position within the electrochemical cell.

Prior to photoelectrochemical measurements, the Si wire arrays were etched for 5 s in 5% HF(aq), rinsed with > 18 MΩ-cm resistivity H_2O, and dried thoroughly under a stream of N_2(g). The electrochemical cells were vigorously stirred during *J-E* measurements. Data were collected and averaged for seven wire array samples, for both wire array photoelectrodes tested in $Me_2Fc^{+/0}$ and $CoCp_2^{+/0}$ electrochemical cells.

3.9.7 Corrections of *J-E* data

Corrections for the concentration overpotential and series resistance losses were performed according to eq. A.1 and A.2, as described in Appendix A. The limiting anodic current density was 72 mA cm^{-2} and the limiting cathodic current densities were 0.15 and 15 mA cm^{-2}, for 0.4 mM and 40 mM Me_2FcBF_4, respectively. The measured value of R_s was dependent on the placement of the Pt working electrode with respect to the Luggin capillary, and typically varied from 40–300 Ω. A value of R_s = 50 Ω was used in the calculations to avoid overcorrection of the data, resulting in conservative values for the intrinsic fill factor and efficiencies of the Si microwire photoelectrodes in contact with $Me_2Fc^{+/0}$–CH_3OH.

3.10 References

1. A. Luque and S. Hegedus, eds., *Handbook of Photovoltaic Science and Engineering*, Wiley, Chichester, 2003.

2. R. F. Pierret, *Advanced Semiconductor Fundamentals*, Pearson Education, Upper Saddle River, 2003.
3. R. M. Swanson, S. K. Beckwith, R. A. Crane, W. D. Eades, Y. H. Kwark, R. A. Sinton and S. E. Swirhun, *IEEE Trans. Electron Dev.*, 1984, **31**, 661-664.
4. R. A. Sinton, Y. Kwark, S. Swirhun and R. M. Swanson, *IEEE Electron Dev. Lett.*, 1985, **6**, 405-407.
5. R. A. Sinton, Y. Kwark, J. Y. Gan and R. M. Swanson, *IEEE Electron Dev. Lett.*, 1986, **7**, 567-569.
6. A. Kumar and N. S. Lewis, *Appl. Phys. Lett.*, 1990, **57**, 2730-2732.
7. M. X. Tan, C. N. Kenyon, O. Kruger and N. S. Lewis, *J. Phys. Chem. B*, 1997, **101**, 2830-2839.
8. F. Gstrein, D. J. Michalak, W. J. Royea and N. S. Lewis, *J. Phys. Chem. B*, 2002, **106**, 2950-2961.
9. M. D. Kelzenberg Ph.D., *Silicon Microwire Photovoltaics*, California Institute of Technology, Pasadena, 2010.
10. J. M. Foley, M. J. Price, J. I. Feldblyum and S. Maldonado, *Energy Environ. Sci.*, 2012, **5**, 5203-5220.
11. W. J. Royea, D. J. Michalak and N. S. Lewis, *Appl. Phys. Lett.*, 2000, **77**, 2566-2568.
12. P. E. Laibinis, C. E. Stanton and N. S. Lewis, *J. Phys. Chem.*, 1994, **98**, 8765-8774.
13. M. D. Kelzenberg, D. B. Turner-Evans, M. C. Putnam, S. W. Boettcher, R. M. Briggs, J. Y. Baek, N. S. Lewis and H. A. Atwater, *Energy Environ. Sci.*, 2011, **4**, 866-871.
14. N. S. Lewis and M. L. Rosenbluth, in *Photocatalysis: Fundamentals and Applications*, eds. N. Serpone and E. Pelizzetti, Wiley Interscience, New York, 1989, pp. 45-121.
15. E. L. Warren, S. W. Boettcher, M. G. Walter, H. A. Atwater and N. S. Lewis, *J. Phys. Chem. C*, 2011, **115**, 594-598.
16. S. W. Boettcher, E. L. Warren, M. C. Putnam, E. A. Santori, D. Turner-Evans, M. D. Kelzenberg, M. G. Walter, J. R. McKone, B. S. Brunschwig, H. A. Atwater and N. S. Lewis, *J. Am. Chem. Soc.*, 2011, **133**, 1216-1219.

17. M. L. Rosenbluth and N. S. Lewis, *J. Amer. Chem. Soc.*, 1986, **108**, 4689-4695.

18. M. L. Rosenbluth and N. S. Lewis, *J. Phys. Chem.*, 1989, **93**, 3735-3740.

19. R. L. Grimm, M. J. Bierman, L. E. O'Leary, N. C. Strandwitz, B. S. Brunschwig and N. S. Lewis, 2012, *In Press*.

20. M. D. Kelzenberg, D. B. Turner-Evans, B. M. Kayes, M. A. Filler, M. C. Putnam, N. S. Lewis and H. A. Atwater, *Nano Lett.*, 2008, **8**, 710-714.

Chapter 4

OPTIMIZATION OF THE PHOTOANODIC PERFORMANCE OF UNDOPED SI MICROWIRES

Summary

To improve the device performance of the undoped Si microwire arrays, strategies were employed to reduce the junction area of the photoelectrochemical devices, and to remove the potentially deleterious Si/Cu interfacial region at the tops of the microwires. To improve the V_{oc} of the device, the junction area of the device was decreased by employing *a*-SiN_x:H and thermal oxide passivation along the side walls of the wires, to create wires with partial and full axial junctions. The resulting axial devices in contact with $Me_2Fc^{+/0}$–CH_3OH typically showed a decrease in both photocurrent and photovoltage, and further investigation is required to understand the trade-off between increasing the V_{oc} of the device and maximizing the carrier-collection efficiency. One particular sample of undoped Si microwires with thermal oxide passivation at the bottom of the wires produced large V_{oc} values exceeding 500 mV, demonstrating that these wires were operating under high-level injection conditions. The interfacial region located at the top of the wire was also removed by mechanical polishing, and the resulting wire arrays showed increases in both the J_{sc} and V_{oc}, with photovoltages again exceeding 500 mV. Thus, the interfacial region was indeed limiting the performance of i-Si photoelectrodes, as a region of low lifetime located at the top of the wires.

In addition, radial p^+ emitters were fabricated on n^+-i-Si microwire arrays, and the resulting junctions were measured in contact with the $Me_2Fc^{+/0}$–CH_3OH redox system and other redox systems. In particular, these arrays with deposited Pt catalyst attained photoelectrode efficiencies for the oxidation of HI to I_2/I_3^- of ~ 3.5%, making these buried junction arrays promising for use as photoanodes in fuel–forming reactions.

4.1 Introduction and motivation

Although radial junctions allow for enhanced carrier-collection efficiency in materials with short diffusion lengths, the photovoltage of structured semiconductors with radial junctions is expected to decrease relative to that of planar devices, given the increase in junction area. The dilution of the photogenerated carrier flux over an increased junction area results in a reduction in the quasi-Fermi level splitting, and therefore a lower V_{oc} value. This relationship between the increase in geometric area and the expected V_{oc} is expressed by eq. 4.1,

$$V_{oc} = \frac{nkT}{q} \ln\left(\frac{J_{ph}}{\gamma J_0}\right) \tag{4.1}$$

where n is the diode quality factor, k is the Boltzmann constant, T is the temperature, q is the unsigned charge on an electron, J_{ph} is the photocurrent density, J_o is the exchange current density, and γ is the ratio of the actual junction area to the projected surface area of the device.[1-4] Thus, for every 10-fold increase in junction area, the generated photovoltage of the electrochemical devices is expected to decrease by at least 59 mV, for devices with $n \sim 1.0$. Such a relationship has been confirmed in measurements of

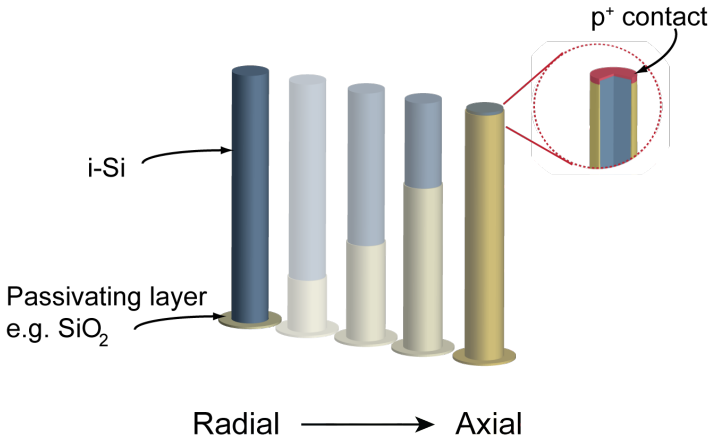

Figure 4.1. Schematic of the progression from a radial to axial wire junction, using variable coverage of surface passivation, including thermal SiO_2 and *a*-SiN_x:H

macroporous n-Si in contact with the $Me_2Fc^{+/0}$–CH_3OH, demonstrating the trade-off between an increase in the carrier-collection efficiency and a decrease in the photovoltage in structured devices.

The undoped Si microwire arrays, as typically grown, possess heights of ~ 75 μm and diameters of ~ 2.5 μm in a hexagonal array, resulting in a geometric enhancement γ ~ 5.6; this enhancement of the junction area should correspond to an expected decrease in the V_{oc} of ~ 45 mV and ~ 89 mV, for diode quality factors n of 1.0 and 2.0, respectively. This calculation does not take into account the concentration of light into the wires in an array, which would serve to mitigate the expected decrease in V_{oc} with structuring.[5] However, it is clear that fabricating wires with a more axial junction should increase the expected photovoltage, within the limit that the photogenerated carriers can still be collected. Thus, n^+-i-Si microwire arrays with both thermal oxide (SiO_2) and silicon nitride (a-SiN_x:H) passivation on the sides of the wires were fabricated, to create devices with more axial junctions (Figure 4.1). The *J-E* performance of these arrays was subsequently measured in contact with $Me_2Fc^{+/0}$–CH_3OH.

The presence of an interfacial Si/Cu region (Figure 4.2) at the tops of the wires may also be limiting the *J-E* performance and the carrier-collection efficiency of the

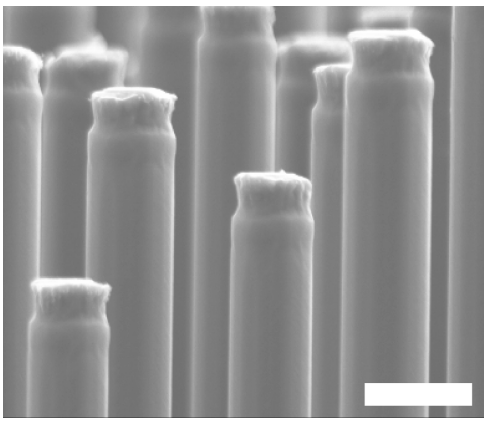

Figure 4.2. SEM image of a Si microwire array after the BHF/RCA2 catalyst removal procedure, with the wires displaying a prominent Si/Cu interfacial region of ~ 800 nm in thickness, scale bar = 2 μm

undoped Si microwire photoanodes. This region was consistently present on wires grown in the Dorothy reactor, and varied in thickness from ~ 50–800 nm. This region was removed through the chemical–mechanical polishing of the tops of the wires in an array and the *J-E* performance of the polished microwire arrays was subsequently measured in the $Me_2Fc^{+/0}$–CH_3OH system.

In addition, radial p^+ emitters were fabricated on n^+-i-Si microwire arrays, to produce optimized photoanodes to perform fuel–forming reactions such as the production of H_2 and I_2/I_3^- from HI. Previous work on radial junction p^+n-Si microwire arrays has shown that these arrays demonstrated improved efficiencies as photocathodes for the reduction H^+ to H_2, as compared to p-Si microwire photocathodes.[3] The formation of a metallurgical junction in the wires, as opposed to the formation of a semiconductor/liquid junction or a pinned semiconductor/metal junction with the deposited catalyst, resulted in a high photovoltage in the device that was decoupled from the energetics of the solution.[6] The emitter also provided an ohmic contact to the deposited Pt metal catalyst, enabling the fabrication of higher efficiency devices. The understanding gained in the use of n^+p-Si microwire arrays for fuel–forming reactions can subsequently be applied to the photoanode, where n^+-i-Si microwire arrays with diffused p^+ emitters can be employed.

4.2 *J-E* response of thermally oxidized, undoped Si microwire arrays

To both decrease the junction area of the electrochemical Si microwire device and remove the interfacial region at the top of the wires, arrays of undoped Si microwires with SiO_2 'boots' were fabricated. As described in previously in Chapter 2.8, after a standard catalyst removal procedure and subsequent KOH etch, the undoped Si microwire arrays were thermally oxidized at 1070–1100ºC for > 1.5 hr, to produce a thermal oxide with a thickness of ~ 200 nm, as measured by SEM. To selectively etch the oxide at the tops of the wires, a PDMS polymer mask was infilled into the array at a height of ~ 10 μm from the base of the wires. The exposed Si oxide was subsequently etched in buffered HF, resulting in wire arrays with oxide passivation at the bottom of the wires (Figure 4.3A).

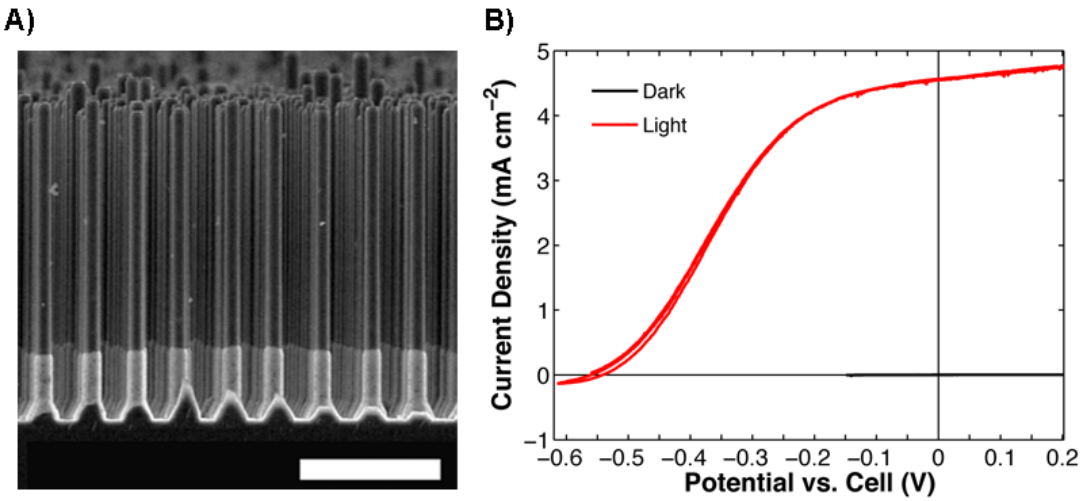

Figure 4.3. A) SEM image of the undoped Si microwire array on an n^+ substrate, with a thermal oxide 'boot,' scale bar = 20 μm. *SEM image from Nick Strandwitz.* B) *J-E* behavior of the wire arrays shown in Figure 3A, with thermal oxide boots, in contact with $Me_2Fc^{+/0}$–CH_3OH under 1 Sun's ELH-type illumination and in the dark

Current density vs. potential (*J-E*) measurements of the undoped Si microwire arrays with SiO_2 passivating boots were measured in contact with 200 mM Me_2Fc-0.4 mM Me_2FcBF_4 in CH_3OH under 100 mW cm^{-2} of simulated 1 Sun's ELH-type illumination (Figure 4.3B). The Si wire array electrodes demonstrated V_{oc} = 563 ± 17 mV, J_{sc} = 4.28 ± 0.74 mA cm^{-2}, and fill factors, *ff* = 0.35 ± 0.06, with a photoelectrode energy-conversion efficiency η = 0.83 ± 0.12%. With the thermal oxide boot, the wire array electrodes displayed large photovoltages, with V_{oc} values more than 100 mV higher than typically measured for undoped wire arrays in contact with the $Me_2Fc^{+/0}$–CH_3OH system. This increase in photovoltage may be attributed to several factors, including the formation of an insulating layer between the degenerate growth substrate and the redox solution; the decrease in the geometric enhancement from $\gamma \sim 8.6$ to 6.9 (~ 14 mV expected increase, assuming n = 2.41); and potential improvement in the bulk properties of the wires with thermal oxidation.

The same electrodes were also measured at varying light intensities, under 808 nm illumination from ~ 0.11 to 2.7 Suns (Figure 4.4). The array showed diode quality factors n = 2.41 ± 0.35 (Figure 4.5). As shown for other undoped Si microwire arrays, the *ff* reached a

maximum value at ~ 0.25 Sun's illumination intensity, and subsequently decreased at higher light intensities due to the parasitic R_s of the electrochemical cell.

Unfortunately, multiple attempts to repeat this result fell short, with the arrays of undoped wires with SiO_2 boots producing both lower V_{oc} and J_{sc} values as well as more resistive devices, as compared to as-grown undoped wires (Figure 4.6). For this particular wire array, the as-grown wires produced V_{oc} = 395 ± 19 mV, J_{sc} = 13.9 ± 0.8 mA cm^{-2}, and *ff* = 0.36 ± 0.03, while the portion of the array with thermal oxide boots produced V_{oc} = 374 ± 10 mV, J_{sc} = 11.0 ± 2.0 mA cm^{-2}, and *ff* = 0.32 ± 0.03. It is likely that the initially high V_{oc} values can be attributed to an improvement of the material properties of the wires themselves, with potential gettering of Cu within the wire and the removal of the top interfacial region with thermal oxidation. The decrease in junction

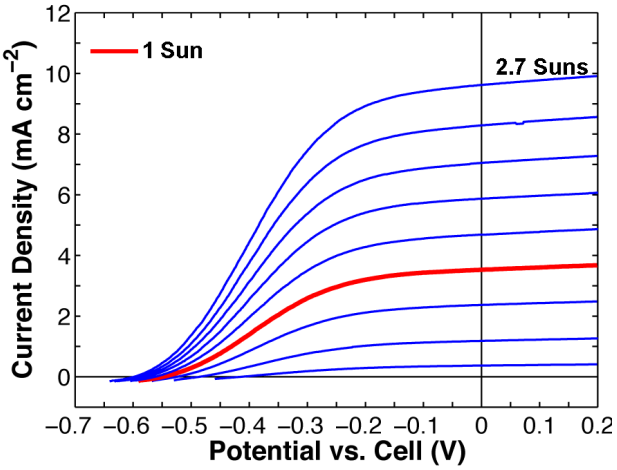

Figure 4.4. *J-E* data at various light intensities under 808 nm illumination for a representative 'booted' n^+-i-Si microwire array photoelectrode measured in contact with 200 mM Me_2Fc/0.4 mM Me_2FcBF_4 in methanol

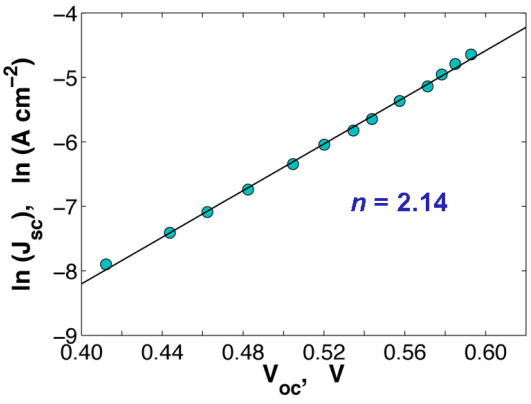

Figure 4.5. The corresponding natural logarithm of the short-circuit photocurrent density vs. the open-circuit photovoltage for the n^+-i-Si microwire array photoelectrode with a thermal oxide boot, yielding a diode quality factor of A = 2.14. *Experiment conducted by Nick Strandwitz*

area should result in modest increases in V_{oc} (~ 15 mV). In addition, all of the electrodes with thermal oxide boots displayed lower dark currents in reverse bias than as-grown Si microwires, attesting to the formation of an insulating barrier between the degenerate substrate and the conformal electrochemical contact. Further attempts to repeat this promising result should focus on improving and monitoring the quality of the dry thermal oxide, as well as potentially growing thicker thermal oxides, on the order of ~ 200 nm. In particular, annealing a dry thermal oxide in Ar has been shown to improve decrease its surface recombination velocity and was standard procedure in the fabrication of Si point-contact cells.[7, 8] From single-wire measurements, the effective diffusion length of radial junction n^+p-Si microwires with SiO_2 diffusion barriers improved by annealing the grown oxide under Ar.[9]

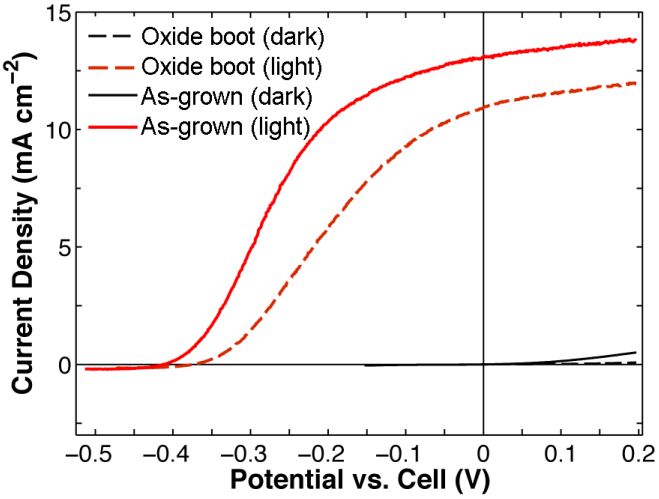

Figure 4.6. The typical *J-E* behavior of an array of n^+-i-Si microwires, with and without a thermal oxide boot, measured in contact with $Me_2Fc^{+/0}$–CH_3OH

4.3 *J-E* response of undoped Si microwire arrays with axial *a*-SiN_x:H passivation

To improve the photovoltage of n^+-i-Si microwire arrays, more axial devices were fabricated, through passivation of the length of the wire with *a*-SiN_x:H. In contrast to the dry thermal oxide, the PECVD SiH_x:H films deposited on Si microwires area expected to create a highly passivated surface with a low surface recombination velocity. The wires with axial passivation using *a*-SiN_x:H were fabricated as described in Chapter 3, using mounting wax as a mask for the chemical etching of the deposited *a*-SiH_x:H films. Figure 4.7A shows an array of n^+-i-Si microwires, with 1–3 μm of exposed Si surface at the tops of the wires, and the remaining length of the wire and substrate coated with an *a*-SiN_x:H film. A control array with an almost fully radial junction was also measured for comparison, with *a*-SiN_x:H passivation on ~ 5 μm of the bottom length of the wire and on the substrate (Figure 4.7B).

The *J-E* behavior of these wire arrays is shown in Figure 4.8. These undoped wires with a full axial junction demonstrated significantly reduced photocurrents, with J_{sc} ~ 2 mA cm^{-2}, while the control wires with a more radial junction displayed a *J-E* response similar to that typically produced by as-grown n^+-i-Si microwire arrays. The axial devices were also significantly more resistive than the radial devices, consistent with the relatively high resistance of the wires and the increased distance that a collected carrier must traverse to be collected at the top of the wire. The increase in the observed resistance of the device might also be attributed to the lack of a high concentration of holes along the length of the wire, with the passivation of the surface insulating the wire from the $Me_2Fc^{+/0}$–CH_3OH contact. Further investigations are warranted to fully understand the source of the observed increase in resistance. Certainly, within these wires, the effective carrier-collection length was less than the total length of the wire (~ 50 μm), due to the significant loss in photocurrent with the formation of the axial junction. From this experiment, it is unclear whether the wires have a diffusion length shorter than the approximate length of the wire, or whether the Si/Cu interfacial region at the top of the wire severely diminished the carrier-collection efficiency, as a region of lower lifetime than the bulk lifetime of the wire.

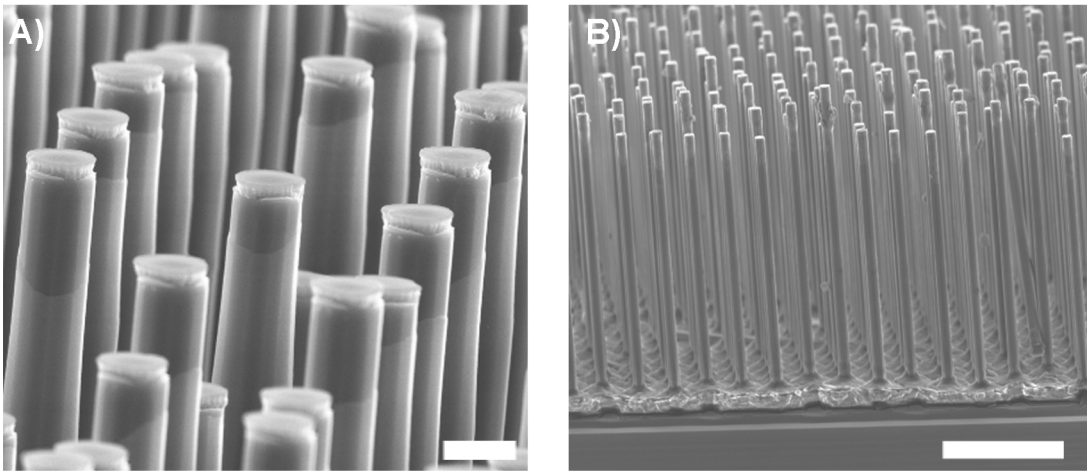

Figure 4.7. SEM images of the n^+-i-Si microwire array with a-SiNx:H surface passivation A) almost to the tops of the wires to form a full axial junction, and B) covering the bottom 5 μm of the wires, with PEVA at the bottom of the array, for an almost fully radial junction. Scale bars = 2 μm and 20 μm, respectively.

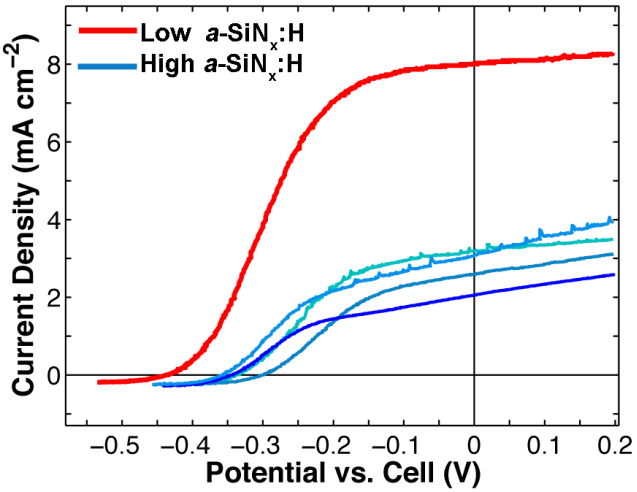

Figure 4.8. *J-E* performance of the two n^+-i-Si microwire arrays shown in Figure 4.7, with high coverage and low coverage of *a*-SiN_x:H along the length of the wires, in contact with $Me_2Fc^{+/0}$–CH_3OH

4.4 Removal of the interfacial region through mechanical polishing

To preferentially remove the top of the wires, arrays of Si microwires were fully infilled with mounting wax (Quickstick 135, South Bay Technology) and hand polished, ultimately removing several microns of Si from the top of the array. For a particular Si microwire array growth, after removing the Cu catalyst, the array was cleaved in half length-wise, and half of the array was reserved for control photoelectrodes. The other portion of the array was fully infilled with mounting wax just to the tops of the wires (Figure 4.9), as previously described for the fabrication of axial junction wires with *a*-SiN_x:H passivation. This wax provided mechanically support for the wires, in addition to selectively exposing the tops of the wires for polishing. The wires were then polished by hand, using a polishing cloth and Al_2O_3 power suspensions with decreasing sizes, from 3–0.3 μm, ultimately finishing with a chemical–mechanical polish of 0.02–0.06 μm colloidal silica (SBT, South Bay Technology). The wax was subsequently removed using acetone, followed by a piranha etch to remove all residual organics.

This method was favored over employing chemical etches, which are not typically anisotropic for the <111> face of Si due to its higher relative stability. In particular, KOH preferentially etched the 100 and the 110 faces of Si,[10, 11] while etches for Si

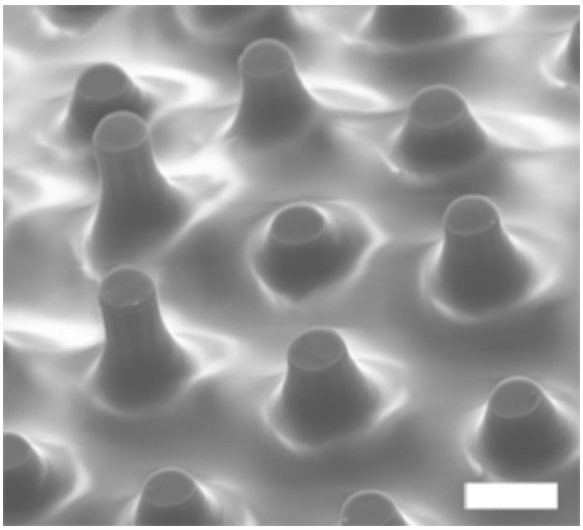

Figure 4.9. SEM image of a wire array with a mounting wax infill, without plasma etching in O_2, scale bar = 3 μm

defects, such as the Secco etch using HF/Cr(VI), created etch pits along the length and at the base of the wires.[1] Also, hand polishing was favored over using a polishing wheel for several reasons. First, the high filling fraction of wax within the array made polishing on a wheel challenging, as the array would tend to 'stick' to the lapping films and immediately destroy a nicely polished surface. To ameliorate this problem, harder waxes (Crystalbond 590, Ted Pella) that could still be removed with solvent were employed, though still unsuccessfully. Second, a precision of on the order of microns is required to uniformly polish a sample of Si microwires, and could not be attained on the polishing wheel. The process was further complicated by the non-uniformity of wire heights over an array, such that the tallest wires would have a considerable amount of material removed and the shortest wires would not be polished at all.

Through hand polishing, ~ 5 μm of material was removed from the top of the array, resulting in arrays with locally uniform heights. The amount of material removed from each wire varied, given their initial heights. As grown, wires in close proximity vary in heights by ± 2–3 μm; thus, a considerable amount of material was removed from the tallest wires, while the shortest wires were only slightly polished. Some portions of the polished arrays still possessed wires with the interfacial region (Figure 4.10).

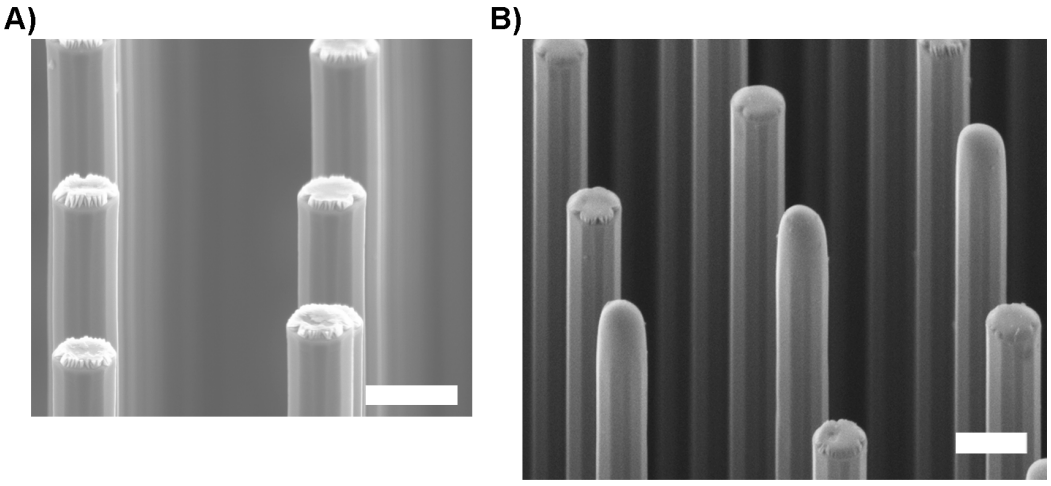

Figure 4.10. SEM images of the same array of Si microwires A) prior to polishing, displaying an interfacial layer at the top of the wires, and B) after polishing

[1] Chromium is also one of the top contaminants of concern found in Superfund sites in the United States and Cr(VI), in particular, is extremely toxic and a known carcinogen. I drew the line.

Moreover, the most highly polished wires were rounded at the top, due to the higher polishing rate of the surrounding wax relative to that of the Si.

The *J-E* behavior of both the polished and control n^+-i-Si microwire array was measured in contact with 200 mM Me_2Fc-0.4 mM Me_2FcBF_4 in CH_3OH under 100 mW cm^{-2} of simulated 1 Sun's ELH-type illumination (Figure 4.11). The polished Si wire array electrodes demonstrated V_{oc} = 523 ± 5 mV, J_{sc} = 10.8 ± 0.9 mA cm^{-2}, and *ff* = 0.37 ± 0.02, while the unpolished, control electrodes produced V_{oc} = 420 ± 10 mV, J_{sc} = 8.6 ± 0.4 mA cm^{-2}, and *ff* = 0.39 ± 0.01. The measured photoresponse of the as-grown control was consistent with what has been previously measured for undoped Si microwires with heights of ~ 70 μm.[12] However, the measured photovoltage of the polished electrodes greatly exceeded the V_{oc} values of all n^+-i-Si electrodes that had been previously measured, definitively demonstrating that the Si/Cu region adversely impacts the device performance of the Si microwire arrays. The considerable increase in the measured V_{oc} indicated that the interfacial region was a region of low lifetime within the wire, and not just a source of parasitic absorption at the top of the wires. In addition, other unpolished portions of the array with longer wires of ~140 μm in height were also measured, and produced V_{oc} = 467 ± 12 mV and J_{sc} = 15.4 ± 0.3 mA cm^{-2}. Thus, the significant increase in photovoltage of the polished array was not from the wires being slightly longer or absorbing more light due

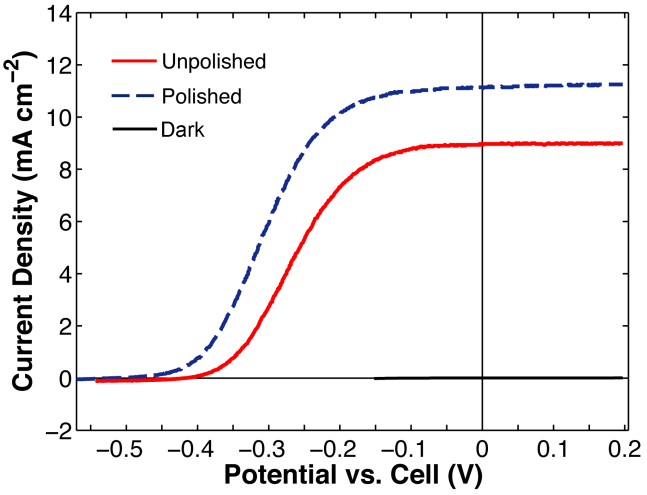

Figure 4.11. The *J-E* behavior of polished and unpolished electrodes from the same array of n+-i-Si microwires, and the corresponding dark curve for the unpolished wires

to their slightly different morphology. Given that there were still some wires remaining on the substrate that had not been polished, the V_{oc} could be expected to increase with total removal of the tops of every wire.

In addition, a piece of the n^+-i-Si microwire array as measured in Chapter 3.3 was also mechanically polished and the *J-E* performance of the polished and unpolished electrodes is given in Figure 4.12. The polished photoelectrodes showed V_{oc} = 463 ± 12 mV, J_{sc} = 13.9 ± 1.2 mA cm^{-2}, and *ff* = 0.46 ± 0.02, while the unpolished electrodes, as described in Chapter 3.3, displayed V_{oc} = 445 ± 13 mV, J_{sc} = 12.8 ± 2.1 mA cm^{-2}, and *ff* = 0.41 ± 0.03. Thus, these electrodes also demonstrated an increase in the photovoltage with the removal of the interfacial region at the top of the wires. However, as shown in Figure 4.12, the amount of the Si/Cu interfacial region was not significant in this wire array (< 100 nm), leading to the less pronounced difference in the response of the polished and unpolished photoelectrodes. Also, approximately 25% of the wires in the polished electrodes remained unpolished; thus, the increase expected for the complete removal of the interfacial region was most likely underestimated in these experiments.

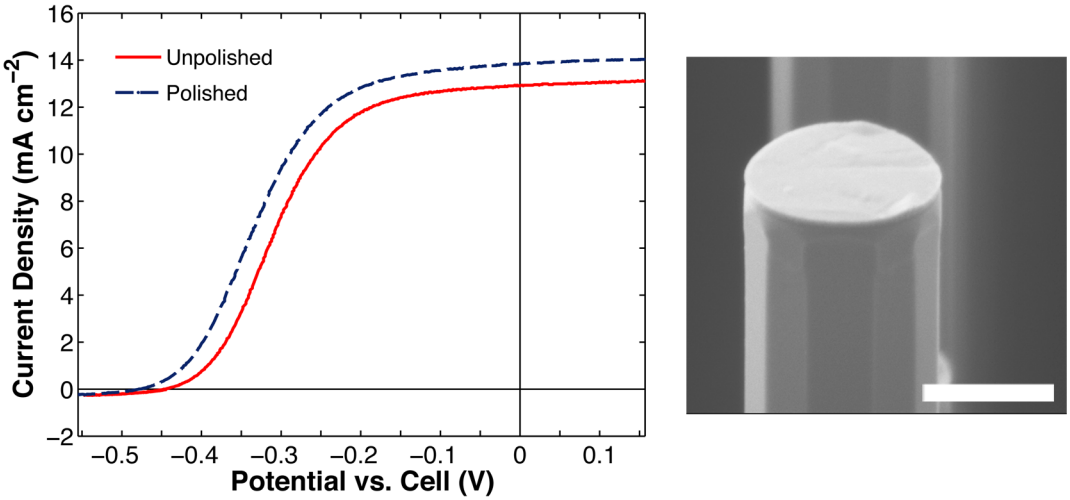

Figure 4.12. *J-E* behavior of undoped Si microwire array electrodes, with unpolished and polished tops of the wires, in contact with $Me_2Fc^{+/0}$, with the corresponding SEM image of the top of the unpolished microwires, scale bar = 2 μm

4.5 Radial p^+ emitter on n^+-i-Si microwire arrays

To fabricate microwire arrays that can be employed to perform fuel–forming reactions, radial p^+ emitters were fabricated on arrays of n^+-i-Si microwires, to form radial junction p^+-i-n^+-Si microwire arrays. These arrays were fabricated using techniques previously employed for fabricating radial junction n^+p-Si microwire arrays.[3, 13, 14] After the Cu VLS catalyst was removed and the wires were thoroughly cleaned, a conformal, dry thermal oxide was grown on the undoped Si microwire arrays. The thermal oxide was selectively etched by employing a PDMS polymer mask, as described in Section 4.2, to form a SiO_2 'boot' that would serve as the diffusion barrier during the formation of the p^+ emitter. The arrays were thoroughly cleaned, to remove residual PDMS, other organics, and trace metal contaminants. To form the radial p^+ emitter, the wire arrays were etched for 5 s in 10% HF(aq) and thermal B diffusion was performed using solid-source boron nitride wafers (Saint-Gobain).

The *J-E* performance of a p^+-i-n^+-Si photoelectrode measured in contact with $Me_2Fc^{+/0}$–CH_3OH (200 mM Me_2Fc, ~ 3.3 mM Me_2FcBF_4) under ~ 0.73 Suns ELH-type illumination is shown in Figure 4.13. This array produced V_{oc} values of ~ 520 mV with a

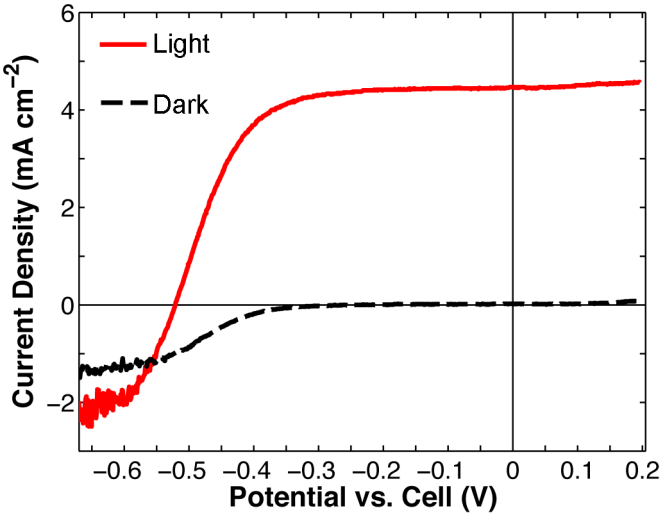

Figure 4.13. *J-E* behavior of a radial junction p^+-i-n^+-Si array electrode measured in contact with $Me_2Fc^{+/0}$ under ELH-type illumination and in the dark. *Experiment conducted by Shane Ardo*

greatly increased *ff* value of ~ 0.64. However, in contact with other redox couples such as aq. $MV^{2+/+}$ and $CoCp^{+/0}$–CH_3CN, the *J-E* performance varied considerably, with the photoelectrodes producing greatly diminished V_{oc} values of ~ 200–300 mV, indicating that the junction formed in these measurements was both electrochemical and metallurgical. Even with the lack of a completely buried junction, processing to form the emitter greatly improved the material properties of the Si microwires, as indicated by the increase in the photovoltage of the p^+-i-n^+-Si in contact with $Me_2Fc^{+/0}$–CH_3OH.

With the promising performance of the p^+-i-n^+-Si arrays in regenerative electrochemical cells, the p^+-i-n^+-Si arrays were also measured in fuming HI, to performing the oxidation of HI to I_2/I_3^-. To facilitate the reaction, Pt nanoparticles (~ 100 mC cm^{-2}) were deposited on the arrays, using an electrochemical deposition process. Under 1 Sun's illumination, a photoelectrode of a Pt/p^+-i-n^+-Si wire array produced a V_{oc} ~ 430 mV, J_{sc} ~ 13.1 mA cm^{-2}, *ff* ~ 0.62, and a photoelectrode energy-conversion efficiency of ~ 3.5% (Figure 4.14). The performance of the photoelectrode did not diminish significantly with multiple (5) *J-E* scans, demonstrating the stability of the Pt/p^+-i-n^+-Si microwire arrays under oxidizing conditions in aqueous solution.

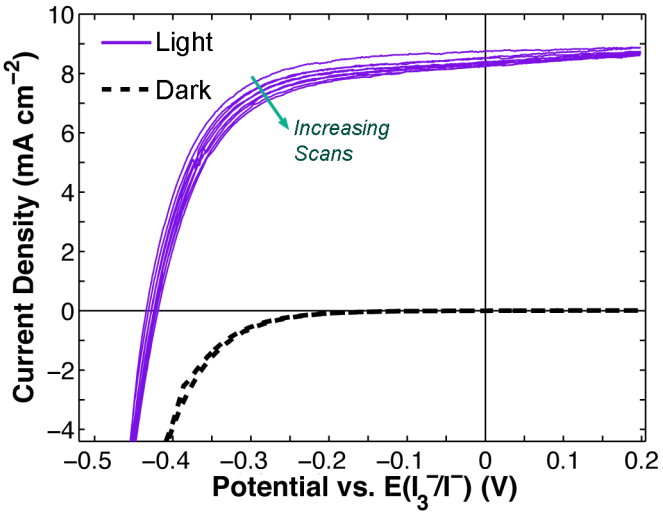

Figure 4.14. *J-E* behavior of a radial junction p^+-i-n^+-Si array electrode measured in contact with fuming HI under 100 mW cm^{-2} ELH-type W illumination and in the dark. Multiple scans are shown, showing the stability of the photoelectrode. *Experiment conducted by Shane Ardo*

4.6 Experimental methods

4.6.1 Fabrication of undoped Si microwires with a thermal oxide boot

A 6N Cu–catalyzed, undoped Si microwire array was grown under standard conditions, and the resulting wires had diameters of ~ 2.6–2.7 μm in a square 3 x 7 μm geometry, and were 45 μm in height. The Cu catalyst was subsequently removed by HF/RCA2 etching procedure, completed twice to ensure the removal of all of the Cu catalyst, followed by etching in 30 % wt. KOH(aq) for 60 s. The array was then oxidized at 1100ºC for 1.5 hr under a pure O_2 ambient, producing a conformal, dry SiO_2 layer with a thickness of ~200 nm. To produce the polymer mask, the array was then coated with a solution that contained 1 g polydimethylsiloxane PDMS and 0.10 g of PDMS curing agent (Sylgard 184, Dow Corning) in 4.35 g (5 mL) of toluene. These samples were then spun at 1000 RPM for 30 s and immediately cured at 150 °C for 30 min to produce a 10 μm thick PDMS layer at the base of the wire array. Residual PDMS was removed from the tops of the wires by employing a ~ 5 s etch in a 1:3 mixture of 75 wt. % tetrabutylammonium fluoride in water (Sigma-Aldrich) and *N*-Methyl-2-pyrrolidone, followed by a H_2O rinse. The arrays were then etched for 5 min in BHF to remove the exposed thermal oxide. The PDMS was then completely removed by etching for 30 min in a 1:1 mixture of 1.0 M tetrabutylammonium fluoride in THF (Sigma-Aldrich) and dimethylformamide, followed by a H_2O rinse. To remove residual organics on the array, a 10 min piranha etch (3:1 aq. conc. H_2SO_4:H_2O_2) was used.

4.6.2 Fabrication of Si microwire arrays with axial *a*-SiN_x:H passivation

To fabricate arrays of Si microwires with axial a-SiN_x:H passivation, the procedures given in Chapter 3.9.4 were followed, for the PECVD *a*-SiN_x:H deposition, mounting wax infill, etching of the exposed *a*-SiN_x:H, and final cleaning of the arrays to remove residual organics.

4.6.3 Chemical–mechanical polishing of Si microwire arrays

After removing the Cu VLS catalyst, arrays of Si microwires of dimensions of ~ 3 cm x 2 cm were cleaved in half longitudinally. Half of the array was reserved for the fabrication of unpolished, control electrodes. The other half of the array was again cut in half, to create to smaller chips for more uniform polishing. All consumable materials for polishing were supplied by South Bay Technology. Each chip was mounted on a flat, 1 inch diameter stainless steel mounting block using a small amount of mounting wax (Quickstick 135, South Bay Technology) on a hot plate at ~ 150ºC. The array was subsequently infilled with mounting wax, and the wax was allowed to equilibrate and flow in the array until the array was slightly shiny; lens paper was not used to remove excess wax, as this removal resulted in rounding of the exposed Si microwires. The array was also not subjected to O_2 plasma ashing. After completion of the mounting wax infill procedure, where the array is completely filled to the tops of the wire arrays with wax, small chips of mounting wax were melted on the mounting block, around the array, but not touching the array. The mounting block was subsequently taken off the hot plate, and the surrounding wax was pushed to the edge of the array, to form a perimeter of wax directly around the array. The wax at the edge was only slightly higher than the wires and infilled ~ 0.5 mm into the array. This wax served as small barrier during polishing, to prevent the removal of wires at the edge of the array.

After the wax cooled, the array was polished using a succession of aluminum oxide suspensions of 3 μm, 1 μm and 0.3 μm. Pieces of polishing cloth (MultiTex™, South Bay Technology) affixed to a glassy-carbon working electrode (outer diameter ~ 6 mm) served as the hand-held polishing implement, so that the sample could be polished by applying downward force over small areas across the sample. Polishing the array 'face down' on the cloth resulted in uneven polishing across the sample. A new polishing cloth was employed for each grit size, and the array was also thoroughly rinsed in > 18 M Ω-cm resistivity H_2O periodically and between grits. The sample was closely observed in an optical microscope, using the focal planes of the top most wires and the shortest wires to gauge the polishing rate. Polishing was terminated when all the wires were the same height, and the array was finally polished using a colloidal silica suspension (SBT, 0.02–0.06 μm). Both Hulu and

Netflix streaming (Gossip Girl: Seasons 1–3) were employed for entertainment, and passers-by were questioned about the weather, current affairs, and their experiments to pass the time. The polishing of an individual chip proceeded for ~ 4 hours. However, from SEM images of the polished arrays, the interfacial region was not polished on the shortest wires within the array; in future attempts, the wire array should be polished a few microns below the shortest wires in the array.

4.7 References

1. B. M. Kayes, H. A. Atwater and N. S. Lewis, *J. Appl. Phys.*, 2005, **97**, 114302.
2. A. P. Goodey, S. M. Eichfeld, K. K. Lew, J. M. Redwing and T. E. Mallouk, *J. Am. Chem. Soc.*, 2007, **129**, 12344-12345.
3. S. W. Boettcher, E. L. Warren, M. C. Putnam, E. A. Santori, D. Turner-Evans, M. D. Kelzenberg, M. G. Walter, J. R. McKone, B. S. Brunschwig, H. A. Atwater and N. S. Lewis, *J. Am. Chem. Soc.*, 2011, **133**, 1216-1219.
4. J. R. Maiolo, H. A. Atwater and N. S. Lewis, *J. Phys. Chem. C*, 2008, **112**, 6194-6201.
5. M. D. Kelzenberg, M. C. Putnam, D. B. Turner-Evans, N. S. Lewis and H. A. Atwater, *IEEE Phot. Spec. Conf.*, 2009, 001948 - 001953.
6. E. L. Warren, S. W. Boettcher, M. G. Walter, H. A. Atwater and N. S. Lewis, *J. Phys. Chem. C*, 2011, **115**, 594-598.
7. R. M. Swanson, S. K. Beckwith, R. A. Crane, W. D. Eades, Y. H. Kwark, R. A. Sinton and S. E. Swirhun, *IEEE Trans. Electron Dev.*, 1984, **31**, 661-664.
8. R. A. Sinton, Y. Kwark, S. Swirhun and R. M. Swanson, *IEEE Electron Dev. Lett.*, 1985, **6**, 405-407.
9. H. Emmer, personal communication. March, 2012.
10. H. Seidel, L. Csepregi, A. Heuberger and H. Baumgartel, *J. Electrochem. Soc.*, 1990, **137**, 3626-3632.
11. H. Seidel, L. Csepregi, A. Heuberger and H. Baumgartel, *J. Electrochem. Soc.*, 1990, **137**, 3612-3626.

12. E. A. Santori, J. R. Maiolo III, M. J. Bierman, N. C. Strandwitz, M. D. Kelzenberg, B. S. Brunschwig, H. A. Atwater and N. S. Lewis, *Energy Environ. Sci.*, 2012, **5**, 6867-6871.

13. M. C. Putnam, S. W. Boettcher, M. D. Kelzenberg, D. B. Turner-Evans, J. M. Spurgeon, E. L. Warren, R. M. Briggs, N. S. Lewis and H. A. Atwater, *Energy Environ. Sci.*, 2010, **3**, 1037-1041.

14. M. D. Kelzenberg, D. B. Turner-Evans, M. C. Putnam, S. W. Boettcher, R. M. Briggs, J. Y. Baek, N. S. Lewis and H. A. Atwater, *Energy Environ. Sci.*, 2011, **4**, 866-871.

C h a p t e r 5

ANGLE–RESOLVED SPECTRAL RESPONSE OF N^+-I-SI MICROWIRE ARRAYS

Components of this chapter were published in

E. A. Santori, J. R. Maiolo III, M. J. Bierman, N. C. Strandwitz, M. D. Kelzenberg, B. S. Brunschwig, H. A. Atwater and N. S. Lewis, *Energy Environ. Sci.*, 2012, **5**, 6867-6871.

Summary

To investigate the carrier-collection efficiency of the undoped Si microwire arrays, the external quantum yield, $\Gamma_{ext,}$ of the arrays in contact with $Me_2Fe^{+/0}$–CH_3OH was measured. Given the angularly anisotropic optical properties of the microwire arrays, the $\Gamma_{ext,}$ was measured as a function of incident illumination. The arrays displayed low external quantum yields at normal incidence, with Γ_{ext} of ~ 0.28 under visible illumination. However at higher angles of incident illumination, the external quantum yield greatly increased with a maximum measured Γ_{ext} of ~ 0.86. The measured external quantum yield values of the undoped Si microwire arrays were similar to those of optimally doped p-Si microwires. Corresponding measurements of the optical properties of the arrays were also made, and an internal quantum yield of ~ 0.75 was subsequently calculated.

Additionally, complementary device physics simulations of wires in radial contact with $Me_2Fe^{+/0}$ showed that the lightly doped wires are completely depleted of electrons, with a hole-rich inversion layer in the near-surface region, ~ 100 nm in depth into the wires. As a consequence, small diameter (D < 200 nm) wires suffer extremely low quantum yield values, due to strong inversion throughout the radial dimension. Larger diameter wires (D > 2 μm) are not strongly inverted in the core of the wire, providing a collection pathway for electrons that is relatively free of holes, and resulting in near-unity quantum yield for wire lifetimes exceeding 5 μs. These numerical simulations can be further leveraged to optimize the device geometry of lightly doped, 1-D semiconductors operating under high-level injection conditions.

5.1 Introduction and motivation

As discussed in Chapter 1, structuring semiconductors with short lifetimes in a radial device geometry should result in an increase in the device efficiency relative to that of a planar device, with the decreased collection lengths allowing for the efficient collection of photogenerated carriers. Device physics modeling of Si wires with radial p-n junctions predicts unity carrier collection for a device with a minority-carrier diffusion length L_n exceeds the radius R of the wire.[1, 2] Internal quantum yields greater than 0.9 have been previously measured for p-Si microwire photocathodes in contact with aq. $MV^{2+/+}$, in good agreement with radial junction theory.[3]

The undoped Si microwires, with diameters of ~ 3 μm and $N_a \sim 1 \times 10^{13} - 1 \times 10^{14}$ cm^{-3}, are fully depleted. Device physics modeling of radial p-n junction wire arrays has indicated that the carrier-collection efficiency precipitously drops off, when the depletion width is greater than the radius of the wire and the wires are thus fully depleted.[4] However, as discussed in Chapter 3, there are several differences between the n^+-i-Si/Me_2Fc–CH_3OH junction and the modeled p-n junction that ultimately warrant an expansion of the model, specifically for the electrochemical device. Therefore, a model of the semiconductor/liquid junction was developed in Sentaurus, to model the n^+-i-Si/Me_2Fc–CH_3OH electrochemical device. In particular, the carrier profile was modeled within an undoped wire in contact with Me_2Fc–CH_3OH. Measurements of the wire's carrier-collection efficiency as a function of distance from the selective back contact were made, by simulating a scanning photocurrent measurement for a single wire.

To investigate the carrier-collection efficiency of the undoped Si microwire arrays, in comparison to doped p-Si microwires, measurements of the external quantum yield with respect to the wavelength of incident illumination ('spectral response') were made on n^+-i-Si photoelectrodes in contact with the $Me_2Fc^{+/0}$–CH_3OH redox system. Given the anisotropy of light absorption within an array with respect to the angle of incident illumination, the spectral response measurements were also performed with respect to the angle of incident illumination. Using measurement techniques developed by M. Kelzenberg,[3, 4] both the angle–resolved external quantum yield and the absorption of an array can be measured experimentally. From these two measurements, the internal

quantum yield of an array in electrochemical contact can be determined, providing insight into the carrier-collection efficiency of the undoped Si microwire arrays.

5.2 Device physics model of n^+-i-Si/Me_2Fc–CH_3OH

5.2.1 Carrier concentration within a single wire

The carrier concentration within a single n^+-i-Si microwire in contact with Me_2Fc–CH_3OH in the dark was calculated using device physics simulations in Sentaurus Device, for a wire with a N_d = 1 x 10^{13} cm^{-3}. As shown in Figure 5.1, the lightly doped n-Si wires, with diameters D = 0.2 and 2.4 μm, possessed high concentrations of holes throughout the diameter of the wires. The smaller diameter D = 0.2 μm wire was strongly inverted, with a background concentration of holes exceeding 1 x 10^{16} cm^{-3} within the core and approaching 1 x 10^{20} cm^{-3} at the surface of the wire. The larger diameter D = 2.4 μm wire was less strongly inverted, but still possessed hole carrier concentrations exceeding the background concentration of the wire when not in contact with Me_2Fc–CH_3OH.

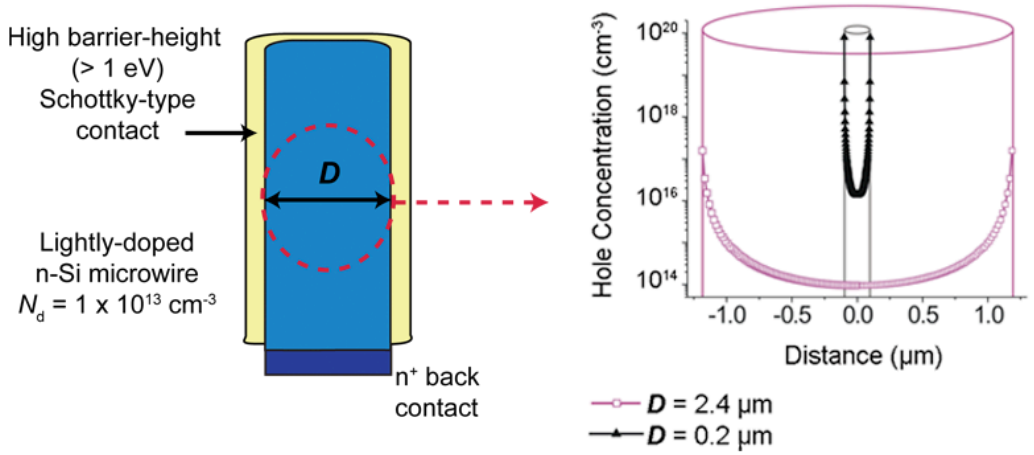

Figure 5.1. Concentration of holes within a single undoped wire in contact with $Me_2Fc^{+/0}$–CH_3OH system in the dark, as a function of the distance radially within the wire, for two different wire diameters D = 0.2 and 2.4 μm. *Simulations performed by Nicholas Strandwitz.*

5.2.2 Scanning internal quantum yield measurement

The internal quantum yield Γ_{int} of a single wire was calculated as a function of the distance of the excited carriers from the top of the wire D_T, as illustrated in Figure 5.2. This type of 'scanning' simulation was preferred to a measurement of the full spectral response or the *I-V* characteristics of a single wire, since the actual excitation profile is not well known, for wires with diameters on the microscale and particularly for wires within an array. The absorption profile would also vary considerably for wires from the nano- to micron-range; a scanning illumination measurement effectively removes the unknown variable of the excitation profile within the wire, measuring the efficiency of carrier-collection at each point along the axial direction of a single wire.

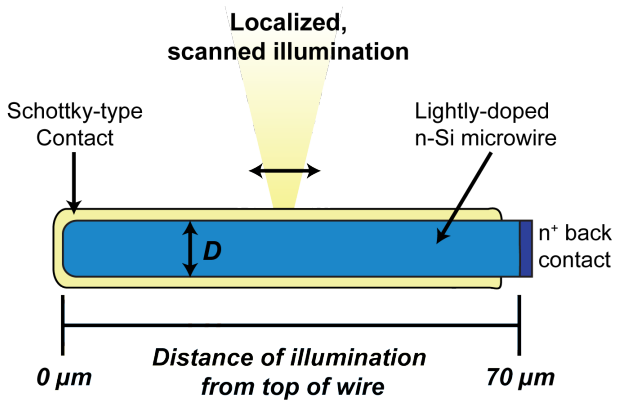

Figure 5.2. Schematic of the scanning internal quantum yield simulation for a single wire, where the internal quantum yield is calculated as a function of the distance of the excitation from the top of the wire

5.2.2A Internal quantum yield vs. N_d

The carrier-collection efficiency within a single wire was calculated for a wire with a typical diameter of D = 2.4 μm, varying the dopant density from N_d = 1 x 10^{11} – 3 x 10^{19} cm^{-3} (Figure 5.3). A Shockley–Read–Hall lifetime was fixed at a value of τ_{SRH} = 1 μs, which corresponds to an effective diffusion length for electrons of ~ 60 μm assuming an electron mobility μ_e ~ 1400 cm^2 V^{-1} s^{-1}. This lifetime was a realistic value for a first simulation, given that L_{eff} ranging from 10 μm to >> 30 μm have been measured for single-

wire p-n junctions. The use of this particular lifetime also guaranteed that, for the fixed D employed, radial collection would be unity for moderately doped wires, in agreement with previous work on radial p-n junction theory. However, for wires with $N_d < 1 \times 10^{15}$ cm^{-3}, the carrier-collection efficiency deviated from unity, particularly for carriers generated at the top of the wire. This result can be understood in light of the carrier concentration within the wire; given that the wires were fully inverted under the simulation conditions, with a high concentration of holes throughout the n-type wire, the recombination rate for electrons increased within the wire. The photogenerated electrons at the top of the wire, which must be transported down the length of the wire to be collected at the back contact, will recombine with the large concentration of holes throughout the wire. Thus, under these simulation conditions, this device architecture was limited by electron transport down the length of the wire.

Wires with $N_d \sim 1 \times 10^{15} - 1 \times 10^{18}$ cm^{-3} possessed $\Gamma_{int} = 1$, in agreement with previous simulations for wires with radii $R < L_{eff}$, providing validation of the current model. For wires with N_d exceeding $\sim 5 \times 10^{18}$ cm^{-3}, other recombination mechanisms such as Auger recombination began to dominate, decreasing the overall lifetime and ultimately limiting the radial collection of carriers.

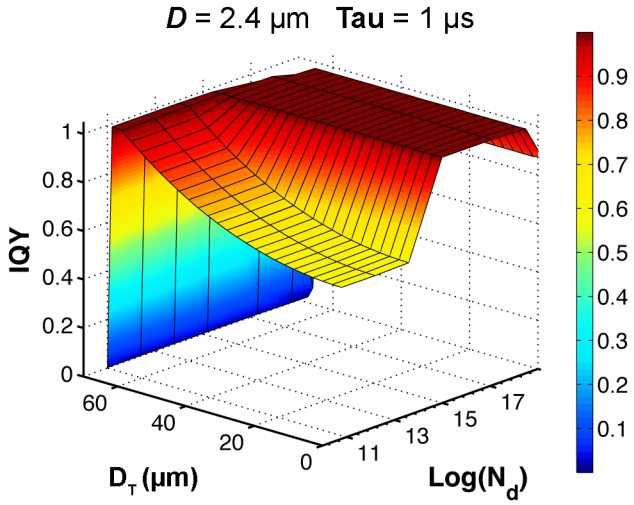

Figure 5.3. Variation of the carrier-collection efficiency along the axial direction of a single wire with the dopant density N_d, for a wire with a typical diameter D = 2.4 µm and a fixed lifetime of 1 µs. *Simulations performed by Nicholas Strandwitz.*

5.2.2B Internal quantum yield vs. wire radius and lifetime

The carrier-collection efficiency within a single, lightly doped wire was also calculated as a function of the radius of the wire and the Shockley–Read–Hall lifetime (Figure 5.4). Both varied parameters had a significant effect on the internal quantum yield; for wires with $R < 0.5$ μm, the carrier-collection efficiency precipitously decreased. This result was consistent with the expected complete depletion of electrons within the wire at these diameters, and the presence of a hole-rich inversion layer in the near-surface region, ~ 100 nm in depth into the wires. At these radii, the wires are strongly inverted throughout the radial dimension, resulting in high recombination rates for electrons traversing down the length of the wire.

In addition, the internal quantum yield demonstrated a strong dependence on the fixed lifetime within the range of 1–10 μs, with Γ_{int} approaching values > 0.9 in wires with $\tau_{SRH} = 10$ μs. Again, assuming an electron mobility $\mu_e \sim 1400$ cm^2 V^{-1} s^{-1}, this lifetime corresponds to $L_{eff} = 60$–190 μm. Thus, to collect the majority of carriers in a 70 μm long wire, the effective diffusion length must be ~ 3 times greater than the length of the wire. Thus, even though the device is structured to facilitate the radial collection of carriers, the axial transport of electrons ultimately limits the carrier-collection within the device, necessitating the use of a material with a long diffusion length.

A)

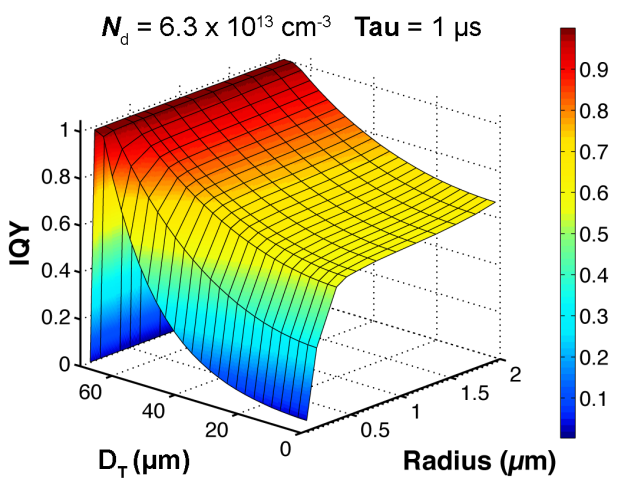

B)

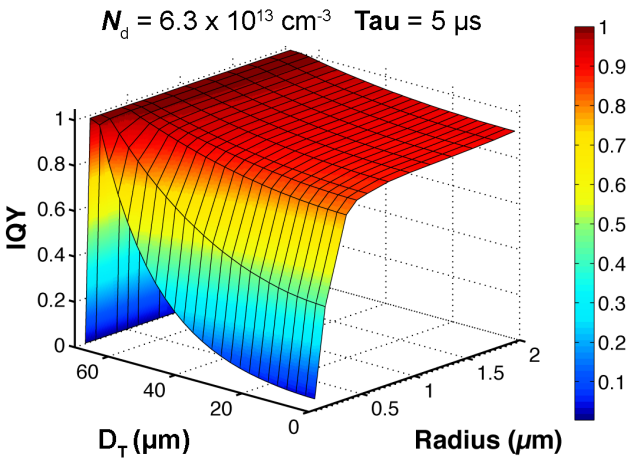

C)

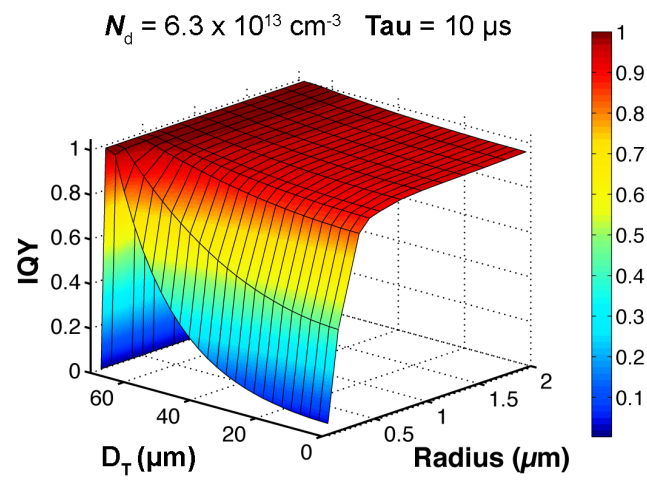

Figure 5.4. Variation of the carrier-collection efficiency along the axial direction of a single wire with the change in the radius of the wire for a fixed dopant density N_d = 6.3 x 10^{13} cm^{-3} and for lifetimes of A) 1 µs, B) 5 µs, and C) 10 µs. *Simulations performed by Nicholas Strandwitz.*

5.3 Angle–resolved spectral response of n^+-i-Si microwire arrays

To investigate the carrier-collection efficiency of n^+-i-Si microwires in contact with $Me_2Fc^{+/0}$–CH_3OH, the external quantum yield, Γ_{ext}, of the Si microwire photoanodes was recorded as a function of the incident angle of illumination. A custom electrochemical cell was constructed, to allow for the rotation of the electrode about a single axis (θ_y) within an Ar purged electrochemical cell (Figure 5.5). Large photoelectrodes were fabricated from high-fidelity arrays of undoped Si microwires grown on degenerate n^+ substrates in a hexagonal array. The lightly doped Si microwire arrays were as given in Section 2.4, with microwire diameters of 2.0–2.5 μm and heights of 70–80 μm, with an average areal packing fraction (η_f) of 9.4% (Figure 5.6). The photoelectrodes were rotated about the θ_y

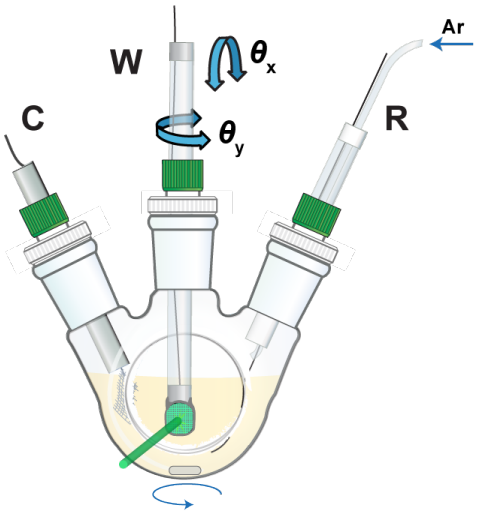

Figure 5.5. Schematic of the electrochemical cell used for angle-resolved spectral response with the $Me_2Fc^{+/0}$–CH_3OH system

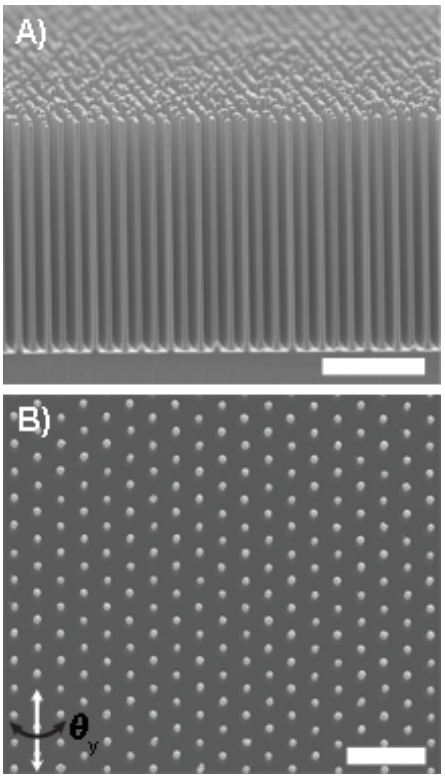

Figure 5.6. A) SEM image of the array of i-Si microwires measured for their spectral response, scale bar = 40 μm. (b) Top view of the i-Si microwire hexagonal array, and the noted axis of rotation θ_y, scale bar = 20 μm

axis of the wire array, as shown in Figure 5.6B, from $\theta_y = 0 - 60^o$.

At normal incidence of illumination (θ_x, $\theta_y = 0^o$), the arrays showed the lowest external quantum yield, with $\Gamma_{ext} \sim 0.28$ under visible illumination (Figure 5.7), corresponding to high transmission through an array that had an average $\eta_f = 9.4\%$. The prominent resonant peaks in the external quantum yield can be attributed to whispering-gallery modes in the hexagonal wires, in which light can circularly propagate at the periphery due to multiple total internal reflections.[5, 6] These peaks had the highest magnitude around normal incidence, and were greatly diminished at higher angles of incident illumination. In addition, in transmission measurements of the peeled wire arrays, these oscillations were only present when the array was illuminated first from the tops of the wires, as opposed to illumination the array with backside illumination (Figure 5.8). This difference could be due to the differing morphologies of the top versus the back of the wire, particularly when the wires are peeled from the substrate, with tops of the wires retaining their circular shape, and the bottom of the wires are strongly tapered or even broken at the base, diminishing the coupling into the cylindrical structures.

Despite the low packing fraction of wires, the arrays effectively collected 28% of

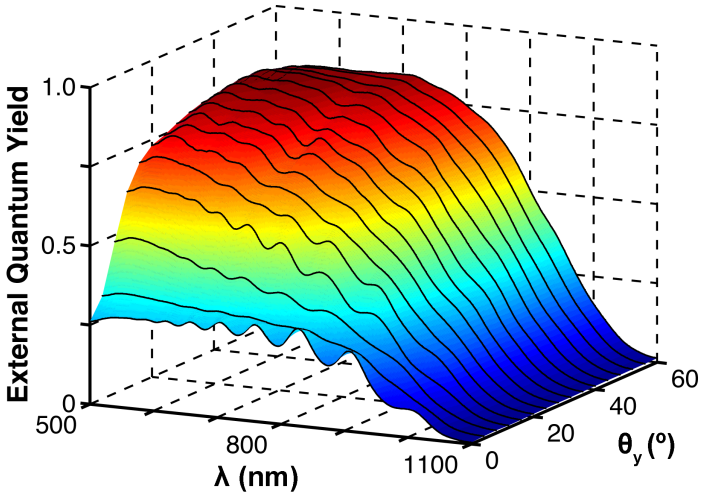

Figure 5.7. Angle–resolved spectral response of n^+-i-Si microwire photoelectrodes in contact with the $Me_2Fc^{+/0}$–CH_3OH system

the incident photons, demonstrating optical concentration within the array. The spectral response of the wire arrays strongly depended on the angle of incident illumination, with a peak $\Gamma_{ext} = 0.86$ at $\theta_y > 52°$. In contrast, photoanodes for which the Si wires had been physically removed from the substrate exhibited negligible photocurrent, with $\Gamma_{ext} < .03$. The current of such electrodes also did not vary with angle, further indicating that the degenerately doped Si substrate did not substantially contribute to the response of the Si wire array photoanodes. The significant increase in Γ_{ext} as θ_y increased indicates that the J_{sc} of the wire arrays previously measured under 1 Sun's illumination was primarily limited by light absorption in the array, and not by carrier collection. Convolution of the spectral response at $\theta_y > 52°$ with the AM 1.5 G spectra resulted in a predicted J_{sc} value of 26 mA cm^{-2}. As has been demonstrated recently, this calculated J_{sc} can be attained by incorporating light-trapping elements such as a back-reflector, anti-reflective coatings, and/or scattering particles into the device structure.[3, 7]

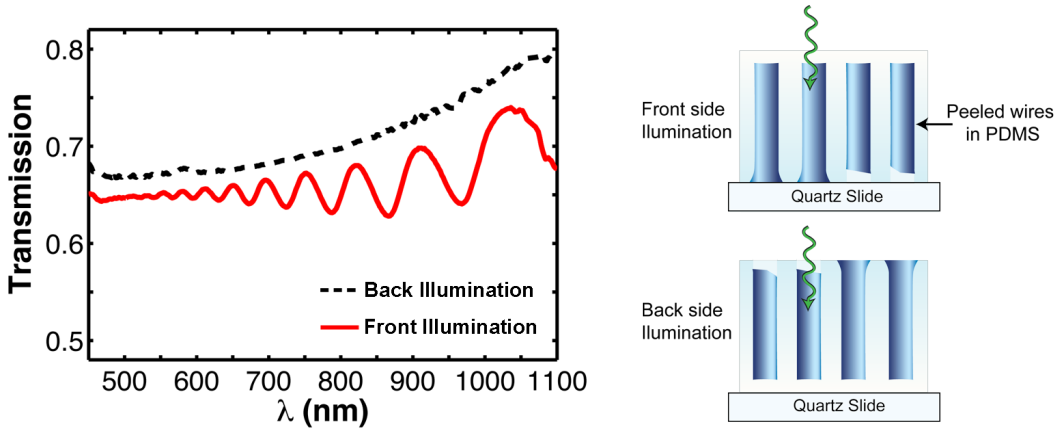

Figure 5.8. Transmission measurements of a peeled array of Si microwires, illuminated from the front and back side of the array

5.4 Angle-resolved optical measurements of n$^+$-i-Si microwire arrays

To calculate the internal quantum yield, Γ_{int}, of the Cu–catalyzed Si microwire array photoanodes, optical absorption measurements as a function of wavelength and angle

were performed on the same wire arrays that were used for collection of the external quantum yield data. An integrating sphere was used to perform optical transmission and reflection measurements on peeled films of wires that had been embedded in polydimethylsiloxane (PDMS), as described previously.[3] As expected, the measured absorption was lowest at normal incidence, corresponding to large transmission through the sparsely packed, highly oriented array (Figure 5.9). The absorption rapidly increased with increasing angle of incident illumination, reaching a plateau value of 0.86.

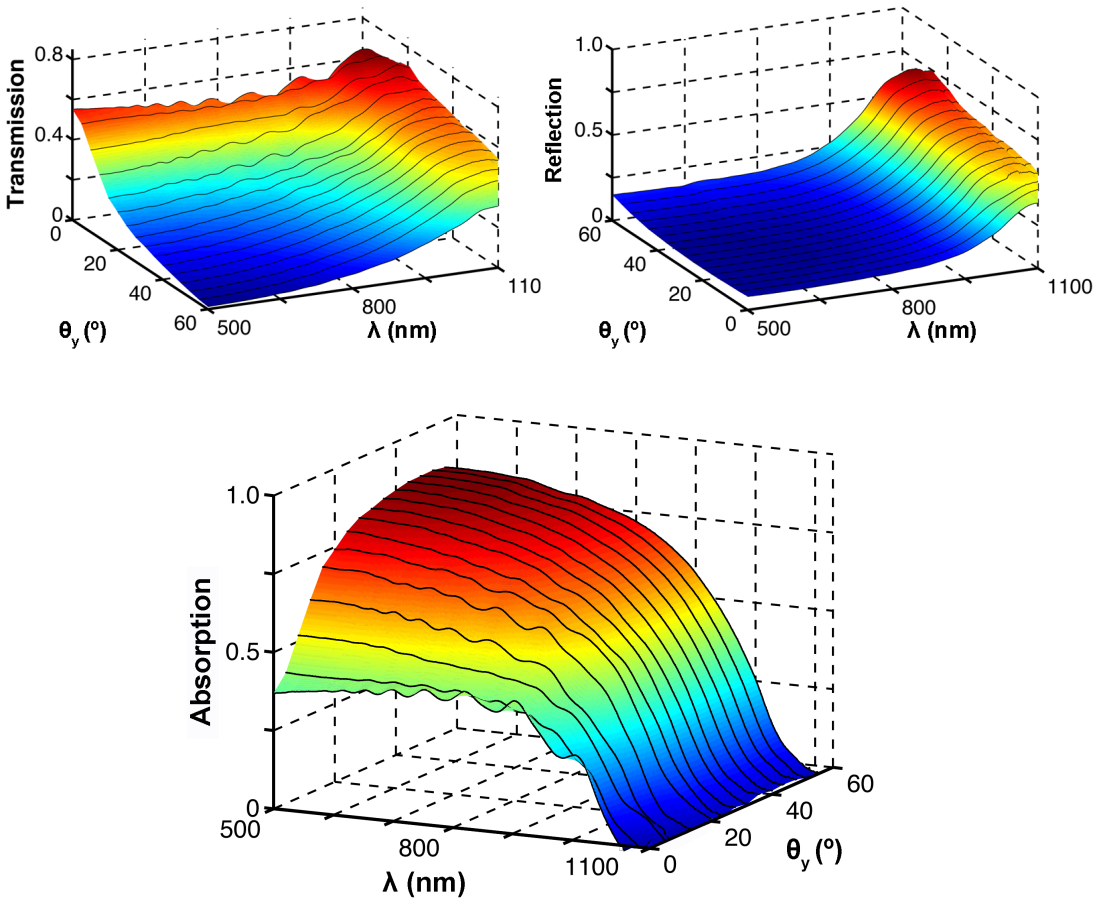

Figure 5.9. Angle–resolved optical measurements of the peeled array of Si microwires

5.5 Internal quantum yield of n^+-i-Si microwire arrays

The value of Γ_{int} for the Si microwire array photoelectrodes was subsequently calculated by dividing the Γ_{ext} at normal incidence by the absorption of the array at normal incidence. Figure 5.10 compares the value of Γ_{ext} and absorption at normal incidence, resulting in a peak Γ_{int} value of 0.73 ± 0.05. Thus, the measured internal quantum yield for the n+-i-Si microwire arrays in contact with $Me_2Fc^{+/0}$–CH_3OH deviated from the value of unity previously measured for p-type Si microwire photocathodes, and from the unity value that is predicted by radial junction theory for a wire having a radius smaller than the minority-carrier diffusion length. The Γ_{int} of the wire array photoanodes at normal incidence was also lower than the Γ_{ext} value that was measured at high angles, implying a change in Γ_{int} with a change in the angle of incident illumination. The Si microwires, however, are not expected to have a minority-carrier diffusion length smaller than their 1.25 μm radius, given that 30 μm minority-carrier diffusion lengths have been reported previously for Cu–catalyzed VLS–grown Si microwires.

These apparent discrepancies can be explained by the presence of the interfacial Si/Cu silicide located at the tops of the wires, as visualized by a high-contrast region in

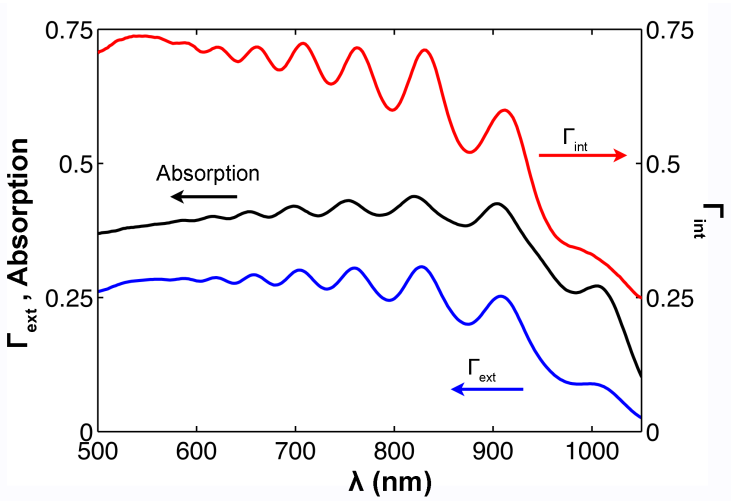

Figure 5.10. The absorption and external quantum yield at normal incidence, with the corresponding calculated internal quantum yield at normal incidence, for n^+-i-Si microwire arrays

scanning electron microscopy images, as shown in Chapter 4. This region persisted after chemical etching to remove the metallic Cu VLS catalyst, and varied in thickness from 200–900 nm, depending on the cooling conditions after VLS growth. This silicide most likely acted as a region of low lifetime for carriers that were generated at the tops of the wires, where a significant fraction of the light is absorbed,[26] thus decreasing the internal quantum yield, particularly at normal incidence. The quantum yield would therefore not only deviate from unity due to this electronically defective region, but would also vary as the excitation profile changes with incident angle of illumination, consistent with the observations reported herein.

However, the device physics modeling of these wires in contact with $Me_2Fc^{+/0}$–CH_3OH predicted that unity quantum yields were only attainable in wires with long lifetimes, exceeding 5 μs.[1] Thus, the measured non-unity quantum yield may be a convolution of the increased recombination from the presence of the Cu/Si interfacial region or other localized defects in the wires, and the decrease in carrier-collection efficiency expected in this device, from the recombination of electrons before they are collected axially.

From the values of Γ_{int} and the optical absorption coefficient $\alpha(\lambda)$, the minority-carrier diffusion length L_n, for a planar device can be approximated by use of eq 5.1.[8, 9]

$$\Gamma_{int} = \frac{1}{1+\frac{1}{\alpha(\lambda)L_n}} \tag{5.1}$$

Analysis of Γ_{int} for the Cu–catalyzed Si microwire array photoanodes in the near-infrared region (800 nm ≤ λ ≤ 950 nm), in which the optical penetration depth α^{-1} did not exceed the length of the wires, yielded an effective diffusion length, $L_{,eff}$, of 75–85 μm. This value is not a true diffusion length, given that the assumptions of eq 5.1 do not apply in a radial geometry, but rather a comparison to the diffusion length that would be needed to produce similar near-IR carrier collection efficiencies in a planar Si device structure (Figure 5.11).

[1] Assuming an electron mobility μ_e consistent with the doping density of the wires of ~ 1400 $cm^2\ V^{-1}\ s^{-1}$, this lifetime corresponds to an effective diffusion length of electrons of ~ 130 μm.

The calculated L_{eff} value is significantly larger than the 30 μm minority-carrier diffusion length that has been measured previously for moderately doped, Cu–catalyzed, VLS–grown Si microwires.[7, 10] This observation further demonstrates the advantages of using a radial junction, which produces a longer effective diffusion length than the actual minority-carrier diffusion length, by extending the device response further into the near-IR region of the spectrum as compared to planar Si-based devices with comparable bulk electronic properties.

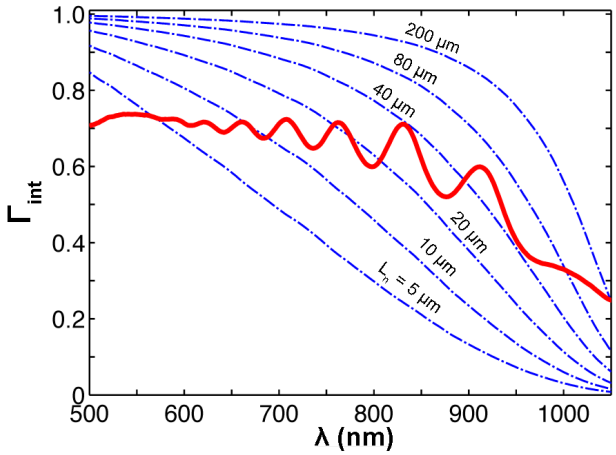

Figure 5.11. A comparison of the measured Γ_{int} of the n^+-i-Si microwire array photoanodes and several calculated Γ_{int} responses for planar Si photoelectrodes, with L_n, ranging from 5–200 μm

5.6 IQY of mechanically polished n^+-i-Si microwire array photoanodes

To determine the effect of the Cu/Si interfacial region on the carrier-collection efficiency of undoped Si microwires, this region located at the tops of the wires was selectively removed through chemical-mechanical polishing. Arrays of n^+-i-Si microwires were fully embedded with mounting wax and subsequently polished by hand using powder Al_2O_3 and silica suspensions (see Chapter 4 for polishing experimental details). Half of each array was reserved as a control, to provide a direct comparison between the same wires in measurements of polished and unpolished electrodes and films. The polishing technique employed removed material at an even rate across the entire array, despite large height variations > 40 μm across the chip. Locally, where neighboring wires possess

height differences of ± 2 μm, material was removed from the tallest wires first, while the shorter wires remained fully embedded in the protective mounting wax infill. Thus, to polish the shortest wires, a total of ~ 6 μm of Si was removed from the tops of the wires, with the tallest wires polished by ~ 6 μm and the shortest polished by 2 μm. The resulting wires had locally uniform heights with flat, non-rounded tops (Figure 5.12).

A)

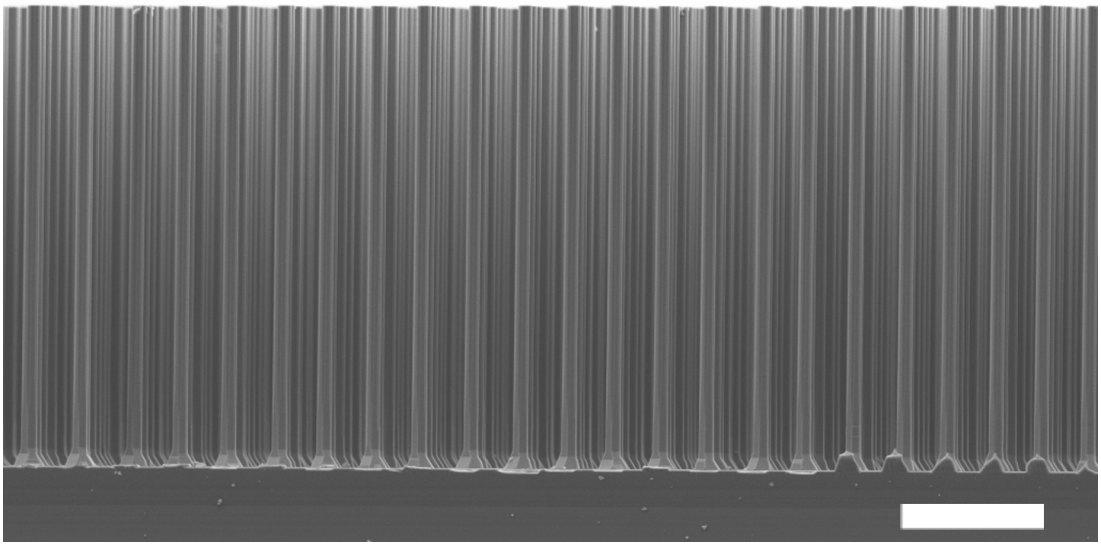

B)

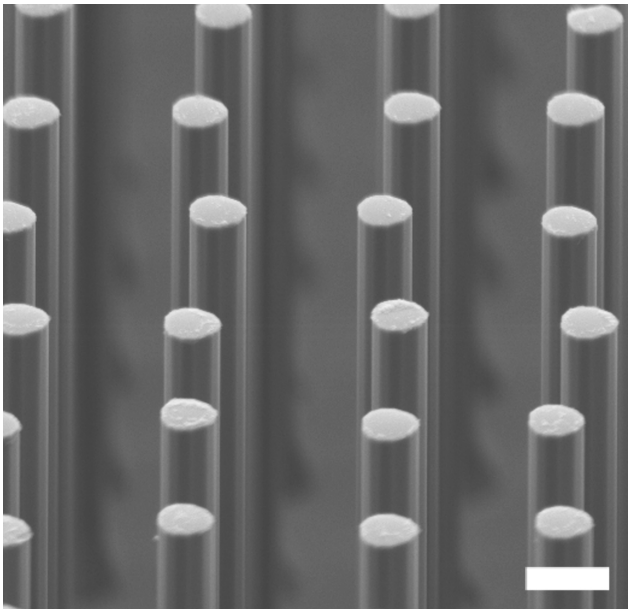

Figure 5.12. A) Side view SEM image of a mechanically polished Si microwire array, scale bar = 20 μm, and B) Top view SEM image of the same array, scale bar = 3 μm

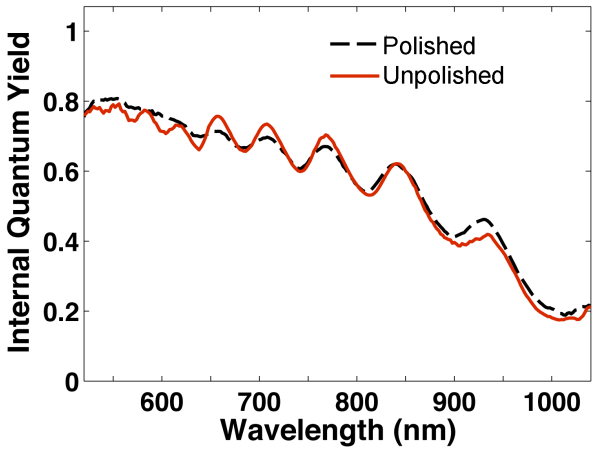

Figure 5.13. The measured Γ_{int} for an array of n^+-i-Si microwire photoelectrodes in contact with the $Me_2Fc^{+/0}$–CH_3OH system, for both polished and as grown wires

The external quantum yield and optical properties of arrays of the unpolished and polished n^+-i-Si microwire array photoelectrodes were subsequently measured, and the Γ_{int} were calculated, as described in Section 5.5. Figure 5.13 shows the measured Γ_{int} for an array of n^+-i-Si microwire photoelectrodes in contact with the $Me_2Fc^{+/0}$–CH_3OH system, for both polished and unpolished portions of the same array. The Γ_{int} showed no change between as grown wires with the Cu/Si interfacial region and polished wires where the silicide had been removed. Thus, for the undoped Si microwire arrays, the presence of the interfacial region at the tops of the wires had no effect on the carrier-collection efficiency within the wires.

With this measurement, deviations in the measured internal quantum yield from unity can more confidently be attributed to the limiting axial transport of electrons in the inverted microwires. Other localized defects, such as defects present at the base of the wire from a high concentration of Cu metal, or from crystallographic defects at the strongly tapered base, could also be contributing to the lower observed internal quantum yield. Indeed, experiments using defect etchants, such as the Secco etch, have revealed a high concentration of defects at the base of the Si microwires. However, these defects would also be present in p-type Si microwires, and should also have a negative impact on the carrier-collection efficiency within radial p-n junction wires. Further modelling and

experimental work is required to understand the effect that these defects would have on the device physics properties of both radial p-n and n^+-i-Si microwire devices.

5.7 Conclusions

The carrier-collection efficiency of lightly doped Si microwires in contact with a high barrier-height contact, $Me_2Fc^{+/0}$–CH_3OH, was determined to deviate from unity, through both simulation and experiments. The Cu silicide region at the top of the wires, which had previously been hypothesized to contribute to the photoanode's low internal quantum yield, was demonstrated to have no effect on the carrier-collection efficiency within these devices. The experimental non-unity internal quantum yield was consistent with results from the device physics model of the electrochemical system, where strong inversion through the radial dimension of the Si wire limited the axial transport of carriers. The relatively high, experimentally measured, carrier-collection efficiency of the n^+-i-Si/$Me_2Fc^{+/0}$–CH_3OH system, with peak Γ_{int} exceeding 0.8, suggests that the Cu VLS–grown Si microwires were of high electronic quality, with lifetimes exceeding 5 μs.

Despite the limitations in carrier transport, the n^+-i-Si microwire arrays in contact with $Me_2Fc^{+/0}$–CH_3OH have demonstrated both *J-E* and external quantum yields similar to optimally doped p-Si microwire array photocathodes. This type of device, which could include solid-state radial junction p^+-i-n^+-Si or n^+-i-p^+-Si microwire arrays, has the advantage of increased process simplicity, without the need for doping optimization and calibration within a nano- or microstructured device. However, if one were to further pursue this device architecture, wires must be fabricated on the microscale using a material with a moderately long lifetime; in addition, highly selective contacts for both carriers and low effective surface recombination velocity are required to fabricate an efficient device. Future work should potentially be directed at fabricating wire devices on the nanoscale, to experimentally verify that complete depletion or inversion within the structure results in a precipitous decay in the device performance.

5.8 Experimental methods

5.8.1 Angle-resolved spectral response

For angle-resolved spectral response measurements, side-facing electrodes of high-fidelity Si microwire arrays with dimensions of ~ 7 x 7 mm were fabricated. The electrodes were fabricated so that the Si microwire arrays would ultimately be eucentric with respect to the rotational axes, θ_y and θ_x. First, the Cu wire coil was threaded through the glass tube and the wire coil was centered with respect to the glass tube (x and y directions) and with little to no pitch ($\theta_x \sim 0^o$). The wire was then secured at the opposite end of the glass tube with tape, to prevent the wire coil from moving during electrode fabrication. The backs of the samples were scratched with a SiC scribe that was coated in Ga:In eutectic (76:24 Ga:In wt.), to make ohmic contact to the Si substrate. The samples were then mounted with Ag print (GC Electronics) onto the coiled wire. Care was taken to ensure that all electrodes had the same orientation in all three dimensions, but examining and adjusting the microwire array under an optical microscope during the fabrication of electrodes. For hexagonally patterned arrays, the long 14 μm axis was oriented vertically, as the axis of rotation (θ_y) (Figure 5.14A). For square patterned arrays, the square pattern of the array was oriented such that the 7 μm axis was at 0 or 90º from the axis of rotation (θ_y) (Figure 5.14B).

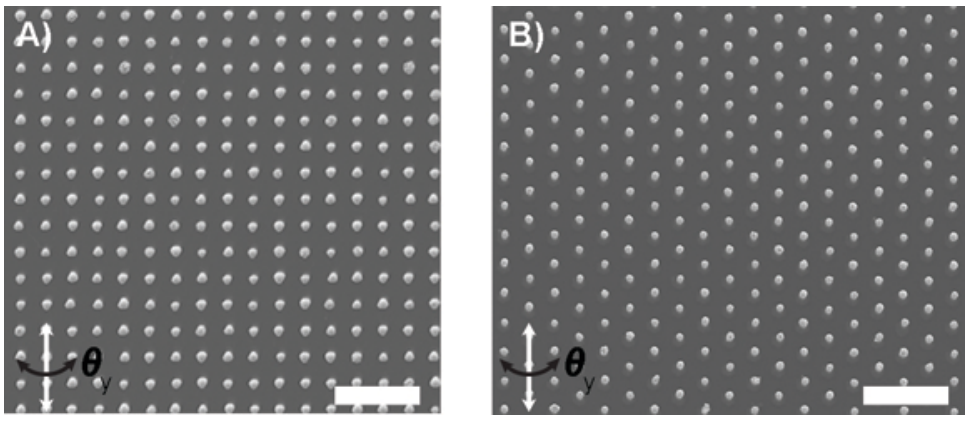

Figure 5.14. Top views of a Si microwire arrays for spectral response, with the noted axis of rotation θ_y, for A) square arrays and B) hexagonal arrays, scale bars = 20 μm

Angle-resolved spectral response measurements were performed using an apparatus that has been described previously, which consisted of a chopped (f = 30 Hz) Fianium supercontinuum laser coupled to a monochromator, with two rotational stages to allow for rotation around both the θ_x and θ_y axes.[3] A custom, air-tight, round-bottom flask with a side window was utilized for angle-resolved spectral response measurements (Figure 2). The electrochemical cell was constructed from a 25 mL round-bottom, heavy wall, three-neck flask with 19/22 fittings (Chemglass). To add a side-facing window, the side of the round-bottom flask was sanded off using a polishing wheel, and a Pyrex glass optical window was adhered onto the modified round-bottom flask with epoxy (Hysol 1C). The side-facing window was positioned to allow for the working electrode to rotate a full 90º within the cell, while minimizing the optical path length within the cell. To allow for an Ar purge in the sealed cell, a small diameter polyethylene tube was threaded through the reference electrode glass tube, along with the reference electrode Pt/Cu wire. The tube was subsequently sealed with epoxy (Hysol 1C) at both ends, providing an inlet for Ar into the cell.

The electrolyte solution consisted of 10 mM of Me_2Fc, ~ 0.4 mM of Me_2FcBF_4, and 1.0 M $LiClO_4$ in 25 mL of methanol. The solution was made under inert atmosphere (< 10 ppm O_2), and added to the cell in air with a strong Ar flow through the electrochemical cell. The electrochemical cell was subsequently held under positive Ar pressure, and a methanol bubbler was used to prevent evaporation of the solution during an Ar purge. The three-electrode cell consisted of a high-area Pt mesh as the counter electrode, a Pt wire directly in solution as the reference electrode, and a Si working electrode. The working electrode was poised at the solution potential of the cell, referenced by a Pt wire in solution. To allow for free rotation of the working electrode in the cell, the thermometer adaptor fitting for the electrode was loosened for the duration of the experiment. The photoelectrode was aligned in the cell by utilizing the reflected optical diffraction pattern, and normal incidence ($\theta_{x,y}$ = 0º) was determined by minimizing the photocurrent of each electrode. A calibrated Si photodiode (FDS-100, Thorlabs) that was positioned inside the cell was used to calculate the Γ_{ext} of the Si microwire array photoelectrodes. The cell was constantly purged with Ar, with the outlet provided by the

loosened fitting of the working electrode. No degradation of the response of the Si working electrode was observed over the duration of the experiment (> 4 h).

5.8.2 Angle-resolved optical measurements

Optical measurements were made on peeled arrays from both photoelectrodes and from pieces of the Si microwire array that were adjacent to those pieces used measured for their spectral response (Figure 5.11). Since the heights of the wires can vary considerably across one growth chip, care was taken to measure wires with the same heights for the optical and photoelectrochemical measurements, by using adjacent portions of the same array with equal distance from the growth front on the chip. For measurements of the wires from photoelectrodes, after electrochemical measurements, the electrodes were thoroughly rinsed with methanol, water and isopropyl alcohol, and dried under N_2. Polydimethylsiloxane (PDMS; Sylgard 184, Dow Corning) was drop-cast into the electrodes. To ensure a uniform thin film, a transparency was placed on top of the curing PDMS, to create a thin film (< 1 mm) of PDMS that exhibited little optical distortion. The PDMS was allowed to cure at room temperature for 48 h, and then at 80ºC for 2 h. The transparency was then removed from the top of the film. Si wires embedded in PDMS were subsequently peeled off of the electrode using a scalpel blade, which when compared to using a razor blade, more consistently peeled the bases of the wire arrays. To temporarily mount the films onto the quartz slide, the films were wetted with a drop of

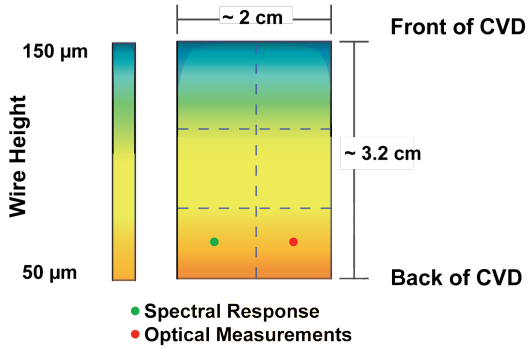

Figure 5.15. Schematic of the approximate height distribution on a chip of Si microwire arrays, with indication of how nearby portions of a chip were used for spectral response and optical measurements

methanol and allowed to dry on the slide. This method provided good adhesion of the film to the slide, with little air in between the film and the glass.

Optical transmission and reflection measurements as a function of wavelength (λ) and incident angle of illumination (θ_y) were performed on the peeled–off films using an integrating sphere.[3] The optical diffraction patterns of the arrays were used to orient the films relative to the rotational axes (θ_x, θ_y). The maximization of transmission in the films was taken to be normal incidence to the wire array.

5.8.3 Device physics simulations

Device physics simulations were carried out using Sentaurus Device from Synopsis Inc. Wires were defined in 2D using cylindrical coordinates. A liquid contact was simulated using a Schottky-type contact that formed a high barrier-height contact with n-Si. Default values were used for interfacial properties unless otherwise noted. Scanning photocurrent simulations were conducted by scanning a simulated light beam axially along a wire. The contacts for the wire included the high barrier-height contact, which was applied radially to the wire, and an n^+ back surface field as an electron selective contact. Distance = 0 μm was defined as the tip of the wire (far from the n^+ back surface field), and the wire was 70 μm in length. The quantum yield for carrier collection at zero applied voltage was determined by integrating the total number of excitations per unit time in the wire and dividing that quantity by the number of electrons collected per unit time derived from the current at the contacts. The dopant density was uniform throughout the wire except at the base. The mobility assumed bulk values that decreased with increasing dopant densities according to empirically developed relationships.[11] A Shockley–Read–Hall lifetime was set for each simulation ($\tau_n = \tau_p$) and adjusted based on the empirical relationship with the dopant density given in eq. 5.2

$$\tau_{SRH} = \frac{\tau_n}{(1+\frac{N}{N_{ref}})} \tag{5.2}$$

where N is the dopant density, N_{ref} = 1 x 10^{16} cm^{-3}, τ_n is the initial value set for the carrier lifetime, and τ_{SRH} is the final value used in computing recombination rates.

5.9 References

1. B. M. Kayes, H. A. Atwater and N. S. Lewis, *J. Appl. Phys.*, 2005, **97**, 114302.
2. M. D. Kelzenberg, M. C. Putnam, D. B. Turner-Evans, N. S. Lewis and H. A. Atwater, *IEEE Phot. Spec. Conf.*, 2009, 001948 - 001953.
3. M. D. Kelzenberg, S. W. Boettcher, J. A. Petykiewicz, D. B. Turner-Evans, M. C. Putnam, E. L. Warren, J. M. Spurgeon, R. M. Briggs, N. S. Lewis and H. A. Atwater, *Nat. Mater.*, 2010, **9**, 239-244.
4. M. D. Kelzenberg Ph.D., *Silicon Microwire Photovoltaics*, California Institute of Technology, Pasadena, 2010.
5. L. Y. Cao, J. S. White, J. S. Park, J. A. Schuller, B. M. Clemens and M. L. Brongersma, *Nat. Mater.*, 2009, **8**, 643-647.
6. T. Nobis, E. M. Kaidashev, A. Rahm, M. Lorenz and M. Grundmann, *Phys. Rev. Lett.*, 2004, **93**.
7. M. C. Putnam, S. W. Boettcher, M. D. Kelzenberg, D. B. Turner-Evans, J. M. Spurgeon, E. L. Warren, R. M. Briggs, N. S. Lewis and H. A. Atwater, *Energy Environ. Sci.*, 2010, **3**, 1037-1041.
8. W. W. Gartner, *Phys. Rev.*, 1959, **116**, 84-87.
9. M. L. Rosenbluth and N. S. Lewis, *J. Am. Chem. Soc.*, 1986, **108**, 4689-4695.
10. M. D. Kelzenberg, D. B. Turner-Evans, M. C. Putnam, S. W. Boettcher, R. M. Briggs, J. Y. Baek, N. S. Lewis and H. A. Atwater, *Energy Environ. Sci.*, 2011, **4**, 866-871.
11. G. Masetti, M. Severi and S. Solmi, *IEEE Trans. Electron. Dev.*, 1983, **30**, 764-769.

A p p e n d i x

NON-AQUEOUS DIMETHYLFERROCENE ELECTROCHEMICAL MEASUREMENTS

A.1 Introduction and motivation

The non-aqueous 1,1′–dimethylferrocene $(Me_2Fc)^{+/0}$ redox system in methanol (CH_3OH) makes a reproducible, high barrier-height contact with n-Si, making it a well–defined regenerative electrochemical system in which to measure the photoanodic properties of n-type and undoped silicon electrodes. The $Me_2Fc^{+/0}$–CH_3OH redox system has been shown to yield excellent junctions with n-type Si, producing open-circuit voltage, $V_{oc,}$ values that are only limited by bulk recombination/generation.[1] For single crystalline, planar n-Si in contact with $Me_2Fc^{+/0}$–CH_3OH, energy conversion efficiencies of over 10%[2-4] and photovoltages in excess of 670 mV under 100 mW cm^{-2} of air mass (AM) 1.5 conditions have been attained.[1]

Additionally, the $Me_2Fc^{+/0}$–CH_3OH system generates an inversion layer in contact with n-Si, and the resulting semiconductor/liquid interface has a low effective surface recombination velocity S of ~ 20 cm s^{-1}.[5] This low S remained when the samples were removed from solution and measured under a N_2 atmosphere, indicating surface functionalization of n-Si in methanol in the presence of a one-electron oxidant, most likely due to the formation of a monolayer of methoxy groups on the Si surface.

Recent studies on the *J-E* behavior of methoxy–terminated n-Si(111) surfaces in $Me_2Fc^{+/0}$ have further elucidated the critical role of the surface chemistry of the Si surface

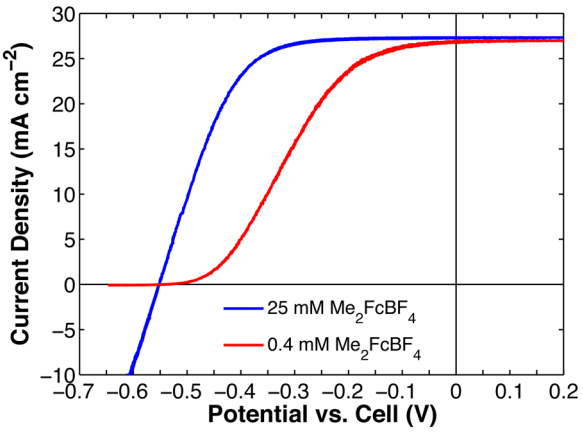

Figure A.1. Typical *J-E* performance of n-Si in contact with $Me_2Fc^{+/0}$–MeOH with 0.4 mM and 25 mM of the oxidized form of the redox couple

on its photoelectrochemical performance in this redox system.[6] Planar, hydride (H)-terminated n-Si electrodes initially measured in contact with $Me_2Fc^{+/0}$–CH_3CN displayed V_{oc} values of ~ 330 mV (Figure A.2). The same electrodes subsequently measured in contact with $Me_2Fc^{+/0}$– CH_3OH attained V_{oc} values of ~ 550 mV, close to the bulk recombination/generation limited photovoltage for the Si used in this system. The electrodes measured in the original $Me_2Fc^{+/0}$– CH_3CN redox solution displayed photovoltages similar to those measured in the $Me_2Fc^{+/0}$– CH_3OH cell. In addition, placing the Si electrodes in methanol prior to measuring those electrodes in the $Me_2Fc^{+/0}$– CH_3CN cell resulted in V_{oc} values of ~ 550 mV, confirming that the surface reaction of the H-terminated Si with methanol led to the demonstrated increase in the photovoltage. In contrast, n-Si photoelectrodes with methyl (CH_3)-termination demonstrated little variation in photovoltage with changes in solvent. These results indicated that surface methoxylation is critical to achieving maximum performance in $Me_2Fc^{+/0}$ electrochemical systems.

The well–defined junction properties of $Me_2Fc^{+/0}$–CH_3OH make it an ideal system to test new n-type materials or the surface properties of existing materials. Herein, key

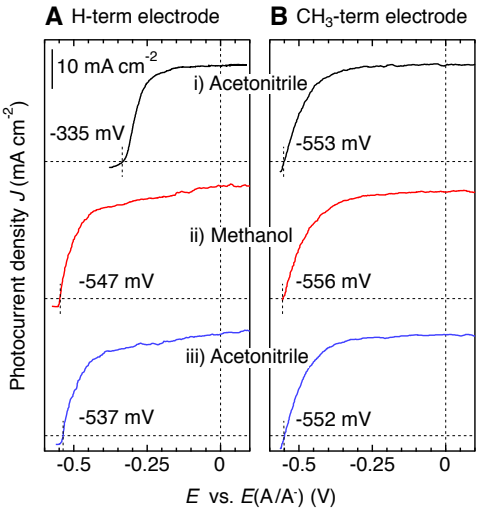

Figure A.2. Sequence of *J-E* scans under illumination for A) H-terminated and B) CH_3-terminated n-Si(111) in contact with $Me_2Fc^{+/0}$ in both methanol and acetonitrile. The same electrodes are (i) initially measured in a $Me_2Fc^{+/0}$–CH_3CN cell, (ii) subsequently measured in a $Me_2Fc^{+/0}$–CH_3OH cell, and (iii) finally measured back in the $Me_2Fc^{+/0}$–CH_3CN cell.

experimental conditions will be given explicitly, to guide future users of this cell.

A.2 Experimental methods

A.2.1 Materials

Methanol (BakerDRY, Mallinckrodt Baker) and lithium perchlorate ($LiClO_4$, battery grade, Sigma-Aldrich) were used as received, without further purification. $LiClO_4$ (95%, Sigma-Aldrich) can also be subsequently dried and used, but such further purification was not necessary to obtain stable, reproducible performance of Si photoelectrodes in the $Me_2Fc^{+/0}$–CH_3OH system. For planar Si control electrodes, wafers of Czochralski-grown, single-side polished, P-doped n-Si(100) with $\rho \sim 4$–8 Ω-cm and thicknesses of 500 ± 25 μm (Wacker Siltronic) were employed.

A.2.2 Purification of $LiClO_4$

$LiClO_4$ (95%, Sigma-Aldrich) was fused in a custom quartz vessel under vacuum (5 mT) at ~ 240ºC. To prepare the quartz vessel, the quartz vessel was initially rinsed with solvent, to remove residual grease from the glass joint. After thoroughly rinsing the vessel with water, the vessel was filled with an aqua regia (1:3 HNO_3:HCl) solution for 1 h, and rinsed with H_2O. Subsequently, a piranha solution (7:3 H_2SO_4:H_2O_2) was used to remove all organics from the vessel. This step was critical, given that any residual organics will react with the liquid $LiClO_4$ in a highly exothermic and explosive reaction. The vessel was then rinsed with H_2O and dried in the low temperature oven at ~ 80º C. Using a custom glass funnel with a long stem, ~ 10 g of $LiClO_4$ were placed in the quartz vessel, such that the reagent fills approximately 1 inch of the vessel. Attempting to fuse more reagent than specified will result in increased hazard when cooling the reagent (see 'dangerous step' below). Using the funnel ensures that the $LiClO_4$ is placed at the bottom of the vessel, where the vessel will be heated. $LiClO_4$ on the sidewalls of the vessel will not reach a sufficiently high temperature to be fused, resulting in incomplete drying of the reagent. A small amount of grease (Dow Corning high vacuum grease) was placed at the bottom of the

ground glass joint on the vessel. This small amount of grease was sufficient to make a good seal, while preventing grease from entering the top of the vessel where the grease has a higher likelihood of encountering liquid $LiClO_4$ during the 'dangerous step.'

The vessel was subsequently immersed in a heating mantle with a sand bath to as great a depth as possible, to expedite the heating of the $LiClO_4$. A thermometer was placed in the sand bath, in close proximity to the quartz vessel. The quartz vessel was then placed under vacuum on the Schlenk line using a liquid nitrogen trap, to prevent water from entering the vacuum pump. A blast shield was placed in front of the reaction, and a Variac used to control the heating mantle was set to ~ 45 V, which should slowly bring the sand bath to ~ 240º C in 1.5 h. To check if all of the $LiClO_4$ had melted, a large mirror was used to examine the bottom of the quartz vessel. *Do not* remove the blast shield or peer around the blast shield while the $LiClO_4$ is being heated. Use the mirror.

Once all of the $LiClO_4$ had melted, the quartz vessel was removed from the sand bath, using the high temperature–compatible white gloves for protection. ***Dangerous step***: keeping the quartz vessel behind the blast shield, ***carefully*** tilt and rotate the vessel, to allow for the $LiClO_4$ to cool on the middle sidewalls of the vessel. By employing this step, the $LiClO_4$ was therefore assessable for removal, instead of cooling as a big, hard block at the very bottom of the vessel. Once the vessel had cooled to close to room temperature, the vessel was isolated from vacuum to remain under passive vacuum, and brought into the dry box. The $LiClO_4$ was removed from the sidewalls using a metal spatula, and was stored in the dry box until use.

A.2.3 Sublimation of Me_2Fc

Me_2Fc (95%, Sigma-Aldrich) was sublimated at room temperature and reduced pressure (~ 10 mT). Me_2Fc sublimates at atmospheric pressure, so heating the reagent is not strictly necessary. To facilitate the sublimation, the reagent can be sublimated at ~ 45ºC. The reagent was stored under an inert atmosphere in the dry box until use.

A.2.4 Synthesis of Me_2FcBF_4

Dimethylferrocenium tetrafluoroborate (Me_2FcBF_4) was synthesized as described previously.[7] Briefly, Me_2FcBF_4 was synthesized from Me_2Fc (either sublimated or used as received) by addition of excess tetrafluoroboric acid (HBF_4, 55% w/w in diethyl ether, Sigma-Aldrich) in the presence of 0.5 equivalents of *p*-benzoquinone (reagent grade ≥ 98%, Sigma Aldrich) in THF (ACS grade). First, the Me_2Fc (2.55 g) was dissolved in THF (80 mL). The solution was stirred in an ice water bath until thoroughly chilled. The reaction was successfully run under Ar (as published) or in air (JRM III, book 2, p. 129). The *p*-benzoquinone (0.66 g) was added with stirring, and the solution subsequently changed to a brown color. HBF_4 (8 mL) was subsequently added and the solution immediately turned a dark blue. The reaction was stirred on ice for ~ 30 min, then vacuum filtered and washed 3 times with 30 mL of cold THF. The resulting solid was dried under vacuum and stored under an inert atmosphere in the dry box until use.

A.2.5 Electrode fabrication

To fabricate electrodes for photoelectrochemical measurements, wire arrays were cleaved into 4 x 4 mm samples. The backs of the samples were scratched with a SiC scribe that was coated in Ga:In eutectic (76:24 Ga:In wt.), to make ohmic contact to the Si substrate. The samples were then mounted with Ag print (GC Electronics) on a coiled wire that was passed through a glass tube, so that the electrode was positioned in a face-down configuration to ultimately mitigate solution absorption. The glass tube has a z-like bend, to enable the working electrode's overlap with the Luggin capillary in the electrochemical cell. The active areas of the electrodes were defined using Loctite 9460 F epoxy, which does not significantly creep into the microwire arrays or form a chemical residue on the surface of planar electrodes. The epoxy was applied as a thin layer (< 0.5 mm) on the face of the electrode, so that mass transport into the electrode was not significantly hindered. The back contact and wire coil were typically insulated using Hysol 1C epoxy, which has increased chemical stability over Loctite 9460 F in methanol. Prior to electrochemical measurements, the electrodes were placed in an oven heated to 70º C for at least 2 h

(usually overnight), to further cure the epoxy to obtain enhanced chemical stability. Electrode areas were measured with a high-resolution scanner, and were calculated using Adobe Photoshop software. Electrode areas were less than 0.03 cm^{-2}, to limit resistance losses within the electrochemical cell, but greater than 0.02 cm^{-2}, such that the electrode areas could be accurately measured. Smaller electrode arrays had increasing effects from epoxy creeping into the array, and also artificially enhanced photocurrent from light scattering into the array from the surrounding epoxy.

A.2.6 Photoelectrochemical measurements

Current density vs. potential (*J-E*) measurements were performed with bottom illumination in an air-tight, flat-bottomed glass cell (Figure 3). The cell was thoroughly

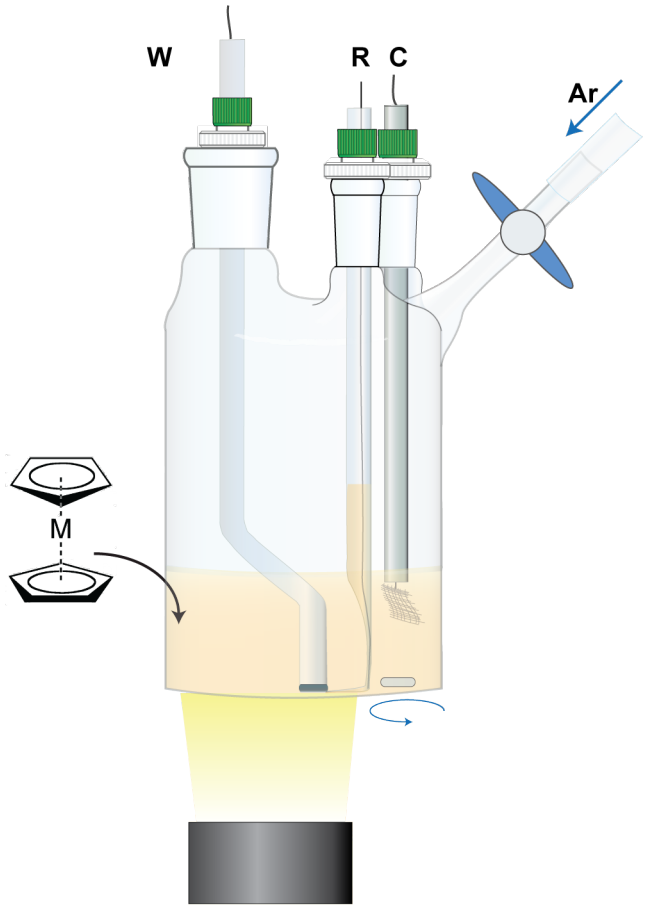

Figure 3. Schematic of the non-aqueous $Me_2Fc^{+/0}$–CH_3OH electrochemical cell

cleaned with piranha and aqua regia solutions, thoroughly rinsed with H_2O, and ultimately dried at high temperatures of ~ 120ºC. The Pt wire and Pt mesh counter electrodes were etched for 5 s in aqua regia, thoroughly rinsed in H_2O and dried at ~ 80ºC. For measurements under 1 Sun's illumination, the electrolyte solution consisted of 200 mM of Me_2Fc, ~ 0.4 mM of Me_2FcBF_4, and 1.0 M $LiClO_4$ in 30 mL of methanol. Small quantities of the oxidized form of the redox couple, Me_2FcBF_4, were employed due to its strong absorption peak in the visible at $\lambda \sim 650$ nm. The cell was assembled and sealed under an inert atmosphere (< 10 ppm O_2) before being placed under positive Ar pressure outside of the dry box. A methanol bubbler was used to prevent evaporation of the solution during an Ar purge. The three-electrode cell consisted of a high-area Pt mesh as the counter electrode, a Pt wire in a Luggin capillary filled with the cell's solution as the reference electrode, and a Si working electrode. In particular, the use of a Luggin capillary allowed for a well–defined, stable reference in the non-aqueous electrochemical cell, and allowed for the reference and working electrode to be in close proximity to limit resistance losses in the cell. The working electrode was consistently placed as close as possible to the Luggin capillary, typically within less than 1 mm of the electrode surface. At these distances, the Luggin capillary was in contact with the epoxy of the working electrode, providing the ultimate limit of the proximity of the working and reference electrodes. When changing working electrodes, the Ar flow was increased, to prevent O_2 from entering the electrochemical cell. The Ar flow was increased to the point that thermometer adaptor could 'float' in the glass fitting. After the electrode was changed, the high Ar flow was maintained for a few seconds, to purge the headspace of the electrochemical cell. The Ar flow was subsequently decreased, to maintain positive Ar pressure to the cell.

The solution potential (as measured at the counter electrode) versus the reference was continuously monitored using a 4-digit voltmeter (Keithley), and deviated from the reference by < 10 mV. If large deviations in potential occurred between the working and reference electrodes, the Luggin was re-equilibrated with the bulk solution by temporarily applying increased Ar pressure to the cell. A Princeton Applied Research (PAR) Model 273 potentiostat in conjunction with CoreWare software was typically employed for electrochemical experiments. The *J-E* behavior of an electrode was initially measured in the dark at a scan rate of 10 mV s^{-1}. By measuring the electrode's dark behavior prior to its

V_{oc} or *J-E* response under illumination, the electrode demonstrated a stable response under illumination, presumably from the completion of surface reactions during these dark scans. The V_{oc} was then measured in the dark and then under illumination. Finally, the *J-E* behavior of an electrode was measured under illumination, with a typical voltage sweep consisting of the following voltage steps: 1) the V_{oc}, 2) -0.05 V vs. $V_{oc,}$ 3) 0.2 V vs. reference, and 4) V_{oc}. A scan rate of 5 mV s^{-1} was employed for the measurement of Si microwire photoelectrodes, to limit hysteresis associated with poor mass transport in the microwire array. In addition, the cell was vigorously stirred during *J-E* measurements (stir motor setting $\geq$ 35), and the stir bar was located in close proximity to the working electrode. Prior to photoelectrochemical measurements, the Si electrodes were etched for 5 s in 5% HF(aq), rinsed with > 18 MΩ-cm resistivity H_2O, and dried thoroughly under a stream of N_2(g).

For electrochemical measurements under simulated 1 Sun's illumination, a 300 W ELH-type tungsten halogen bulb with a dichroic rear reflector was used as the illumination source. The lamp was coupled to a ground glass diffuser, to produce a more uniform field of illumination, and the illumination was directed directly through the bottom of the glass cell without the use of a mirror. The incident light intensity was calibrated using a Si photodiode (FDS-100, Thorlabs) that was placed in the solution at the position of the working electrode. The light intensity was adjusted until the short-circuit photocurrent density on the Si diode was the same as the value produced by 100 mW cm^{-2} of ELH-type illumination. This Si photodiode was previously calibrated relative to a secondary standard Si solar cell (Solarex), by measuring the current of the Si photodiode when placed under 100 mW cm^{-2} ELH-type illumination, as measured by the Solarex calibrated Si solar cell. To confirm this calibration, a planar, single crystal n-Si photoelectrode was also measured in the electrochemical cell, and the light intensity was adjusted such that the J_{sc} of the working electrode was ~ 27 mA cm^{-2}, as was previously measured for shiny, n-Si photoelectrodes under 100 mW cm^{-2} illumination.[3, 4] This method proved to be the most accurate way to calibrate the light intensity at the working electrode position, since the lamps generally have large intensity variations across the illumination area.

For electrochemical measurements under simulated AM 1.5 G illumination, the cell was illuminated using a 150 W Xe lamp with an AM 1.5 G filter (Newport/Oriel) coupled to a UV-enhanced Al mirror (PF10-03-F01, Thorlabs), to direct the light through the bottom of the cell. The illumination intensity was calibrated as described above. For experiments using the Xe lamp, the measurement of a planar, n-Si photoelectrode in solution gave the most accurate calibration of the incident light intensity, given the arc lamp's non-uniform light intensity.

To demonstrate the correction for concentration overpotential losses, 25 mM Me_2FcBF_4 was added directly to the cell after completing measurements under 1 Sun illumination. A 1 W 808 nm diode laser (Thorlabs) was used as the illumination source, and *J-E* data were collected by matching the J_{sc} value to the value of J_{sc} that was obtained under simulated 1 Sun (ELH-type or AM 1.5 G) illumination. This process typically required ~ 60 mW cm^{-2} of 808 nm illumination, as measured by a calibrated photodiode (FDS-100, Thorlabs), which was *underfilled* with the incident illumination at the position of the working electrode.

A.2.7 Corrections for series resistance and concentration overpotential losses

Corrections for the concentration overpotential (η_{conc}) and series resistance (R_s) losses were performed according to eqs. A.1 and A.2.

$$\eta_{conc} = \frac{k_B T}{nq}\left\{\ln\left(\frac{J_{l,a}}{-J_{l,c}}\right) - \ln\left(\frac{J_{l,a} - J}{J - J_{l,c}}\right)\right\} \tag{A.1}$$

$$E_{corr} = E_{meas} - iR_s - \eta_{conc} \tag{A.2}$$

where k_B is Boltzmann's constant; T is the absolute temperature; q is the (unsigned) charge on an electron; n is stoichiometric number of electrons transferred in the electrode reaction (n = 1 for $Me_2Fc^{+/0}$); and $J_{l,a}$ and $J_{l,c}$ are the anodic and cathodic mass transport–limited current densities, respectively. A Pt foil (0.025 mm thick, 99.9% Alfa Aesar) working electrode of comparable area and geometric configuration to the Si working electrodes was used to measure the $J_{l,a}$, $J_{l,c}$, and R_s of the cell. Typically, the Pt electrode's measured $J_{l,a}$

was ~ 80 mA cm^{-2}, and $J_{l,c}$ were ~ 0.15 and ~ 10 mA cm^{-2}, for 0.4 mM and 25 mM Me_2FcBF_4, respectively. To obtain the series resistance of the cell, the *J-E* data of the Pt electrode was first corrected for η_{conc} losses using eq. 1. The inverse of the slope of the linear portion of the resulting *J-E* data was then evaluated to produce a value for R_s. The measured value of R_s was dependent on the placement of the working electrode with respect to the Luggin capillary, and typically varied from 50–150 Ω. A value of R_s = 50 Ω was used in the calculations to avoid overcorrection of the data, resulting in conservative, potentially underestimated, values for the intrinsic fill factor and photoelectrode efficiency of the Si/$Me_2Fc^{+/0}$–CH_3OH contact.

A.3. References

1. M. L. Rosenbluth and N. S. Lewis, *J. Am. Chem. Soc.*, 1986, **108**, 4689-4695.
2. C. M. Gronet, N. S. Lewis, G. Cogan and J. Gibbons, *Proc. Natl. Acad. Sci. U.S.A.*, 1983, **80**, 1152-1156.
3. J. F. Gibbons, G. W. Cogan, C. M. Gronet and N. S. Lewis, *Appl. Phys. Lett.*, 1984, **45**, 1095-1097.
4. M. L. Rosenbluth, C. M. Lieber and N. S. Lewis, *Appl. Phys. Lett.*, 1984, **45**, 423-425.
5. F. Gstrein, D. J. Michalak, W. J. Royea and N. S. Lewis, *J. Phys. Chem. B*, 2002, **106**, 2950-2961.
6. R. L. Grimm, M. J. Bierman, L. E. O'Leary, N. C. Strandwitz, B. S. Brunschwig and N. S. Lewis, 2012, *In Press.*
7. J. R. Maiolo, H. A. Atwater and N. S. Lewis, *J. Phys. Chem. C*, 2008, **112**, 6194-6201.